Theories and Experiments on Nonlinear Optics

Final Report

June 1, 1965 - May 31, 1969

Contract Nonr 3656(32)

ARPA Order Number 306

Program Code Number 4730

Name of Contractor: The Regents of the University of California

Project Scientist: Y. R. Shen

I. INTRODUCTION

The research project proposed in the original contract was to investigate the physical mechanisms responsible for the many anomalous effects associated with the stimulated Raman scattering in various media. In the early stage of the investigation, we soon realized that an intense laser beam propagating in liquid tends to self-focus into hot filaments. Self-focusing is apparently responsible for most of the anomalous effects observed in stimulated Raman scattering. It was then clear that one must first understand self-focusing before all mysteries about stimulated Raman scattering can be solved.

We studied both theoretically and experimentally the physical mechanisms for the intensity-dependent refractive index and hence for self-focusing. Our results showed that in most liquids, the optical Kerr effect is the dominant mechanism, but in some liquids, the electrostrictive effect also plays a non-negligible role. Both stimulated Raman and Brillouin scattering are initiated and enhanced by self-focusing and the formation of hot filaments.

It was believed by most people that the observed hot filaments of few microns in diameter are just the self-trapped filaments predicted by Chiao, Garmire, and Townes. In our recent experiments, however, we showed that by using a single-mode laser, the observed hot filaments are in fact tracks of moving focal spots resulting from self-focusing. This result has important far-reaching consequences on many effects connected with self-focusing.

We also constructed a set-up with two simultaneously Q-switched lasers at different frequencies. We used the set-up to generate

far-infrared radiation by beating the two laser beams in a nonlinear crystal. We were able to demonstrate for the first time the feasibility of obtaining an intense, tunable far-infrared pulse from difference-frequency generation.

II. RESEARCH ACCOMPLISHMENTS

A. Self-Focusing and Stimulated Scattering

Results of early investigation on stimulated Raman scattering in liquids showed that the Raman gain was two orders of magnitude larger than the theoretical prediction. It was conceived by us that this anomalous gain could be explained if the laser beam propagating in the liquid was inhomogeneous or contained hot filaments. By using a two-cell method, we showed that this is indeed the case. (See Appendix I). As a result of intensity-dependent refractive index of the liquid, the laser beam tends to self-focus into hot filaments in the liquid. We then investigated the physical mechanisms responsible for the intensity-dependent change of refractive index. From the variation of the self-focusing strength with temperature, we concluded that in most liquids, the optical Kerr effect is the dominant mechanism for self-focusing, but in some liquids, the electrostrictive effect is also important (Appendices II and III). By assuming that the laser beam breaks into filaments after self-focusing, some qualitative features of the observed stimulated Raman and Brillouin scattering were explained (Appendix III); however, no quantitative agreement was achieved.

It was believed for some time that the observed hot filaments of a few microns were the demonstration of self-trapping predicted by Chiao, Garmire, and Townes. Nevertheless, the small size and high intensity

of the filaments received no explanation. Recently, we made careful measurements on the duration, the intensity, and the spectrum of light in the filaments (Appendix IV). The results obtained from a single-mode laser indicated that it was not likely that the self-trapped filaments existed in our experiments. Closer investigation on the filaments and related effects showed that the filaments are actually composed of continuous series of moving focal points (Appendix V). This discovery clearly changes the current status of research on self-focusing and self-trapping.

B. Far-Infrared Difference-Frequency Generation

It was suggested earlier by several people that using two temperature-tuned ruby lasers can provide a tunable source of coherent far-infrared radiation. Many research workers tried, but failed. Only recently, we were able to demonstrate for the first time that such a tunable far-infrared source can indeed be achieved. In our experiments, we used two temperature-tuned Q-switched ruby lasers. The main difficulty which we had overcome was to synchronize the two laser pulses. We were able to obtain 1 mW of far-infrared radiation out of a 1/2 mm crystal of $LiNbO_3$. (See Appendix VI). By varying the ruby temperature from room to liquid N_2 temperature, we can obtain a tuning range of 0 - 22 cm^{-1} for the far-infrared output. In addition, we were able to make the laser lase at either R_1 or R_2 line. This extends the possible tuning range from 0 - 51 cm^{-1}. The device would be extremely useful for the investigation of transcient or lifetime measurements on the low-lying resonance excitations.

C. Theoretical Calculations

1) On Self-Trapped Filaments. (Appendix VII) We showed from steady-state thermodynamic consideration that the assumption of possible field-induced phase transition can lead to the formation of self-trapped filaments of light in liquids. The model is an analog of Abrikosor vortex state in superconductors.

2) On Optical Nonlinearities of a Plasma. (Appendix VIII) Second-harmonic generation and stimulated Raman effects in a plasma were discussed. The second-harmonic generation from a solid-state plasma boundary was investigated. It was shown that second-harmonic generation from metals is dominated by the contribution from bound electrons in the surface layer. The prediction has been verified by N. Bloembergen et al Phys. Rev. 174, 813 (1968).

3) On Photon-Magnon Interaction. (Appendices IX and X) It was predicted that light scattering from magnons in ferro-, ferri-, and anti-ferro-magnets can be observed. The similarity between the spin-Raman effect and the vibrational Raman effect was emphasized and the possibility of stimulated Raman scattering from magnons was discussed. It was also suggested that the magnon-phonon coupling can enhance light scattering intensity. The results were presented as an invited talk in the 1967 Annual Conference on Magnetism and Magnetic Materials. The prediction was verified by P. A. Fleury et al. (Phys. Rev. Letters 17, 84 (1966)).

4) On Quantum Statistics of Nonlinear Optics. (Appendix XI) Nonlinear interaction of light with matter was discussed from the quantum statistical point of view. It was shown that the rate of nonlinear interaction depends on the mode structure of the light fields and measurements of the statistical properties of the output fields can yield infor-

mation about statistics of the input fields and the properties of the medium. The paper was given as an invited talk in the 1967 Enrico Fermi Summer Institute.

5) On Permutation Symmetry of Nonlinear Susceptibilities. (Appendix XII) Permutation symmetry of nonlinear susceptibilities was derived from the microscipic theory. It was shown that the permutation symmetry is essential for the existence of a time-averaged free energy.

Security Classification

DOCUMENT CONTROL DATA R&D

(Security classification of title, body of abstract and indexing annotation must be entered when the overall report is classified)

1. ORIGINATING ACTIVITY *(Corporate author)*

University of California, Berkeley, California

2a. REPORT SECURITY CLASSIFICATION

Unclassified

2b. GROUP

3. REPORT TITLE

Theories and Experiments on Nonlinear Optics

4. DESCRIPTIVE NOTES *(Type of report and inclusive dates)*

Final Report June 1, 1965 - May 31, 1969

5. AUTHOR(S) *(Last name, first name, initial)*

Y. R. Shen

6. REPORT DATE	7a. TOTAL NO. OF PAGES	7b. NO. OF REFS
June 30, 1969	95	

8a. CONTRACT OR GRANT NO.	9a. ORIGINATOR'S REPORT NUMBER(S)
b. PROJECT NO.	
c.	9b. OTHER REPORT NO(S) *(Any other numbers that may be assigned this report)*
d.	ARPA, The Office of Naval Research

10. AVAILABILITY/LIMITATION NOTICES

Qualified requesters may obtain copies of the report from DDC.

11. SUPPLEMENTARY NOTES	12 SPONSORING MILITARY ACTIVITY

13. ABSTRACT

Experimental results on self-focusing and self-trapping of laser light in liquids and on tunable far-infrared difference-frequency generation are presented. Theoretical investigation on various problems on nonlinear optics is described.

DD FORM 1 JAN 64 1473

Unclassified

Security Classification

Security Classification

14. KEY WORDS	LINK A		LINK B		LINK C	
	ROLE	WT	ROLE	WT	ROLE	WT
Nonlinear optics						
Lasers						

INSTRUCTIONS

1. ORIGINATING ACTIVITY: Enter the name and address of the contractor, subcontractor, grantee, Department of Defense activity or other organization *(corporate author)* issuing the report.

2a. REPORT SECURITY CLASSIFICATION: Enter the overall security classification of the report. Indicate whether "Restricted Data" is included. Marking is to be in accordance with appropriate security regulations.

2b. GROUP: Automatic downgrading is specified in DoD Directive 5200.10 and Armed Forces Industrial Manual. Enter the group number. Also, when applicable, show that optional markings have been used for Group 3 and Group 4 as authorized.

3. REPORT TITLE: Enter the complete report title in all capital letters. Titles in all cases should be unclassified. If a meaningful title cannot be selected without classification, show title classification in all capitals in parenthesis immediately following the title.

4. DESCRIPTIVE NOTES: If appropriate, enter the type of report, e.g., interim, progress, summary, annual, or final. Give the inclusive dates when a specific reporting period is covered.

5. AUTHOR(S): Enter the name(s) of author(s) as shown on or in the report. Enter last name, first name, middle initial. If military, show rank and branch of service. The name of the principal author is an absolute minimum requirement.

6. REPORT DATE: Enter the date of the report as day, month, year; or month, year. If more than one date appears on the report, use date of publication.

7a. TOTAL NUMBER OF PAGES: The total page count should follow normal pagination procedures, i.e., enter the number of pages containing information.

7b. NUMBER OF REFERENCES: Enter the total number of references cited in the report.

8a. CONTRACT OR GRANT NUMBER: If appropriate, enter the applicable number of the contract or grant under which the report was written.

8b, 8c, & 8d. PROJECT NUMBER: Enter the appropriate military department identification, such as project number, subproject number, system numbers, task number, etc.

9a. ORIGINATOR'S REPORT NUMBER(S): Enter the official report number by which the document will be identified and controlled by the originating activity. This number must be unique to this report.

9b. OTHER REPORT NUMBER(S): If the report has been assigned any other report numbers *(either by the originator or by the sponsor)*, also enter this number(s).

10. AVAILABILITY/LIMITATION NOTICES: Enter any limitations on further dissemination of the report, other than those imposed by security classification, using standard statements such as:

(1) "Qualified requesters may obtain copies of this report from DDC."

(2) "Foreign announcement and dissemination of this report by DDC is not authorized."

(3) "U. S. Government agencies may obtain copies of this report directly from DDC. Other qualified DDC users shall request through _____."

(4) "U. S. military agencies may obtain copies of this report directly from DDC. Other qualified users shall request through _____."

(5) "All distribution of this report is controlled. Qualified DDC users shall request through _____."

If the report has been furnished to the Office of Technical Services, Department of Commerce, for sale to the public, indicate this fact and enter the price, if known.

11. SUPPLEMENTARY NOTES: Use for additional explanatory notes.

12. SPONSORING MILITARY ACTIVITY: Enter the name of the departmental project office or laboratory sponsoring *(paying for)* the research and development. Include address.

13. ABSTRACT: Enter an abstract giving a brief and factual summary of the document indicative of the report, even though it may also appear elsewhere in the body of the technical report. If additional space is required, a continuation sheet shall be attached.

It is highly desirable that the abstract of classified reports be unclassified. Each paragraph of the abstract shall end with an indication of the military security classification of the information in the paragraph, represented as *(TS)*, *(S)*, *(C)*, or *(U)*.

There is no limitation on the length of the abstract. However, the suggested length is from 150 to 225 words.

14. KEY WORDS: Key words are technically meaningful terms or short phrases that characterize a report and may be used as index entries for cataloging the report. Key words must be selected so that no security classification is required. Identifiers, such as equipment model designation, trade name, military project code name, geographic location, may be used as key words but will be followed by an indication of technical context. The assignment of links, roles, and weights is optional.

APPENDIX I

BEAM DETERIORATION AND STIMULATED RAMAN EFFECT*

Y. R. Shen and Y. J. Shaham

Physics Department, University of California, Berkeley, California
(Received 11 October 1965; revised manuscript received 10 November 1965)

The most important fundamental discrepancy between theory and experiments in the stimulated Raman effect is that the observed Raman gain is one to two orders of magnitude larger than the theoretical value.[1] The latter is given by[2]

$$g = (2\pi\omega_S^2/k_{Sz}c^2)|\chi_s''|^2|E_l|^2,$$

where ω_S is the Stokes frequency, k_S the Stokes wave vector, E_l the laser field amplitude, and χ_s'' the resonant Raman susceptibility whose magnitude can be obtained from the spontaneous Raman-scattering data. It was suggested that the observed anomalous gain might be the result of the multimode structure (or hot filaments) of the laser (pumping) beam,[3] but McClung, Wagner, and Weiner, using a nearly single-mode laser beam in the experiments, still found the presence of such an anomalous gain.[1] This, however, does not eliminate the possibility of deterioration of the laser beam into multimodes as the beam interacts with the medium. In this paper, experimental evidence is presented to suggest that scattering mechanisms in a medium can produce inhomogeneities or filamentary structure in an initially homogeneous beam. We believe that these hot filaments are responsible for the many anomalous effects previously observed.

A laser beam, Q switched by cryptocyanine solution and limited in cross section by an aperture in the cavity, was used to generate Stokes radiation in a 20-cm toluene cell (cell A). The laser intensity was varied by a Polaroid prism outside the laser cavity. Another cell (cell B) of variable length, filled with water, benzene, acetophenone, or nitrobenzene, was inserted between the laser and the toluene cell. The threshold of the stimulated Raman scattering was then measured as a function of the length of cell B. The results are shown in Fig. 1. The curves clearly show that the medium in cell B can distort the laser beam in such a way as to help significantly the Raman generation in toluene. Here, the Raman threshold of toluene first increases and then decreases sharply as the length of cell B is increased.

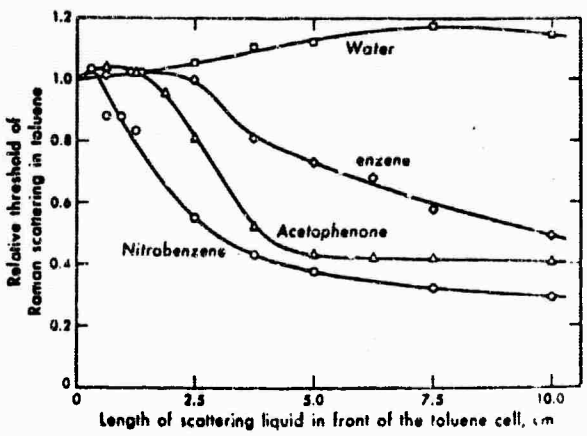

FIG. 1. Raman threshold in toluene versus the cell length of a scattering cell in front of the toluene cell. The scattering cell was filled with water, benzene, acetophenone, or nitrobenzene.

This suggests that the distortion of the beam is due to some kind of stimulated scattering in cell B. The initial rise of the threshold is believed to be the result of insertion loss in cell B. No Raman radiation was generated in cell B, except for the case of nitrobenzene or acetophenone with the cell longer than 3.5 cm. It is therefore reasonable to assert that the beam distortion is due to forward scattering through generation of acoustic and thermal strain (Brillouin and Rayleigh scattering). The maxima and the slopes of these curves show that if forward scattering is responsible for the beam distortion, nitrobenzene should have the largest scattering cross section, followed by acetophenone, benzene, and water. The existing data on incoherent light scattering give the following scattering intensity ratio[4]:

$$I_{NB}:I_{AC}:I_{B}:I_{water}=10.88:5.66:3.15:0.17.$$

Above threshold, the intensity of the toluene Stokes emission was found to increase appreciably when a 7.5-cm nitrobenzene cell is inserted between the laser and the toluene cell, even though the laser power is somewhat depleted by the generation of Raman emission in nitrobenzene. It was also noticed that the laser beam coming out from a Raman cell was generally less homogeneous than the original beam. Hot, thin laser filaments formed in Raman-active media have been observed by other workers.[5]

That the forward scattering may be responsible for the anomalous Raman gain is also reflected in the temperature effect of the Raman emission. Fig. 2 shows the Raman threshold in nitrobenzene and toluene in a 15-cm cell as a function of temperature. The observed effect is too large to be attributed to the change in the Raman scattering itself. This is confirmed by the fact that when a 7.5-cm nitrobenzene cell was inserted in front of the toluene, the toluene Raman threshold remained more or less constant with temperature. If the temperature of the nitrobenzene cell was varied instead, appreciable change in the toluene Raman threshold was again observed. The curves indicate less beam distortion for higher temperature. This suggests that the forward stimulated Brillouin effect may be the dominating mechanism for beam distortion, since the effect would then be stronger for smaller acoustic damping, and hence for lower temperature.

Theoretically, a laser beam can be distorted or deteriorated into multimodes through nonlinear interaction between light waves and pressure (acoustic) and thermal waves in the medium. The interaction is governed by the set of coupled electromagnetic and acoustic wave equations and the heat diffusion equation. In the limiting case where only the static pressure and thermal strain (electrostriction) are considered, this would lead to the beam-trapping phenomenon proposed by Chiao, Garmire, and Townes.[6] More generally, the initial laser intensity distribution in the frequency and wave-vector space would be broadened a great deal by this mechanism. In other words, a single-mode laser beam can be spoiled into many coherent spatial and temporal modes, which then give rise to hot filaments in the beam and intense spikes in the laser pulse. Usually, the thermal effect is negligible compared to the pressure effect. The forward Brillouin scattering (which includes electrostriction) is possibly responsible for the distortion of the beam. It would have a threshold much lower than the Raman threshold in many media, as seen from the estimate for the case of beam trapping.[6]

Most of the anomalous Raman effects can be explained by the multimode theory.[3] In particular, N coherent laser modes of comparable intensities would give a maximum Stokes gain which is about N times larger than the average gain.[7] The details of the theory will be reported elsewhere.

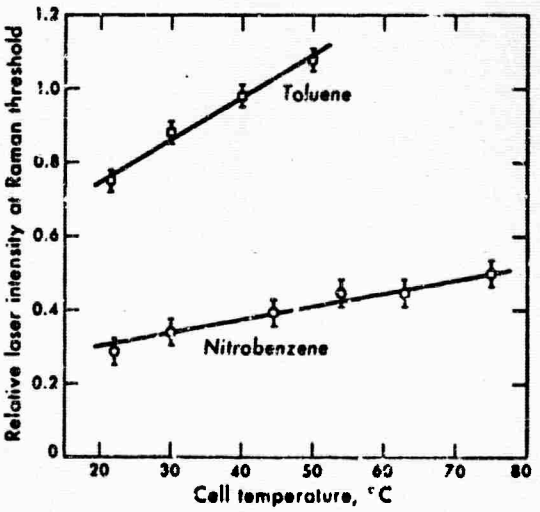

FIG. 2. Raman threshold of toluene and nitrobenzene as a function of temperature.

We would like to thank Professor N. Bloembergen, Dr. F. Quelle, and Professor S. P. Davis for stimulating discussion.

*This research was supported by the U. S. Office of Naval Research under Contract No. Nonr-3656(32).

[1]F. J. McClung, W. G. Wagner, and D. Weiner, Phys. Rev. Letters 15, 96 (1965); D. Weiner, S. Schwarz, and F. J. McClung, J. Appl. Phys. 36, 2395 (1965).

[2]Y. R. Shen and N. Bloembergen, Phys. Rev. 137, 1787 (1965).

[3]N. Bloembergen and Y. R. Shen, Phys. Rev. Letters 13, 720 (1964).

[4]S. Bhagavantam, Scattering of Light and the Raman Effect (Chemical Publishing Company, New York, 1942).

[5]N. Bloembergen and P. Lallemand, private communications.

[6]R. Chiao, E. Garmire, and C. H. Townes, Phys. Rev. Letters 13 479 (1964).

[7]In Ref. 3, the modes are assumed to have random phases. This assumption leads to a factor of $\log N$ in the enhancement of the Stokes gain.

APPENDIX II

Volume 20, number 4 PHYSICS LETTERS 1 March 1966

ELEC 'ROSTRICTION, OPTICAL KERR EFFECT AND SELF-FOCUSING OF LASER BEAMS *

Y. R. SHEN
Physics Department, University of California, Berkeley, California

Received 26 January 1966

Electrostrictive coefficients and optical Kerr constants for liquids are derived. Their relative importance in the self-focusing of a giant-pulse laser beam is discussed.

A laser beam propagating in an isotropic, transparent medium induces an increase in the refractive index proportional to the laser intensity through electrostriction and optical Kerr effect. The intensity-dependent index of refraction can lead to self-focusing of the laser beam, as first envisaged by Arkaryan [1] and by Chiao et al. [2], and recently computed by Kelley [3]. Experimentally, it has been observed that the beam does get highly inhomogeneous after traversing through a liquid medium [4, 5]. The self-focusing action, with the result of hot-filament formation, gives rise to the anomalous gain in the stimulated Raman scattering. Therefore, knowledge about electrostrictive coefficients and optical Kerr constants for various liquids is now extremely helpful in work on stimulated scattering in liquids. The optical Kerr effects in some liquids have been measured by Gires and Mayer [6], and the intensity-dependent refractive indices by Maker et al. [7]. In this note, they are derived in terms of refractive indices, dielectric constants, isothermal compressibilities and d.c. Kerr constants. Their relative importance in self-focusing of a giant-pulse laser beam is discussed.

The Clausius-Mosotti relation gives the change of the refractive index in terms of the variations in density and in polarizability, $\Delta\rho$ and $\Delta\alpha$.

* This research is supported by the U.S. Office of Naval Research under Contract Nonr-3656(32).

$$\Delta n = (\Delta n)_\rho + (\Delta n)_\alpha = \quad (1)$$

$$(n_0^2 - 1)(n_0^2 + 2)[(\Delta\rho/\rho_0) + (\Delta\alpha/\alpha_0)]/6n_0 .$$

In the presence of an optical field $E(r, t)$, $\Delta\rho$ obeys the driven acoustic wave equation

$$\left(-\nabla^2 + \frac{1}{v^2}\frac{\partial^2}{\partial t^2} - \frac{2\Gamma}{v^2}\frac{\partial}{\partial t}\right)\Delta\rho = -\frac{1}{8\pi}\frac{\gamma}{v^2}(\nabla^2 E^2) . \quad (2)$$

Here, $v = (1/\rho_0\beta)^{\frac{1}{2}}$ is the acoustic velocity, β the isothermal compressibility, Γ the acoustic damping, and $\gamma = 2n_0\rho_0(\partial n/\partial\rho) = \frac{1}{3}(n_0^2 - 1)(n_0^2 + 2)$. Since $\Delta\rho$ cannot follow the driven force at optical frequencies, only the low-frequency components of $\Delta\rho$ should be considered. In the case of a monochromatic field $E(r, t) = \epsilon(r)\cos(k\cdot r - \omega t)$, one finds

$$(\Delta n)_\rho = K_\rho\lambda\,\tfrac{1}{2}\epsilon^2 \quad (3)$$

with $K_\rho = \gamma^2\beta/8\pi n_0\lambda$ defined as the electrostrictive coefficient. The electrostrictive coefficients calculated are shown in table 1 for a few liquids *.

The change of the polarizability is assumed to come entirely from the orientational variation of the anisotropic molecules. Let the orientational distribution function be $f(\theta, \varphi, \psi)$, where θ, φ and ψ determine the orientation of a particular molecule. The change of the polarizability can then be calculated from the theory of Lengevin [9]. We have

$$\Delta\alpha = \int p(\Delta f)\sin\theta\,d\theta\,d\varphi\,d\psi / E\int f\sin\theta\,d\theta\,d\varphi\,d\psi . \quad (4)$$

Here, p is the induced dipole moment, and $\Delta f = f - f_0$ obeys the equation

$$[(\partial/\partial t) + (1/\tau)]\,\Delta f = (\Delta f)_\infty/\tau$$
$$(\Delta f)_\infty = C[\exp(-U/kT) - 1] , \quad (5)$$

where $\tau \approx 4\pi a^3\nu/kT$ is the relaxation time, a the dimension of molecules, ν the viscosity coefficient, C the normalization constant, and U the potential energy of the anisotropic molecule in the E field. Again, since Δf cannot follow variations at optical frequencies, only the low-frequency part should be taken into account. In the first order, one finds, for a linearly polarized monochromatic field,

$$(\Delta n)_\alpha = \tfrac{2}{15}K_\alpha\lambda(\tfrac{1}{2}\epsilon^2) \quad (6)$$

* The electrostrictive coefficients are about 4 times larger than those calculated in ref. 2. The error can be traced back to the smaller values of β they used and the missing of a factor 2. Their values of optical Kerr constants should also be smaller by a factor of 2 [8].

Table 1

Electrostrictive coefficients, K_ρ, optical Kerr constants, K_α, and the d.c. Kerr constants, $(K_1)_{dc}$, calculated at the wavelength of the sodium D line for various liquids. In calculating these constants, n_0 is obtained from the International Critical Tables and β and δ from the Handbook of Chemistry and Physics. All physical constants are taken at 20°C if possible.

	$K_\rho \times 10^7$	$K_\alpha \times 10^8$	$(K_1)_{dc} \times 10^8$
Carbon-tetrachloride	1.21	0.67	0.74
Carbon-disulphide	2.53	32.6	32.26
Hexane	1.06	0.45	0.45
Cyclohexane	1.06	0.78	0.74
m-xylene	1.20	7.59	8.58
Benzene	1.33	5.73	5.93
Toluene	1.25	6.55	7.53
Chlorobenzene	1.20	9.93	91
Bromobenzene	1.50	14.35	91
Nitrobenzene	0.92	26.4	2560
Aniline	1.00	3.22	-12.3
Chloroform	1.03	1.70	-33.2
Acetone	0.75	1.03	163
Methylalcohol	0.58	0.17	9.7
Ethylalcohol	0.66	0.21	7.68
Butylalcohol	0.64	0.41	-36.5

and for a circularly polarized field

$$(\Delta n)_\alpha = \tfrac{1}{15}K_\alpha\lambda(\tfrac{1}{2}\epsilon^2) \quad (7)$$

with $K_\alpha = [(n_0^2 + 2)(n_0^2 - 1)(\epsilon + 2)/(\delta + 2)^2(\delta - 1)](K_1)_{dc}$ defined as the optical Kerr constant. Here, δ is the dielectric constant, and ϵ is given by the Debye relation

$$(\delta - 1)/(\delta + 2) = [(\epsilon - 1)/(\epsilon + 2) + 4\pi\rho_0\mu^2/9mkT] ,$$

μ being the permanent dipole moment of the molecules. $(K_1)_{dc}$ is the part of the d.c. Kerr constant originated from the induced dipole moments only and is always positive. For non-polar molecules, one finds $K_\alpha \approx (K_1)_{dc}$. For polar molecules with large μ, the optical Kerr constant can be much smaller than the d.c. Kerr constant in absolute magnitude. The optical Kerr constants, for various liquids, obtained with $(K_1)_{dc}$ calculated by Raman and Krishnan [9], are given in table 1. The d.c. Kerr constants are also given for comparison.

For a giant laser pulse of pulse width Λ, it can easily be shown that if $\tau \ll \Lambda$, eq. (6) is still valid, but $(\Delta n)_\alpha$ is now proportional to $|\epsilon(r, t)|^2$, which varies with time. For most liquids, this is true since $\tau < 10^{-10}$ sec. The density variation $\Delta\rho$, however, cannot follow the giant pulse. Assuming the distribution of laser intensity over the cross section and time to be

$$\epsilon(r,t)^2 = A\exp(-\alpha^2 r^2)\begin{cases} t & \text{for } t \leq \Lambda \\ (-t+2\Lambda) & \text{for } t \geq \Lambda \end{cases} \quad (5)$$

one can get a rough estimate of the density variation by neglecting $\nabla^2(\Delta\rho)$ in eq. (2). This is a good approximation for $\alpha < 100$ and $r < 1/\alpha$. The result, together with the optical Kerr effect, gives a total change of the index of refraction

$$\Delta n = [K_\rho v^2\alpha^2(1-\alpha^2r^2)t^3 + K_\alpha t]\tfrac{1}{3}\lambda A\exp(-\alpha^2r^2) \quad \text{for } t \leq \Lambda$$
$$= [K_\rho v^2\alpha^2(1-\alpha^2r^2)(2\Lambda^3 - 6\Lambda^2 t + 6\Lambda t^2 - t^3) + K_\alpha(2\Lambda - t)]\tfrac{1}{3}\lambda A\exp(-\alpha^2r^2) \quad \text{for } t \geq \Lambda \quad (9)$$

Eq. (9) shows that at $t = \Lambda$, the ratio $(\Delta n)_\rho/(\Delta n)_\alpha$ is about $10^{-2}K_\rho/K_\alpha$ for $v = 1.5\times10^5$ cm/sec, $\Lambda = 2\times10^{-8}$ sec, and $\alpha = 30$ cm^{-1}. This ratio becomes larger at later times.

The increase of refractive index with the laser intensity leads to self-focusing of laser beams in liquids. Experiments [4, 5, 10] show that the self-focusing action is very strong in CS_2, followed in decreasing order by nitrobenzene, bromobenzene, toluene, benzene, chloroform, CCl_4, hexane and methylalcohol. Table 1 shows that the magnitudes of the optical Kerr constants of these liquids follow exactly the same order. We have also seen a large reduction of self-focusing action in these liquids when a circularly polarized laser beam is used [10]. This makes one believe that the optical Kerr effect is responsible for self-focusing. However, for liquids with small optical Kerr constants, electrostriction may also be important. If one uses eq. (9), one would find at $t = \Lambda$, $(\Delta n)_\rho/(\Delta n)_\alpha \approx 0.4$ in CCl_4. The electrostrictive coefficients have a strong positive temperature dependence, while the optical Kerr constants have a weaker negative temperature dependence. Temperature measurements [10] indeed show that in all liquids with large optical Kerr constants, the self-focusing action decreases with increase of temperature, but in CCl_4 and hexane, it increases with increase of temperature. The optical Kerr effect is also responsible for spectral broadening in the stimulated Raman scattering [11], when the laser radiation has two or more modes separated by about 1 cm^{-1}. The electrostriction, however, should have very little effect on spectral broadening, since the component of $\Delta\rho$ at the beat frequencies of the laser modes would be extremely small.

References

1. G.A. Askaryan, Zh. Eksperim. i Teor. Fiz. 42 (1962) 1567; translation Soviet Phys. JETP 15 (1962) 1088.
2. R.Y. Chiao, E. Garmire and C.H. Townes, Phys. Rev. Letters 13 (1964) 479.
3. P.L. Kelley, Phys. Rev. Letters 15 (1965) 1005.
4. Y.R. Shen and Y.J. Shaham, Phys. Rev. Letters 15 (1965) 1008.
5. P. Lallemand and N. Bloembergen, Phys. Rev. Letters 15 (1965) 1010.
6. F. Gires and G. Mayer, Compt. Rend., 258 (1964) 2039.
7. P.D. Maker, R.W. Terhune and C.M. Savage, Phys. Rev. Letters 12 (1964) 507.
8. E. Garmire, Thesis, M.I.T., 1965 (unpublished); R.Y. Chiao, Thesis, M.I.T., 1964 (unpublished).
9. C.V. Raman and K.S. Krishnan, Phil. Mag. 3 (1927) 724.
10. Y.J. Shaham, private communications, to be published.
11. N. Bloembergen and P. Lallemand, to be published.

* * * * *

BLANK PAGE

APPENDIX III

Reprinted from THE PHYSICAL REVIEW, Vol. 163, No. 2, 224-231, 10 November 1967
Printed in U. S. A.

Self-Focusing and Stimulated Raman and Brillouin Scattering in Liquids*

Y. R. SHEN† AND Y. J. SHAHAM
Physics Department, University of California, Berkeley, California

(Received 20 April 1967)

Experimental results on the self-focusing of a laser beam in many liquids are reported. It is shown that the optical Kerr effect and electrostriction cannot explain the temperature variation of self-focusing in some liquids. Forward stimulated Brillouin scattering seems important in such cases. Measurements on the generation of stimulated Raman and Brillouin radiation in liquids are presented. The effect of self-focusing and self-trapping on the forward-backward asymmetry in the Stokes generation is discussed. Other qualitative features in the stimulated Raman and Brillouin scattering are explained.

I. INTRODUCTION

WHEN a high-intensity laser pulse traverses a certain distance in a liquid, the beam cross-section often reduces, and in some liquids, thin filaments of extremely high intensity appear. This phenomenon, which is generally known as self-focusing and self-trapping of light beams, has been the subject of intense theoretical[1-7] and experimental[8-18] investigation recently. It is self-focusing and self-trapping that give rise to the many anomalies observed in stimulated Raman and Brillouin scattering in liquids. Physically, self-focusing arises because the refractive index (real part) of the medium increases with the beam intensity (a coherent elastic-scattering process), and because stimulated Brillouin and Rayleigh scattering near the forward direction occur via acoustic and orientational excitations in the medium (a coherent inelastic-scattering process). An alternative way of describing self-focusing is that the width of the beam intensity distribution over its spatial Fourier components increases with distance.

The intensity dependence of refractive indices has been investigated by many authors.[19] In a nonabsorbing medium, it is due to optical Kerr effect, electrostriction, and nonlinear electronic polarizability.[2] For ordinary Q-switched laser intensity, the steady-state refractive index can be written in the form

$$n=n_0+(n_{2a}+n_{2\rho}+n_{2e})\tfrac{1}{2}\,|\,E\,|^2,$$

where E is the laser field strength, and the coefficients n_{2a}, $n_{2\rho}$, and n_{2e} are associated with Kerr effect, electrostriction, and nonlinear electronic polarizability, respectively. For most liquids which have been subject to investigation, n_{2a} ranges from 10^{-13} to 10^{-11} esu, while $n_{2\rho}$ is of the order of 10^{-11} esu. In the normal dispersion region, n_{2e} is about 10^{-15} or 10^{-14} esu as estimated from the nonlinear polarizability for third-harmonic generation,[20] and should be negligible compared with n_{2a} and $n_{2\rho}$. It is, however, believed that the Kerr effect gives the dominant contribution to the intensity-dependent part of the refractive index in liquids. The reason is simple. The Kerr effect, arising from molecular reorientation[21] and molecular redistribution,[22] responds almost instantaneously to the Q-switched pulse, but the electrostrictive effect, which involves mass transfer to a region of high beam intensity, cannot follow the rapid intensity variation of the pulse. One can actually show that for a 10^{-8}-sec pulse, the electrostrictive contribution to the refractive index would be negligible

* This research was supported by the Office of Naval Research under Contract No. Nonr-3656(32).

† A. P. Sloan Research Fellow.

[1] G. A. Askar'yan, Zh. Eksperim. i Teor. Fiz. **42**, 1567 (1962) [English transl.: Soviet Phys.—JETP **15**, 1088 (1962)].

[2] R. Y. Chiao, E. Garmire, and C. H. Townes, Phys. Rev. Letters **13**, 479 (1964).

[3] P. L. Kelley, Phys. Rev. Letters **15**, 1005 (1965).

[4] V. I. Bespalov and V. I. Talanov, JETP Pis'ma v Redaktsiyu **3**, 471 (1966) [English transl.: JETP Letters **3**, 307 1966)].

[5] K. Grob and M. Wagner, Phys. Rev. Letters **17**, 819 (1966).

[6] S. K. Akhmanov, A. P. Sukhorukov, and R. V. Khokhlov, Zh. Eksperim. i Teor. Fiz. **50**, 1537 (1966) [English transl.: Soviet Phys.—JETP. **23**, 1025 (1966)].

[7] Yu. P. Razier, JETP Pis'ma v Redaktsiyu **4**, 286 (1966) [English transl.: JETP Letters **4**, 193 (1966)].

[8] Y. R. Shen and Y. J. Shaham, Phys. Rev. Letters **15**, 1008 (1965).

[9] P. Lallemand and N. Bloembergen, Phys. Rev. Letters **15**, 1010 (1965); **16**, 81 (1966).

[10] G. Hauchecorne and G. Mayer, Compt. Rend. **261**, 4014 (1965).

[11] E. Garmire, R. Y. Chiao, and C. H. Townes, Phys. Rev. Letters **16**, 347 (1966).

[12] N. F. Pilipetskii and A. R. Rustamov, JETP Pis'ma v Redaktsiyu **2**, 88 (1965) [English transl.: JETP Letters **2**, 55 (1965)].

[13] C. C. Wang, Phys. Rev. Letters **16**, 344 (1966).

[14] R. G. Brewer and J. R. Lifsitz, Phys. Letters **23**, 79 (1966).

[15] R. Y. Chiao, M. A. Johnson, S. Krinsky, H. A. Smith, C. H. Townes, and E. Garmire, IEEE J. Quantum Electron. **2**, 467 (1966).

[16] N. Bloembergen, P. Lallemand, and A. Pine, IEEE J. Quantum Electron. **2**, 246 (1966).

[17] D. H. Close, C. R. Guiliano, R. W. Hellwarth, L. D. Hess, F. J. McClung, and W. G. Wagner, IEEE J. Quantum Electron. **2**, 553 (1966).

[18] R. G. Brewer and C. H. Townes, Phys. Rev. Letters **18**, 196 (1967).

[19] P. D. Maker, R. W. Terhune, and C. M. Savage, Phys. Rev. Letters **12**, 612 (1964); F. Gires and G. Mayer, Compt. Rend. **258**, 2039 (1964).

[20] P. D. Maker, R. W. Terhune, and C. M. Savage, in *Proceedings of the Third International Congress on Quantum Electronics*, edited by P. Grivet and N. Bloembergen (Columbia University Press, New York, 1964), p. 1559.

[21] P. Debye, *Marx's Handbuch der Radiologei, VI* (Academische Verlagsgeselkchaft, Leipzig, Germany, 1925), Chap. V, p. 768; *Polar Molecules* (Dover Publications, Inc., New York, 1929).

[22] S. Kielich, Mol. Phys. **6**, 49 (1963); R. W. Hellwarth, Phys. Rev. **152**, 156 (1966).

compared with the Kerr effect in most liquids. (See Sec. III for more detail.)

Beam components propagating in the off-axis directions can also grow in intensity through stimulated Brillouin and Rayleigh scattering. This also leads to self-focusing phenomenon. Self-focusing by this mechanism has so far received little attention. In fact, the gain of stimulated Brillouin scattering near the forward direction is rather high even for a short Q-switched pulse. For self-focusing of the laser pulse in liquids with small Kerr constants, stimulated Brillouin scattering could be as important as the Kerr effect. In this paper, we show, from our measurements on the temperature variation of self-focusing action in different liquids, that this is indeed the case. The relative importance of the Kerr effect and stimulated Brillouin scattering to self-focusing can be obtained from these measurements since the Kerr effect is inversely proportional to temperature, but stimulated Brillouin gain increases as temperature increases.

While self-focusing in liquids seems to be qualitatively understood, the dynamics with which a beam, after being self-focused, breaks into self-trapped filaments (known as small-scale trapping[15]) is not yet understood,[6] although the size of the filaments seems to be connected to the Kerr constant of the medium.[16] As one would expect, both self-focusing and self-trapping affect dramatically the nonlinear optical processes in liquids, in particular, stimulated Raman scattering and backward stimulated Brillouin scattering. Self-focusing gives rise to the observed threshold in stimulated Raman and Brillouin scattering,[13] and the presence of intense filaments is responsible for the anomalously high Raman and Brillouin gain above threshold.[8–10] Without knowing the dynamics of filament formation, it is, however, difficult to calculate qualitatively the effect of self-focusing on the stimulated scattering. In this paper, we present some experimental results on first-order Stokes and Brillouin generation, and discuss qualitatively how their characteristics, the forward-backward asymmetry of the Stokes radiation, the temperature effect, etc., are dominated by self-focusing and self-trapping. Experimental results will be shown in Sec. II, followed by discussion in Sec. III.

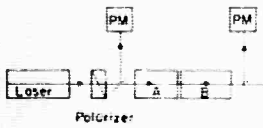

FIG. 1. Experimental set-up of the two-cell method for measuring self-focusing strength of a liquid.

II. EXPERIMENTS

A 3 in. ruby laser, Q-switched by cryptocyanine solution, was used in the experiments. The beam was limited to a diameter of 2 mm. The average peak power of the 15-nsec Q-switched pulses was about 75–100 MW/cm², depending on the cavity parameters. The self-focusing action of the beam in a liquid was investigated by the two-cell scheme.[8] (Figure 1.) Here the laser beam was passed through two cells in series. They were separated by a distance of 2 cm to allow for windows and a beam splitter when the back-scattered radiation was monitored. The first cell was filled with the liquid under investigation, and the second cell with liquid of low Raman threshold or strong self-focusing action, such as nitrobenzene or carbon disulfide. Self-focusing of the beam in the first cell was then easily detected by the decrease of Raman threshold for liquid in the second cell. To avoid complication, the length of the first cell was always kept below its own Raman threshold. This method has much higher sensitivity than the single-cell method in which the self-focusing action is measured by the observed Raman threshold for liquid in the same cell.[13] It is sensitive in the sense that relatively weak self-focusing action in liquids such as hexane and water can now be measured.[22] One can

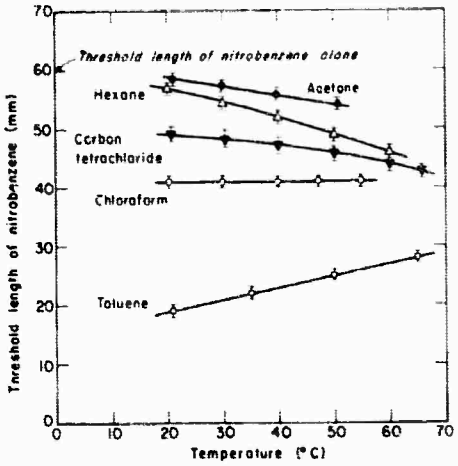

FIG. 2. Temperature variation of self-focusing in different liquids. A longer threshold length of nitrobenzene indicates weaker self-focusing action. See the text.

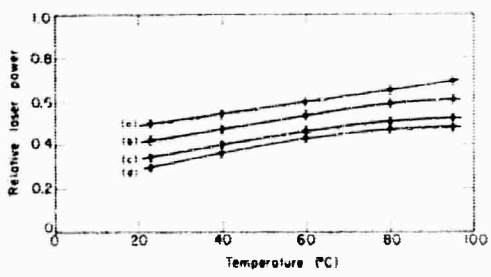

FIG. 3. Effect of a nitrobenzene self-focusing cell on the temperature variation of the Raman threshold of a 15-cm toluene cell. Length of the nitrobenzene cell: (a) 0, (b) 1.3, (c) 2.5, and (d) 5.0 cm.

[22] In liquid with weak self-focusing strength, stimulated Raman and Brillouin scattering may appear before the beam is self-focused to a minimum cross section. Consequently, Raman and Brillouin thresholds of the liquid are no longer a measure of the self-focusing strength. Hexane is a good example.

TABLE I. The relative self-focusing strengths in different liquids measured in terms of the cell length of the liquid which reduces the Raman threshold of 15-cm toluene by 5% when inserted in front of the toluene cell. For nonpolar liquids, n_{2a} are obtained from the dc Kerr constants in Ref. 30. For polar liquids, n_{2a} are either obtained from the experimental values of M. Paillette [Compt. Rend. 262, 264 (1966)] or from the calculated values of Y. R. Shen [Phys. Letters 20, 378 (1966)]. g_R is calculated from Eq. (10) with $k_{zz}=2/d$ and $d=0.1$ cm for a 100-MW/cm² ruby-laser beam. g_B is calculated from Eq. (16) with $k_{zz}=2/d$, $d=0.1$ cm, $\Delta\omega=\Gamma$, and $\delta=2\times10^{-9}$ sec for a 100-MW/cm² ruby-laser beam.

	Observed self-focusing strength (in.)	$10^{12}\,n_{2a}$	$10^{2}\,g_R$	$10^{3}\,g_B$	$10^{2}\,(g_R+g_B)$	(g_B/g_R) (%)
Carbon disulfide	$\frac{3}{8}$	11.3	6.8	7.4	7.54	10.9
Nitrobenzene	$\frac{7}{16}$	8.6	6.1	4.1	6.51	6.7
Bromobenzene	1	4.7	4.5	3.0	4.80	6.7
m-xylene	$1\frac{3}{8}$	3.0	3.7	4.8	4.18	13.0
Benzene	$1\frac{3}{4}$	2.3	3.2	5.0	3.70	15.6
Aniline	4	1.1	2.2	4.0	2.60	18.2
Chloroform	5	0.53	1.57	2.6	1.83	16.6
Carbon tetrachloride	$5\frac{1}{2}$	0.33	1.24	2.5	1.49	20.2
Hexane	$5\frac{7}{8}$	0.23	1.06	3.5	1.41	33.0
Acetone	6	0.23	1.07	2.7	1.34	25.2

easily determine the relative self-focusing strength of different liquids using this method. With the laser peak intensity at about 100 MW/cm², we measured the cell lengths of liquids required to reduce the Raman threshold of toluene in the second cell by 5%. The results, together with n_{2a} are given in Table I. Note that the self-focusing strengths of various liquids, except perhaps acetone and hexane, follow the same order as their optical Kerr constants.

The temperature dependence of self-focusing was investigated by varying the temperature of the first cell (15 cm in length). The second cell was filled with nitrobenzene in this case. The results for a few liquids are shown in Fig. 2. It is seen that the self-focusing action in toluene decreases with increase of temperature. This holds for all liquids with large Kerr constants. The temperature variation is similar to that of Raman and Brillouin threshold of liquid in a single cell.[8] This supports the idea that stimulated Raman and Brillouin scattering in these liquids are initiated by strong self-focusing of the beam into hot filaments. However, in acetone, hexane, and carbon tetrachloride, self-focusing gets stronger with increasing temperature, suggesting that besides the Kerr effect, some other mechanism now comes into play. As we shall show in the next section, the contribution of forward stimulated Brillouin scattering to self-focusing is indeed non-negligible in these liquids. The question also arises on whether self-focusing in the first cell would eliminate the temperature dependence of Raman threshold in the second cell. This was tested by using a 15-cm toluene cell with variable temperature proceded by a nitrobenzene focusing cell. As shown in Fig. 3, the temperature variation of Raman threshold in toluene changes only slightly with the focusing cell. The reason is that a major part of self-focusing of the beam actually happens not in the first cell but in the second cell. The filaments have not yet been formed in the first cell. The temperature variation in toluene did nearly vanish when the nitrobenzene cell was above its own threshold, but the results become less meaningful because of the possibility of depletion of laser power by stimulated Raman and backward Brillouin scattering in the nitrobenzene cell.

Wang[12] has shown that for a single cell, the inverse Raman threshold length varies linearly with the square root of the laser power.[3] We found the same result in CS_2 and nitrobenzene at relatively low power level, as shown in Fig. 4. As the laser power increases, the curves start to deviate from the straight line. This suggests that another mechanism for self-focusing may have set in at higher laser intensity.

We are also interested in the generation of stimulated Raman and backward Brillouin scattering in liquid with strong self-focusing properties. A toluene cell was used in the measurements. One of the interesting anomalies resulting from self-focusing and self-trapping is the forward-backward asymmetry in stimulated Raman process. Figure 5 shows the variation of the first-order Stokes power as a function of the cell length at three different laser powers. Note that the forward-backward asymmetry varies with the cell length, although the backward Stokes power is always higher just above

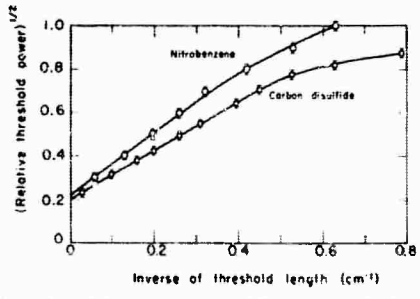

FIG. 4. Variation of the square root of Raman threshold power as a function of inverse of the cell length in CS_2 and nitrobenzene.

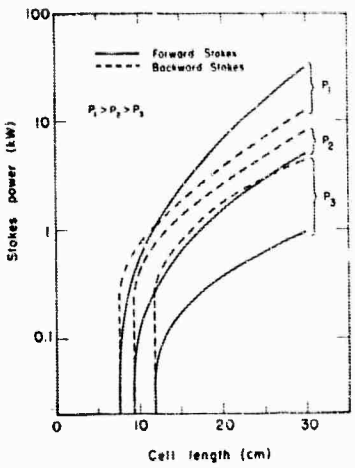

FIG. 5. First-order forward and backward Stokes power versus the cell length at three laser powers, $P_1 = 80$, $P_2 = 67$, and $P_3 = 53$ MW/cm².

threshold. The forward Stokes becomes more intense at long cell lengths. Care was taken to insure that the asymmetry was not induced by reflection from windows. In Fig. 6, the variarion of Stokes power, generated from a 20-cm toluene cell, as a function of laser power is given. The set of curves on the left corresponds to the case where a 2.5-cm nitrobenzene cell was inserted in front of the toluene cell. As expected, the curves look similar to those of Fig. 5. The variation of backward Brillouin power with laser power is also incorporated in Fig. 6.

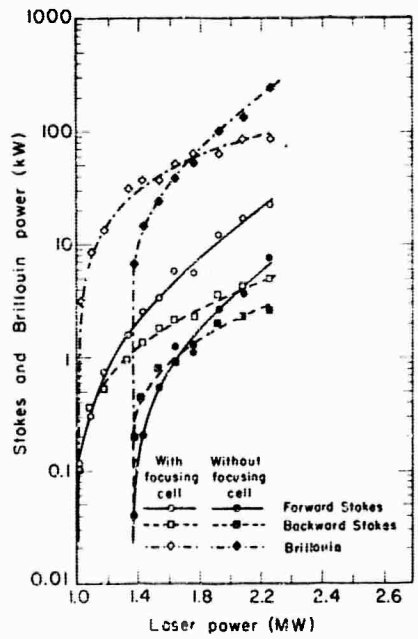

FIG. 6. Variation of Stokes and Brillouin power generated in a 20-cm toluene cell as a function of laser power, with and without a 2.5-cm nitrobenzene self-focusing cell.

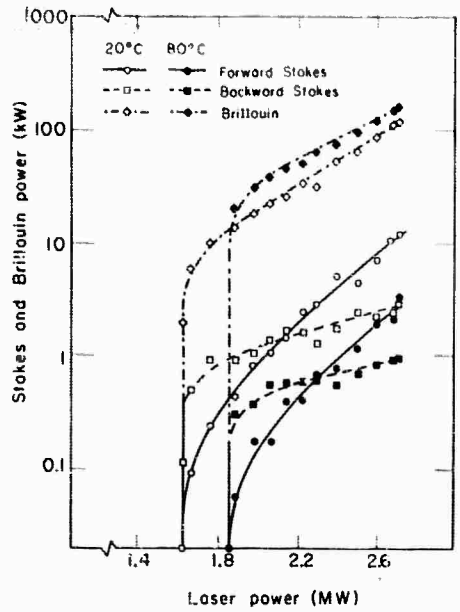

FIG. 7. Variation of Stokes and Brillouin power with laser power in 15-cm toluene at two different temperatures.

Figures 7 and 8 give the variation of Stokes and backward Brillouin power with the laser power in toluene and hexane, respectively, at two different temperatures. It is seen that at the higher temperature, the Raman and Brillouin threshold for toluene is higher, but as the laser power increases, the Brillouin radiation finally becomes more intense than the one at the lower temperature. In hexane, the Brillouin radiation has lower threshold and higher power at the higher temperature. No stimulated Raman radiation from hexane was observed.

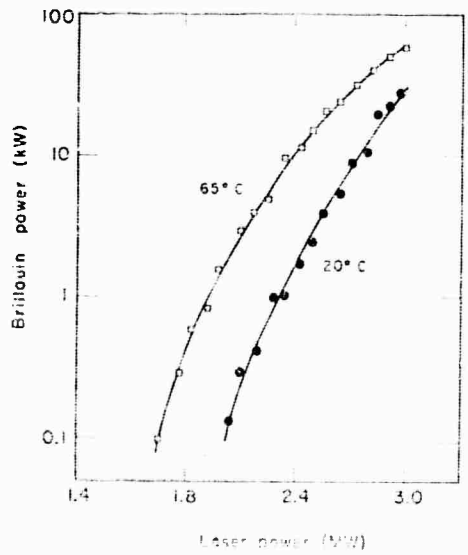

FIG. 8. Variation of Brillouin power with laser power in 15-cm hexane at two different temperatures.

The above measurements of intensities were made by using silicon photodiodes and a Tektronix 555 oscilloscope. The intensity values correspond to the peak values of the integrated pulses. The temporal structure of the generated Stokes and backward Brillouin radiation was investigated by using an FW-114 photodiode and a Tektronix 519 oscilloscope. Both the forward and the backward Stokes radiation from toluene were composed of short pulses of about 10^{-9} sec long, in partial agreement with observations of other workers.[18,24] The Brillouin radiation also contained short pulses, somewhat similar to what was observed by Maier *et al.*,[25] but they are not as sharp as the pulses in the Stokes radiation. Near threshold, both Stokes and Brillouin radiation consists of a single short pulse. Because of the short cells we used in our experiments, the depletion of total laser power in the Raman and Brillouin generation was not nearly as much as in the case of Maier *et al.*[25]

III. CALCULATION AND DISCUSSION

Generally speaking, self-focusing arises as a result of interaction of the light beam with the density variation and molecular reorientation and redistribution in the medium. The propagation of the light beam in liquid is described by the wave equation

$$\left(-\nabla^2+\frac{\epsilon}{c^2}\frac{\partial^2}{\partial t^2}\right)\mathbf{E}(\mathbf{r},t)=-\frac{4\pi}{c^2}\frac{\partial^2}{\partial t^2}\mathbf{P}^{\mathrm{NL}}(\mathbf{r},t). \quad (1)$$

In this case, the polarization of the medium can be written as

$$\mathbf{P}=\chi\cdot\mathbf{E}(\mathbf{r},t),$$

$$\chi=\sum_{m=1,2,\cdots}\rho^m\alpha_m, \quad (2)$$

where terms with $m>1$ arise because of correlation between molecules.[21] The nonlinear polarization P^{NL} appears as a result of change in ρ and α_m induced by the light fields.

$$\mathbf{P}^{\mathrm{NL}}(\mathbf{r},t)=\left[(\partial\chi/\partial\rho)\Delta\rho(\mathbf{r},t)+\sum_m(\partial\chi/\partial\alpha_m)\Delta\alpha_m(\mathbf{r},t)\right]\mathbf{E}(\mathbf{r},t). \quad (3)$$

The density variation $\Delta\rho$ obeys the acoustic wave equation

$$\left(-\nabla^2+\frac{1}{v^2}\frac{\partial^2}{\partial t^2}-\frac{2\Gamma}{v^2}\frac{\partial}{\partial t}\right)\Delta\rho(\mathbf{r},t)=-\frac{\gamma}{8\pi v^2}\nabla^2|E|^2(\mathbf{r},t). \quad (4)$$

Here, $v=(1/\rho\beta)^{1/2}$ is the acoustic velocity, β is the isothermal compressibility, Γ is the acoustic damping, γ is defined as $\gamma=\rho(\partial\epsilon/\partial\rho)$, and $|E|^2(\mathbf{r},t)$ is the slowly varying part of $E^2(\mathbf{r},t)$. The change $\Delta\alpha_1$, reflecting variation in the orientational distribution, is governed by the equation[21]

$$(\partial/\partial t+1/\tau)\Delta\alpha_1(\mathbf{r},t)=(A/\tau)|E|^2(\mathbf{r},t), \quad (5)$$

where A is a constant inversely proportional to temperature, and τ is the orientational relaxation time. Similar equations probably govern $\Delta\alpha_m$ which are changes induced by molecular redistribution. The relaxation time for molecular reorientation and redistribution is usually rather short ($\sim5\times10^{-11}$ sec).[26] If we limit ourselves to the low-frequency variation of $E^2(\mathbf{r},t)$,[27] then $\Delta\alpha_m(\mathbf{r},t)$ would respond almost instantaneously to $|E|^2(\mathbf{r},t)$. To the first order, we can write

$$\sum_m(\partial\chi/\partial\alpha_m)\Delta\alpha_m=(n/2\pi)n_{2\alpha}\tfrac{1}{2}|E|^2(\mathbf{r},t). \quad (6)$$

Self-focusing should therefore be described by the solution of Eqs. (1), (3), (4), and (6). If both $\Delta\rho$ and $|E|^2$ are Fourier-analyzed, then each Fourier component of $\Delta\rho$ consists of two parts. The part in phase with the driving component leads to change in the (real) refractive index: This is known as electrostriction. The part 90° out of phase with the driving component leads to stimulated Brillouin scattering. From Eq. (4), we find that the electrostrictive part is given approximately by

$$\Delta\rho_e(\mathbf{r},t)=\int d^3r'\left(\frac{-\gamma}{8\pi v^2}\right)\nabla^2|E|^2\left(\mathbf{r}',t-\frac{|\mathbf{r}-\mathbf{r}'|}{v}\right)\Big/4\pi|\mathbf{r}-\mathbf{r}'|. \quad (7)$$

It can easily be shown that for a Gaussian beam of radius r_0 and pulse duration δ, the first-order solution of Eq. (7) with $v\delta\ll r_0$ yields at the peak of the laser pulse,

$$(\partial\chi/\partial\rho)\Delta\rho\approx(n\tau^2\delta^2/4\pi r_0^2)n_{2\rho}|E|^2, \quad (8)$$

where

$$n_{2\rho}=\gamma^2\beta/8\pi n.$$

This is because the spatial density variation cannot follow the rapid change in the laser intensity, so that the $-\nabla^2$ term is small compared with the $\partial^2/\partial t^2$ term in Eq. (4). For liquids under investigation, $n_{2\rho}$ is about 1 to 10 times $n_{2\alpha}$. With $v\approx10^5$ cm/sec, $\delta\approx10^{-8}$ sec, and $r_0\approx0.1$ cm, one sees immediately from Eqs. (6) and (8) that the electrostrictive effect is negligible compared with the Kerr effect, and hence is not responsible for the temperature variation of self-focusing in liquids.

Even if the electrostrictive effect is neglected, it is still difficult to find an analytical solution from the

[21] M. Maier, W. Kaiser, and J. A. Giordmaine, Phys. Rev. Letters 17, 1275 (1966).
[25] M. Maier, W. Rother, and W. Kaiser, Appl. Phys. Letters 10, 80 (1967).
[26] C. W. Cho, N. D. Foltz, D. H. Rank, and T. A. Wiggins, Phys. Rev. Letters 18, 107 (1967).
[27] Stimulated Rayleigh scattering with a large frequency shift may be less important for self-focusing, since it is essentially initiated at the noise level.

above equations to describe self-focusing. However, as we mentioned earlier, self-focusing can be described by the amplification of Fourier components propagating in the off-axis direction.

Let us assume a plane wave

$$\mathbf{E}_0=\tfrac{1}{2}\mathcal{E}_0\exp[i\mathbf{k}_0\cdot\mathbf{r}-i\omega_0 t] \tag{9}$$

as the pump field propagating in the medium along the z direction. We are interested in the amplification of a weak wave E_s with wave vector $\mathbf{k}_s$ and frequency ω_s. Bespalov and Talanov[4] and Chiao *et al.*[28] show that the change of refractive index (essentially due to Kerr effect) actually induces an exponential gain for the amplification of E_s.

$$g_R=k_{sz}[-(k_{sz}/k_0)^2+2(n_2/n_0)\mathcal{E}_0^2]^{1/2}, \tag{10}$$

assuming $(\omega_0-\omega_s)\ll 1/\tau$. It turns out that the e-folding length for the growth of E_s with $k_{sz}=2/d$ is just the self-focusing distance z_{foc} of a beam with a diameter d, if $(k_{sz}/k_0)^2\ll 2(n_2/n_0)\mathcal{E}_0^2$.[28]

$$z_{foc}=d/2[2(n_2/n_0)\mathcal{E}_0^2]^{-1/2}. \tag{11}$$

The optimum gain is

$$(g_R)_{opt}=k_0(n_2/n_0)\mathcal{E}_0^2 \tag{12}$$

which occurs at $(k_{sz})_{opt}=k_0[(n_2/n_0)\mathcal{E}_0^2]^{1/2}$. As $\mathcal{E}_0^2$ increases, $(g_R)_{opt}$ would finally become much larger than the gain at $k_{sz}=2/d$. Then, one may find that in a distance less than z_{foc}, the wave E_s with $(k_{sz})_{opt}$ becomes stronger than E_s with $k_{sz}=2/d$, although initially the former is much weaker than the latter. The actual self-focusing distance would then become smaller than z_{foc},[4] and would depend on $\mathcal{E}_0^{-2n}$ with $\frac{1}{2}<n<1$. This is likely to happen in liquids with large Kerr constants. As an example, we have $n_2=1.13\times10^{-11}$ for CS_2. For a 100-MW/cm^2 beam with $d=0.1$ cm, and $\mathcal{E}_0^2=8\times10^5$ esu, we find $(g_R)_{opt}=0.92$ and $(g_R)_{k_{sz}=2/d}=0.067$. This probably explains why in Fig. 4 the inverse of the self-focusing distance depends on the laser intensity as $P^n\propto\mathcal{E}_0^{2n}$ with $n>\frac{1}{2}$ at high intensity. For liquids with small Kerr constants, $(g_R)_{opt}$ is not very different from $(g_R)_{k_{sz}=2/d}$ even at an intensity of 100 MW/cm^2.

The weak wave E_s can also be amplified through forward stimulated Brillouin scattering, governed by the coupled equations

$$(-\nabla^2-\omega_s^2\epsilon_s/c^2)E_s=(4\pi\omega_s^2/c^2)(\gamma/4\pi\rho)E_0\Delta\rho^*,$$
$$(-\nabla^2-\omega_{ac}^2/v^2-i2\omega_{ac}\Gamma/v^2)\Delta\rho^*=-(\gamma/8\pi v^2)\nabla^2(E_0^*E_s), \tag{13}$$

with $\omega_s+\omega_{ac}=\omega_0$. For scattering in the near-forward direction, $\mathbf{k}_s+\mathbf{k}_{ac}=\mathbf{k}_0$, the Brillouin power gain is[29]

$$g_B=(k_s\Gamma/vk_{ac})+[(k_s\Gamma/vk_{ac})^2+(\omega_s^2\gamma^2\beta\mathcal{E}_0^2/32\pi c^2)]^{1/2}. \tag{14}$$

Ordinary liquids have $\gamma\sim1$ and $\beta\sim10^{-10}$. Therefore, at the same laser intensity, g_B would be much greater than g_R, if the laser beam were continuous.

In practice, however, the Q-switched laser generates a short pulse of pulse width δ. The amplification of E_s due to Kerr effect is still given by Eq. (10) with $\mathcal{E}_0^2$ replaced by $\mathcal{E}_0^2(t)$, since the response of Kerr effect to $\mathcal{E}_0^2(t)$ is almost instantaneous. The Brillouin gain, on the other hand, is greatly reduced. To estimate the reduction, let us assume that $\mathbf{E}_0$ and $\mathbf{E}_s$ are infinite plane waves which can be represented by

$$\mathbf{E}_0=\mathbf{A}_0\Delta\omega\sum_{m=-N/2}^{N/2}\exp[i(\omega_0+m\Delta\omega)(n_0\hat{k}_0\cdot\mathbf{r}/c-t)], \tag{15}$$

$$\mathbf{E}_s=\sum_{m=-N/2}^{N/2}A_{sm}(z)\Delta\omega\exp[i(\omega_s+m\Delta\omega)(n_s\hat{k}_s\cdot\mathbf{r}/c-t)],$$

where $N\Delta\omega=1/\delta$ and $A_0\Delta\omega=(\mathcal{E}_0)_{max}/N$. Then, the driving term for $\Delta\rho$ in Eq. (13) with wave vector $\mathbf{k}_{ac}=(\omega_0n_0k_0-\omega_sn_s\hat{k}_s)/c$ and frequency $\omega_{ac}=\omega_0-\omega_s$ is

$$+(\gamma^2/8\pi v^2)k_{ac}^2\sum_{m=-N/2}^{N/2}A_0A_{sm}(\Delta\omega)^2\exp[i\mathbf{k}_{ac}\cdot\mathbf{r}-i\omega_{ac}t]$$

for sufficiently large $\Delta\omega$. The coupling of $\Delta\rho$ with the N frequency modes A_{sm} of E_s leads to $(N+1)$ coupled equations, whose solution is of the form

$$A_{sm}(z)=\sum_i C_i\exp(g_iz),$$

where g_i are the eigenvalues. The maximum g_i gives the reduced Brillouin gain, which can be shown to be

$$g_B=-(k_s\Gamma/vk_{ac})+[(k_s\Gamma/vk_{ac})^2+(\omega_s^2\gamma^2\beta\delta\Delta\omega/32\pi c^2)\mathcal{E}_{0max}^2]^{1/2} \tag{16}$$
$$\simeq(\omega_s^2\gamma^2\beta vk_{ac}\delta\Delta\omega/64\pi c^2k_s\Gamma)\mathcal{E}_{0max}^2.$$

This gain would remain roughly unchanged for a beam of finite cross-section ($d\gg\lambda$). Obviously, for $g_B\lesssim\Gamma/v$, we should take $\Delta\omega\sim\Gamma$. Then, with a 100-MW/cm^2 laser beam of $d=0.1$ cm and $\delta=2\times10^{-8}$ sec, the Brillouin gain at $k_{sz}=2/d$ in CS_2($\gamma=2.2$, $\beta=0.92\times10^{-10}$) is $g_B\sim4.6\times10^{-3}$. This gain is small compared with the gain g_R due to Kerr effect in CS_2, but in media with small Kerr constants, it can be important. We believe that this forward-stimulated Brillouin scattering is responsible for the temperature dependence of self-focusing in chloroform, CCl_4, hexane, and acetone as shown in Fig. 2.

[28] R. Y. Chiao, P. L. Kelley, and E. Garmire, Phys. Rev. Letters 17, 1158 (1966).

[29] Y. R. Shen and N. Bloembergen, Phys. Rev. 137, A1787 (1965). Here, the solution is actually valid only for scattering at a sufficiently large angle such that $k_{ac}/k_0\gg g_B/\bar{\kappa}_{ac}$.

Since the total gain for E_s is $g \approx g_R + g_B$, the temperature dependence of g at $k_{sz} = 2/d$ is

$$dg/dT \simeq -g_R/2T + g_B d\beta/\beta dT, \qquad (17)$$

assuming that the temperature dependence of quantities other than n_{2a} and β in g can be neglected. Figure 2 shows $dg/dT = 0$ for chloroform at about 100 MW/cm^2. With $g_R = 1.57 \times 10^{-2}$ and $d\beta/\beta dT = 0.01$ [30] for chloroform at $T = 300°$K, we should have $g_B = 2.62 \times 10^{-3}$. Equation (16) with $\gamma = 1.27$, and $\beta = 10^{-10}$ for chloroform gives $g_B = 1.7 \times 10^{-3}$. In Table I, we calculated g_R and g_B at $k_{sz} = 2/d$ for various liquids, using the experimental g_B for chloroform as reference and assuming the same dependence of g_B on γ, β and n (Ref. 30) as in Eq. (16). Then, with Eq. (17), one can easily show that for CCl_4, hexane, and acetone, $dg/dT > 0$, and for other liquids in the table besides chloroform, $dg/dT < 0$ in agreement with our observation.

Experiments on stimulated Raman scattering in liquids show many anomalous effects,[31] such as the anomalous gain,[32] spectral broadening,[9] class-II anti-Stokes radiation,[33] etc. Most of the anomalous effects can now be explained by self-focusing and self-trapping. Nevertheless, the anomalous forward-backward asymmetry in the Stokes radiation has not yet received a satisfactory explanation, although it is believed that this must also be a consequence of self-focusing and self-trapping.

In the self-trapped region essentially all the Stokes radiation is generated in the self-trapped filaments. Assume that individual filaments are isolated from the surrounding, and the Stokes generation in each filament can be described by the steady-state equations[34]:

$$\begin{aligned} \partial N_{sF}/\partial z &= \sigma N_l (N_{sF}+1), \\ \partial N_{sB}/\partial z &= -\sigma N_l (N_{sB}+1), \\ \partial N_l/\partial z &= -\sigma (N_l N_{sF} + N_l N_{sB}), \end{aligned} \qquad (18)$$

with $N_{sF}(0) = N_{sB}(L) = 0$, where $N_l(z)$, $N_{sF}(z)$, and $N_{sB}(z)$ are the average photon numbers per unit length for laser, forward, and backward Stokes fields, respectively, and σ is the scattering coefficient. Then, the solution of Eq. (18) is

$$\begin{aligned} N_{sF}(L) &= N_{sB}(0) \\ &= \exp\left[\int_0^L \sigma N_l(z)\,dz\right] - 1 \end{aligned} \qquad (19)$$

which shows that the forward-backward symmetry in the Stokes generation would persist.

The observed forward-backward asymmetry suggests that the filaments are not isolated. The Stokes radiation generated elsewhere in the medium is expected to self-focus together with the laser beam into the self-trapped filaments. Generally, this would increase the rate of forward Stokes generation in the filaments. In fact, the Stokes generation in the filaments is perhaps a transient rather than a steady-state phenomenon. As we mentioned earlier, the Stokes radiation appears as a series of sharp pulses. It was suggested that each filament lasts not much longer than 10^{-10} sec.[18] The Stokes generation in a filament is therefore described by

$$\begin{aligned} (\partial/\partial z + n_s \partial/c\partial t) N_l &= -\sigma N_l (N_{sF} + N_{sB}), \\ (\partial/\partial z + n_s \partial/c\partial t) N_{sF} &= \sigma N_l (N_{sF} + 1), \\ (\partial/\partial z - n_s \partial/c\partial t) N_{sB} &= -\sigma N_l (N_{sB} + 1), \end{aligned} \qquad (20)$$

neglecting other nonlinear processes in the filament. The solution of Eq. (20) is difficult, but it can be shown that when the laser peak power is highly depleted in the Stokes generation, and $N_{sF}(z=0)$ is not too much larger than $N_{sB}(z=L)$, where L is the length of the filament, the peak intensity of N_{sB} can be many times higher than that of N_{sF}.[24] This would then enhance the backward Stokes radiation. Of course, the reverse will be true if $N_{sF}(z=0)$ is sufficiently larger than $N_{sB}(z=L)$. Because of our lack of knowledge on how the self-trapped filaments are formed, and because of other nonlinear processes in the filaments, it is quite impossible to describe the analytical details of stimulated Raman scattering in liquids. However, on the basis of what we have just discussed, we can explain qualitatively the observed forward-backward Stokes asymmetry (Fig. 5). After the laser traverses a distance z_f (the self-focusing length) in the liquid, filaments start to show up. The average number of filaments $W(z)$ increases with distance z rapidly, say

$$W(z) = \exp[f(z - z_f)]$$

and the laser input into individual filaments is nearly a constant depending only on the properties of the liquid. Because of self-focusing of Stokes radiation, we would expect that $N_{sF}(z=z_0) > N_{sB}(z=z_0+L)$ for a filament initiated at z_0, and that $N_{sF}(z=z_0)$ increases with z_0 and the laser intensity in the nontrapped region. Thus, when the cell length is increased above z_f, both forward and backward Stokes radiation begin to be generated in the filaments with extremely high gain before saturation in the Stokes generation sets in. This appears as a sharp threshold for the stimulated scattering. After saturation sets in, the backward Stokes radiation would become more intense than the forward as a result of transients, if $N_{sF}(z=z_0)$ is not too much

[30] *International Critical Tables, National Research Council*, (McGraw-Hill Book Co., New York, 1930). *Handbook of Chemistry*, edited by N. A. Lange (Handbook Publishers, Inc., Sandusky, Ohio, 1956).
[31] See, for example, B. P. Stoicheff, Phys. Letters **7**, 186 (1963).
[32] F. J. McClung, W. G. Wagner, and D. Weiner, Phys. Rev. Letters **15**, 96 (1965).
[33] E. Garmire, Phys. Letters **17**, 251 (1965).
[34] R. W. Hellwarth, Phys. Rev. **130**, 1850 (1963).

larger than $N_{sB}(z=z_0+L)$. As the cell length is increased further, more filaments show up, and the increase of $N_{sF}(z=z_0)$ with z_0 enhances the forward Stokes generation in these filaments. The Stokes intensity in the forward direction now grows faster than in the backward direction. Eventually, for a sufficiently long cell, the forward Stokes radiation will become more intense than the backward Stokes, although the reverse is true near the threshold. This explains the crossover of the forward and the backward Stokes curves in Fig. 5.[35] Since $N_{sF}(z=z_0)$ also increases with the intensity of the laser beam, the crossover would appear closer to the threshold length for higher laser intensity as we have observed. A similar argument explains the qualitative behavior of the Stokes curves in Figs. 6 and 7, if we remember that the self-focusing distance z_f in toluene is nearly proportional to the square root of laser intensity.[3] In Fig. 6, the nitrobenzene focusing cell helps the self-focusing action in toluene, enhances slightly the forward Stokes intensity with respect to the backward Stokes, and hence brings the crossover point closer to threshold. Since most of the Stokes amplification comes from the self-trapped region,[36] the slight change in the threshold would not affect greatly the Stokes generation above threshold. The two sets of Stokes curves, with and without the focusing cell, look very much alike except that one is shifted from the other. The Stokes curves in Fig. 7, however, seem to indicate the fact that the Stokes amplification is greater at lower temperature because of a smaller Raman linewidth.

The sharp rise of the Brillouin curves near Raman threshold in Figs. 6 and 7 show that the stimulated Brillouin scattering in toluene is also initiated by the appearance of self-trapped filaments. Nevertheless, since the lifetime of the filaments is short, the Brillouin generation in these filaments is greatly reduced. Thus, relatively, the Brillouin amplification in the nontrapped region is much more important than in the Stokes case. It has a steady state gain of 0.7 cm^{-1} for a 100 MW/cm^2 laser beam.[37] This large gain is presumably responsible for the higher Brillouin intensity than the Stokes. The Brillouin amplification in the nontrapped region could explain the cross over of the two Brillouin curves in Fig. 6 with and without a focusing cell. At sufficiently high laser intensity, the Brillouin amplification in the nontrapped region would dominate over the Brillouin generation in the filaments. Since the Brillouin amplification depends positively on the isothermal compressibility β, which increases sharply with temperature, the Brillouin intensity is expected to be higher at higher temperature, just as shown in Fig. 7, although the threshold in toluene at higher temperature is higher. In hexane, there is no evidence of the presence of filaments. The Brillouin curves in Fig. 8 also give no indication of sharp threshold. It is believed that in hexane the effect of self-focusing and self-trapping on stimulated Brillouin scattering should be negligible. Then, since the Brillouin amplification increases with temperature, the Brillouin radiation should have higher intensity and hence a lower apparent threshold at higher temperature, as shown in Fig. 8.

IV. CONCLUSION

In most organic liquids, the optical Kerr effect is the dominant mechanism for self-focusing. However, the Kerr effect fails to explain the fact that the self-focusing strength increases with temperature in liquids such as CCl_4, hexane and acetone. For a Q-switched laser pulse, the electrostrictive contribution to self-focusing is often negligible. It is concluded that forward stimulated Brillouin scattering should be responsible for the temperature effect in these liquids. Self-focusing and self-trapping affect drastically the stimulated Raman and Brillouin scattering in liquids. The increase of number of self-trapped filaments with cell length and laser intensity, together with self-focusing and transient effects, explains qualitatively the observed forward-backward asymmetry in the Stokes generation. Other qualitative features in the stimulated Raman and Brillouin scattering can also be explained.

[35] The qualitative features of Fig. 5 can be obtained if we assume that the Stokes radiation generated in each filament is approximated by

$$\left.\begin{aligned} N_{sF}(z_0+L) &= N_{sF}(z_0)\exp(gL) \\ N_{sB}(z_0) &= N_{sB}(z_0+L)\exp(g'L) \end{aligned}\right\}, \qquad 0\le L\le L_{sat}$$

$$N_{sF}(z_0+L) = N_{sF}(z_0)N_{i0}/[N_{sF}(z_0)+fN_{sB}(z_0+L)],$$

$$N_{sB}(z_0) = C,$$

$$L_{sat} = (1/g)\ \ln[N_{i0}/[N_{sF}(z_0)+fN_{sB}(z_0+L)]],$$

$$g' = (1/L_{sat})\ \ln[C/N_{sB}(z_0+L)],$$

and $N_{sF}(z_0)$, $N_{sB}(z_0+L)$, g, f, and C are numerical constants properly chosen.

[36] The Stokes gain in the nontrapped region is only about 0.25 cm^{-1} even for a 100 MW/cm^2 laser beam. See Ref. 29.

[37] See Ref. 29. The acoustic damping used to calculate the gain is taken from R. Y. Chiao and P. A. Fleury, in *Proceedings of Conference on Physics of Quantum Electronics, Puerto Rico, 1965*, edited by P. L. Kelley, *et al.* (McGraw-Hill Book Co., New York, 1966), p. 241.

APPENDIX IV

MEASUREMENTS OF SUBNANOSECOND "FILAMENT" PULSES USING THE CONVOLUTION TECHNIQUE*

Michael M. T. Loy and Y. R. Shen†

Department of Physics

University of California

Berkeley, California

ABSTRACT

The well-known convolution technique was used to measure subnanosecond pulses generated from "filaments" in a self-focused beam. The results showed that in toluene, the pulse width varied from 200 to 100 psec or less, and the peak power was about 30 kwatts.

* Research supported by the U. S. Office of Naval Research under contract No. Nonr-3656(32).

† A. P. Sloan Research Fellow

Self-focusing of an intense light beam[1,2] in a nonlinear medium has recently attracted much attention. In some liquids, direct time-integrated photographs show that a self-focused beam would break into small-scale "filaments" of few microns in diameter.[3,4] Brewer et al[5] found that a "filament" in CS_2 has a lifetime less than 10^{-10} sec. and a peak intensity larger than 10 KW. For theoretical interpretation, more accurate information about the duration and the intensity of a "filament" is of prime importance. However, most of the common techniques for subnanosecond pulse measurements are not easily applicable to the measurements of filament pulses. The combination of a fast diode and a Tektronix 519 oscilloscope has a limited time constant of 300 psec or more.[5] The two-photon fluorescence technique[6] requires an intense beam of fairly large cross-section. The second-harmonic correlation technique[7] needs, in addition, a large number of roughly identical pulses. In this letter, we would like to introduce the well-known convolution technique for subnanosecond pulse measurements. We also present results of the first accurate measurements on the duration of filament pulses.

If the response of a linear system to a δ-function is $g(t)$, then the response to an arbitrary function $s(t)$ is given by the convolution integral

$$R(t) = \int_{-\infty}^{t} g(\tau)\, s(t-\tau)\, d\tau \qquad (1).$$

Knowing $R(t)$ and $g(t)$ one can, in principle, determine $s(t)$ from the integral. This convolution technique is similar to that used in spectroscopy to recover the true spectral lineshape from the observed spectrum. In our case, the linear system consisted of an ITT F4018

photodiode in connection with a Tektronix 519 oscilloscope. A suitable amount of load resistance and capacitance was inserted in the photodiode housing to make the system weakly underdamped. The overall system has a time constant of about 400 psec. To approximate the δ-function, we used the mode-locked pulses from a Nd-glass laser. Two-photon fluorescence measurements on these pulses yielded a value of 8 ± 3 psec. for the pulse width. The response function $g(t)$, obtained directly from the oscilloscope trace of the system response to such a mode-locked pulse, is shown in Fig. 1a.

All oscilloscope traces were taken at a sweep rate of 2 nsec/div, (5 mm/div. on the polaroid pictures). The linearity of the sweep rate was calibrated to within 1.5%. The oscilloscope traces were measured by a cross-feed manipulator,[8] with an accuracy of 1 μ in both coordinates. However, the major source of error in the measurements still came from reading the traces from the pictures. The uncertainty was typically ±0.05 to ±0.15 mm for different parts of the trace depending on its slope. Computer calculation of Eq. (1) was then performed to match the observed response function $R(t)$ by using $g(t)$ of Fig. 1a and by adjusting the width and the shape of $s(t)$ using a Voigt function.[9]

We applied this technique to the measurements of "filament" pulses. A beam of 0.75-mm diameter from a single-mode Q-switched ruby laser was sent through a 33-cm toluene cell. For laser power above the self-focusing threshold, photographs of the beam cross-section at the end of the cell showed an intense bright spot of 10 ± 2 μ in diameter. Diffracted light from the spot was detected by the fast photodiode. Figure 1b shows an oscilloscope trace of a typical "filament" pulse obtained at laser power close to the self-focusing threshold. We found, from computer calculation

of Eq. (1), that the corresponding true pulse s(t) has a full width at half maxima of 190 ± 30 psec, with an asymmetric pulse shape fairly well determined as shown in the insert of Fig. 1b. At higher input power, the oscilloscope trace of a typical "filament" pulse is shown in Fig. 1c. We found in this case that s(t) has a full width of 100 ± 60 psec. Here, the inaccuracy arose mainly because of uncertainty in the pulse shape of s(t). The same difficulty exists in two-photon fluorescence and second-harmonic correlation techniques.[7] The insert in Fig. 1c shows that s(t) assumes very different widths depending on whether it is Gaussian or Lorentzian. If the shape of s(t) were known, the accuracy in determining the pulse width would be as good as ± 15 psec. The observed "filament" pulse width would appear to decrease with increasing input power if we assumed that the pulse shape remained roughly unchanged. The peak powers of all "filament" pulses, estimated from the energy content in the pulses, were about 30 KW within a factor of 2. Measurements on "filaments" in CS_2 yielded essentially the same results with peak power at around 8 KW.

As an independent check on duration and intensity of the "filaments" we used the method suggested by Mayer.[10] Let $I_{2\omega}(\underline{r},t)$ be the intensity of second harmonics generated from a thin KDP crystal by a nearly parallel beam of intensity $I_{\omega}(\underline{r},t)$. Then, the energy in the fundamental and the second-harmonic pulses are given respectively by

$$\begin{aligned} P_{\omega} &= \int I_{\omega}(\underline{r},t)\,dA\,dt \\ P_{2\omega} &= \int I_{2\omega}(\underline{r},t)\,dA\,dt = C\int I_{\omega}^{2}(\underline{r},t)\,dA\,dt \end{aligned} \qquad (2)$$

where the constant coefficient C is obtained from the known effeciency of the second-harmonic generation process. Simultaneous measurements of

P_ω and $P_{2\omega}$ would determine both the pulse width and the peak intensity if the functional form of $I_\omega(\underset{\sim}{r},t)$ is known. In our experiments, the constant C was determined by measuring the second-harmonic generation from a KDP crystal using the input laser beam. Applications of the above method to the "filament" pulses generally yielded for the pulse width a value which is within a factor of two compared with that obtained from the convolution technique. This method is inherently much less accurate than the convolution technique.

This convolution technique can, of course, be applied to measurements of other subnanosecond pulses, such as stimulated Raman pulses. From the experience in our computer calculation, we noticed that rough measurements over a few key points (including the two maxima, the minimum etc.) are usually sufficient to determine the pulse shape and width with an accuracy somewhat less than what we stated earlier. This technique is especially sensitive to the variation in the pulse wing. For instance, we found that it was very useful to have this technique supplement the two-photon fluorescence technique to assure that the mode-locked pulses were "clean" without appreciable ripples at the wings.

ACKNOWLEDGMENT

We would like to thank S. McCall for suggesting to us the convolution technique, and J. Shelton for technical help.

REFERENCES

1. R. Y. Chiao, E. Garmire, and C. H. Townes, Phys. Rev. Letters 13, 479 (1964).
2. P. L. Kelley, Phys. Rev. Letters 15, 1005 (1965).
3. R. Y. Chiao, M. A. Johnson, S. Krinsky, H. A. Smith, C. H. Townes, and E. Garmire, IEEE J. Quan. Electron. 2, 467 (1966).
4. R. G. Brewer and J. R. Lifsitz, Phys. Letters 23, 79 (1966).
5. R. G. Brewer, J. R. Lifsitz, E. Garmire, R. Y. Chiao, and C. H. Townes, Phys. Rev. 166, 326 (1968).
6. J. A. Giordmaine, P. M. Rentzepis, S. L. Shaprio, and K. W. Wecht, Appl. Phys. Letters 11, 216 (1967).
7. J. A. Armstrong, Appl. Phys. Letters 10, 16 (1967).
8. M. Maier, W. Kaiser, and J. A. Giordmaine, Phys. Rev. Letters 17, 1275 (1966).
9. For a description of the cross-feed manipulator and the measuring technique, see, for example, Tektronix 519 Oscilloscope Manual.
10. H. C. van de Hulst and F. F. M. Reesinck, Astrophysical Journal 106, 121 (1947).
11. G. Hauchecorne and G. Mayer, Compt. Rendus 261, 4014 (1965).

FIGURE CAPTION

Fig. 1. Oscilloscope traces of the system response to various light pulses. The system was composed of an ITT F4018 photodiode in connection with a Tektronix 519 oscilloscope.

a) A mode-locked pulse of 8 ± 3 psec in pulse width from a Nd-glass laser.

b) A "filament" pulse with a pulse width of 190 ± 30 psec and an asymmetric pulse shape as shown in the insert.

c) A "filament" pulse with a pulse width of 100 ± 60 psec. The inaccuracy is due to uncertainty in the pulse shape. The insert shows that the pulse width could be very difficult depending on whether the pulse is Gaussian or Lorentzian.

The circles indicate results of computer calculation of Eq. (1), taking the mode-locked pulse as an δ-function.

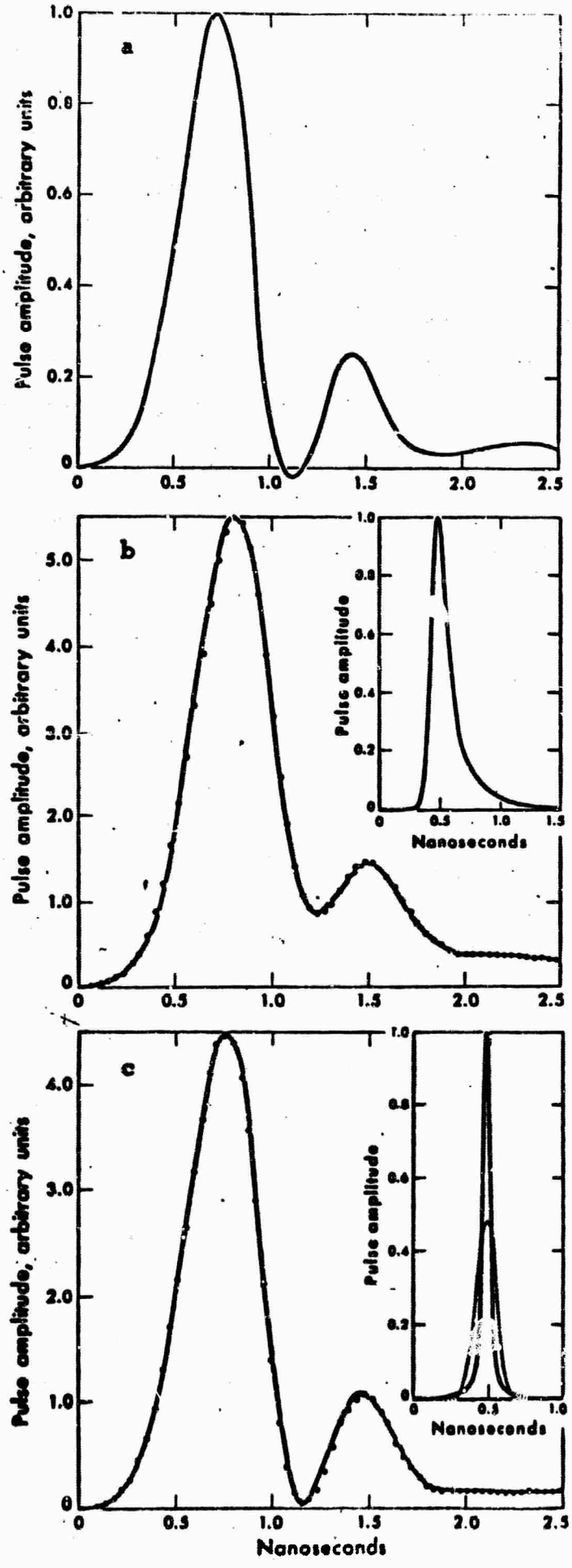
a
b
c
Pulse amplitude, arbitrary units
Nanoseconds
Pulse amplitude
0
0.5
1.0
1.5
2.0
2.5
3.0
4.0
5.0
0.2
0.4
0.6
0.8

APPENDIX V

VOLUME 22, NUMBER 19 PHYSICAL REVIEW LETTERS 12 MAY 1969

SMALL-SCALE FILAMENTS IN LIQUIDS AND TRACKS OF MOVING FOCI*

Michael M. T. Loy and Y. R. Shen†
Physics Department, University of California, Berkeley, California 94720
(Received 13 March 1969)

Experimental results show that the small-scale filaments in liquid, obtained with a single-mode laser, are composed of continuous series of focal spots. Many related observations are shown to be consistent with the picture of moving foci.

Experimental observation on self-focusing of laser light in liquids has shown that the self-focused beam would eventually break into intense filaments a few microns in diameter.[1,2] The existence of these filaments has recently attracted much attention. They have been attributed to self-trapping predicted by Chiao, Garmire, and Townes.[3] Recent experiments[4] on spectral broadening in filaments, obtained by using an inhomogeneous, multimode laser, seem to support this assertion. Lugovoi and Prokhorov[5] however suggest that in some situations filaments are simply tracks of moving foci, in accordance with time variation of the input laser intensity. In this paper, we would like to present some experimental evidence that filaments obtained with a single-mode laser are actually composed of a continuous time series of focal spots. We also show that many effects inherently related to self-focusing are consistent with the picture predicted by Lugovoi and Prokhorov.

A single-mode ruby laser, Q switched by cryptocyanine, was used in the experiments. The beam was passed through a 0.75-mm pinhole before propagating into the liquid cell in order to assure maximum spatial homogeneity. A typical oscilloscope trace of input pulses is shown in Fig. 1(a) together with the Fabry-Perot pattern in Fig. 1(b). "Filaments" or moving focal spots were observed by focusing a camera at the end of the cell. In most cases only one "filament" appeared [Fig. 1(c)]; occasionally, there were two, when the input laser power was exceptionally high. This is in clear contrast to the results obtained with a multimode laser, where tens or even hundreds of filaments are frequently observed on each picture.[4] As the laser power was increased from below to above the self-focusing threshold, the photograph first showed a bright spot of about 50 μ in diameter, which gradually became more intense and shrank to a more or less limiting "filament" size (10 ± 2 μ in diameter in toluene and 5 ± 1 μ in CS_2). The pulse emitted from the filament was detected by an ITT F4018 photodiode in combination with a Tektronix Model No. 519 oscilloscope. A 1-mm disk was inserted somewhere in front of the photodiode to block off the background of non-self-focused laser light.[1] The pulse duration was then measured by the convolution technique.[6] The results on toluene showed that with increasing input laser power, as the bright spot shrank from 50 μ to the limiting 10-μ "filament" size, the pulse duration changed from 1 nsec to 200 psec, and then as the "filament" size remained unchanged, the pulse duration continued to shorten to less than 100 psec. While the pulse became shorter, the energy content in the pulse decreased accordingly, but the peak intensity in the limiting "filament" remained roughly constant at 30 GW/cm^2. Spectral analysis with spectograph and Fabry-Perot on the "filament" pulses yielded a linewidth of less than 1 cm^{-1}.

These results are consistent with the picture of "filaments" formed by moving foci. On the other hand, it would be rather difficult to ex-

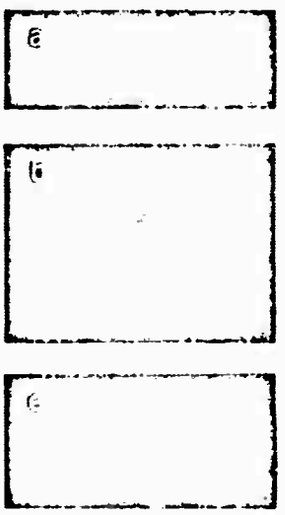

FIG. 1. (a) A typical oscilloscope trace (5 nsec/div) of an input laser pulse. (b) A Fabry-Perot pattern (1.25-cm spacing between plates) of an input laser pulse. (c) A typical "filament" in toluene. The picture was taken by focusing the camera at the end of the cell with a 125× magnification.

plain how a self-trapped filament of such high intensity could last for more than a few millimeters without showing appreciable spectral broadening.[7] A way to help distinguish the two cases is to focus the camera inside rather than at the end of the liquid cell. If the "filament" were indeed a self-trapped filament which terminates at the end of the cell, we would expect to see a blurred defocused image of the filament; otherwise, as the laser power is increased above the self-focusing threshold, we should always see a clear image of the focal spot extended gradually further inside the cell. In our experiments, we took simultaneous photographs with two cameras, one focused at the end of the cell and the other up to a few centimeters inside the cell. For laser power above the self-focusing threshold, we found on both photographs at equivalent positions a bright focal spot of about the same size (10 ± 2 μ in toluene), consistent with the picture of moving foci. The focal spot appeared deeper inside the cell for higher laser power, but not up to the point at which the peak of the laser pulse would self-focus, presumably because stimulated backward Raman and Brillouin scattering effectively terminated self-focusing through depletion of the incoming laser power (see explanation below). One might think that these results could also be interpreted as a self-trapped filament moving along a line. We rule out such a possibility on the following grounds: (1) Calculation[8] shows that a trapped filament of 30-GW/cm^2 peak intensity without appreciable spectral broadening should be depleted by Raman scattering in less than a few millimeters. (2) Focal spots were observed within 1 cm of the point at which the peak of the input pulse should self-focus, when the input peak power was not too far above the self-focusing threshold. This showed that the trapped filaments, if existing, could not be longer than 1 or possibly 0.5 cm. The limit was set by the experimental inaccuracy in determing the self-focusing threshold, assuming the worst case that self-focusing was not terminated by stimulated scattering. Physical results would of course be essentially the same, whether it is a moving focal spot of finite focal region or a moving, short, trapped filament. We also focused the camera up to a few millimeters outside the cell. The observed image was almost an order of magnitude smaller than one would expect from diffraction of a self-trapped filament, indicating some focusing action of the beam extended outside the cell.

Theoretically, knowing the time variation of the input laser power, we can calculate how the focal spot moves along the line. We assume that for a certain laser power P the focal spot appears at the self-focusing distance[9]

$$Z_f = K/[(P/P_{cr})^{1/2} - 1], \quad (1)$$

where P_{cr} is the critical power for self-trapping[3] and K is a constant depending on the geometric factors of the input beam and the nonlinear refractive index of the medium. By measuring the threshold power for self-focusing at various cell lengths we can find K and P_{cr}. The motion of the focal spot can then be determined from Eq. (1), knowing the time variation of the input laser power and taking into account the fact that light propagates with finite velocity. Figure 2 shows the position of the focal spot in toluene

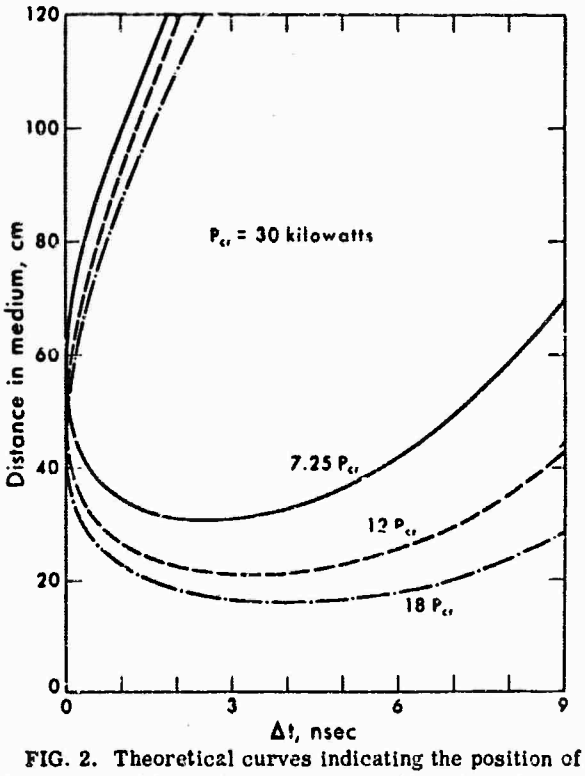

FIG. 2. Theoretical curves indicating the position of the focal spot inside toluene as a function of relative time Δt for several peak powers of a Gaussian laser pulse with 7.6-nsec full width at half-maximum. Here $\Delta t = 0$ refers to the instant the first focal spot is formed. Curves are calculated using Eq. (1) and experimental values of self-focusing threshold at different cell lengths. Note that since light travels with finite velocity, peak of the laser pulse would focus earlier with shorter self-focusing distances than the leading part of the pulse focusing with longer self-focusing distances. This also explains why, at a given Δt, two focal distances can be obtained from Eq. (1).

as a function of time for a set of input Gaussian pulses with various peak powers.[10] These pulses were chosen to match approximately the observed laser pulses in the experiments. However, there could be some residual spatial inhomogeneity in our laser beams; so the curves in Fig. 2 only describe approximately the actual experiments.

One consequence is immediately obvious from the picture of moving foci shown in Fig. 2. For a given cell length, the focal spot would spend more time at the end of the cell when the input laser power is just at the self-focusing threshold than in the case where the input power is considerably above the self-focusing threshold. In the former case, we would expect to see a brighter focal spot at the end of the cell. This is in fact what was observed. We noticed in addition, with the aid of motion pictures, that whenever the input power was near the self-focusing threshold, there appeared a bubble of about 100-μ diam out of the focal region at the end of the cell. Rough estimate shows that while an intense field is necessary to initiate the bubble, an energy of a few ergs is needed to create the bubble. This can therefore happen only if the focal spot stays at a local 10-μ region for more than 10 psec. Most of our experiments were done on toluene with a cell length of 33 cm and an input laser pulse of peak power between $6P_{cr}$ and $12P_{cr}$. From Fig. 2, we expect that the focal spot would first appear in the liquid medium at the end of the cell and then move inward. For higher input power, smaller pulse width, and longer cells the focal spot could first appear inside the cell and then split into two focal spots, one moving towards the front and the other towards the end of the cell. This would happen only at $P > 100\ P_{cr}$ for the 33-cm toluene cell we used. Then the focal spot could also move with a speed greater than the velocity of light.

Figure 2 shows that for input power larger than the self-focusing threshold, if self-focusing were not terminated by other processes, then the duration of a "filament" pulse would be much longer (>1 nsec for $P > 7P_{cr}$) than what was observed (~150 psec) and would increase with increase of input power, opposite to what was observed. However, various stimulated scattering processes can be initiated at the focal region. The backward stimulated Raman and Brillouin scattering would deplete effectively the incoming laser power[11] and consequently terminate the "filament" by depleting the later part of the input laser pulse to a level below the self-focusing threshold. The self-focused light diffracted from the focal spots could also be depleted by forward Raman scattering. Because of longer interaction length, depletion would of course be more appreciable for focal spots deep inside the cell. In all respects, the focal spots near the end of the cell should be less affected by stimulated scattering. Photographs indeed showed that focal spots inside the cell were much less intense than those close to the end of the cell. From Fig. 2, we conclude that to yield the observed "filament" pulse duration, the major part of the pulse must be emitted from a short section of the "filament" presumably within 1 cm towards the end of the cell. This also explains why the pulses were shorter and weaker for higher input power.

In conclusion, we believe that under conditions similar to ours, the so-called "filaments" are actually the result of moving foci. The size of a "filament" should then be the size of the focal spot. Machine calculations,[12] with a simple model of saturable-refractive index, indicate that a self-focused beam would defocus and then refocus again. If the laser power is being depleted by stimulated scattering in the focusing process, then the self-focused beam after defocusing would not have enough self-focusing strength to refocus. For an input laser pulse which is nonhomogeneous and multimoded, self-trapped filaments may still exist[4] because of very different propagation conditions. However, a question yet to be answered is why the size of the observed "filaments" in a given liquid seems to remain roughly constant irrespective of the input pulses.

We are indebted to Dr. P. L. Kelly for numerous discussions and valuable comments on the manuscript. We would also like to thank Professor R. Y. Chiao and Professor C. H. Townes for helpful discussions.

---

*Research supported by the U. S. Office of Naval Research under Contract No. Nonr-3656(32).

†A. P. Sloan Research Fellow.

[1]R. Y. Chiao, M. A. Johnson, S. Krinsky, H. A. Smith, C. H. Townes, and E. Garmire, IEEE J. Quantum Electron. QE-2, 467 (1966).

[2]R. G. Brewer, J. R. Lifsitz, E. Garmire, R. Y. Chiao, and C. H. Townes, Phys. Rev. 166, 326 (1968).

[3]R. Y. Chiao, E. Garmire, and C. H. Townes, Phys. Rev. Letters 13, 479 (1964).

[4]M. M. Denariez Roberge and J. P. Taran, to be published.

[5]V. N. Lugovoi and A. M. Prokhorov, Zh. Eksperim.

i Teor. Fiz.–Pis'ma Redakt. 7, 153 (1968) [translation: JETP Letters 7, 117 (1968)].

[6]M. T. Ley and Y. R. Shen, to be published. The essence of the technique is to extract the pulse signal $s(t)$ from the convolution integral $R(t) = \int_{-\infty}^{t} s(\tau) g(t-\tau) \times d\tau$, where $R(t)$ and $g(t)$ are response functions of the detection system to the pulse signal and to a pulse of δ function, respectively. Allowing the possibility of different pulse shapes, we were able to measure the pulse width with an accuracy of ±30 psec for a 200-psec pulse and of ±60 psec for a 100-psec pulse. The time constant of our detection system was about 100 psec.

[7]T. K. Gustafson, J. P. Taran, H. A. Haus, J. R. Lifsitz, and P. L. Kelley, Phys. Rev. 177, 306 (1969).

[8]Y. R. Shen and N. Bloembergen, Phys. Rev. 137, 1787 (1965). The calculation on the saturation effect in this reference has recently been verified by W. Maier and W. Kaiser, to be published.

[9]P. L. Kelley, Phys. Rev. Letters 15, 1005 (1965).

[10]We have been informed that T. K. Gustafson and J. P. Taran have obtained similar results.

[11]M. Maier, W. Kaiser, and J. A. Giordmaine, Phys. Rev. Letters 17, 1275 (1966).

[12]J. H. Marburger and E. L. Dawes, Phys. Rev. Letters 21, 556 (1968), and Phys. Rev. (to be published).

SIMPLE MODEL FOR SEMICONDUCTOR-METAL TRANSITIONS: SmB_6 AND TRANSITION-METAL OXIDES

L. M. Falicov*

Department of Physics, University of California, Berkeley, California 94720

and

J. C. Kimball†

Department of Physics, and The James Franck Institute, University of Chicago, Chicago, Illinois 60637

(Received 12 March 1969)

We propose a simple model for a semiconductor-metal transition, based on the existence of both localized (ionic) and band (Bloch) states. It differs from other theories in that we assume the one-electron states to be essentially unchanged by the transition. The electron-hole interaction is responsible for the anomalous temperature dependence of the number of conduction electrons. For interactions larger than a critical value, a first-order semiconductor-metal phase transition takes place.

Many substances, including SmB_6[1] and a number of transition-metal oxides,[2] exhibit semiconductor-metal transitions.[3] The transitions are in many cases first-order phase transitions (e.g., in V_2O_3); however, they can also result from a gradual but anomalously large increase in conductivity over a range of temperatures (e.g., in SmB_6 and Ti_2O_3). In addition, measurements of large magnetic susceptibilities with anomalous temperature dependences suggest that in many of these materials localized magnetic moments exist and that they are intimately connected with the transition. As an example, it has been hypothesized[1] that in SmB_6 the conduction electrons and the localized moments are produced simultaneously by the promotion of a single localized electron from the spherically symmetric Sm^{++} ion ($J=0$) into a conduction band. The Sm^{+++} ion left behind ($J=\frac{7}{2}$) acts as a localized moment.

We present here a simple theory of the semiconductor-metal transition based on a model having both localized and itinerant interacting quasiparticle states. The relevant single-electron states consist of (a) bands of extended Bloch functions and (b) a set of localized states centered at the sites of the metallic ions in the crystal. As $T \to 0$ the localized states are lower in energy than the band states and are fully occupied by electrons. Therefore the quasiparticle excitations are either localized holes or itinerant electrons. In the language of second quantization and in the spirit of the Landau theory of Fermi liquids, we write the one-particle terms as

$$H_0 = \sum_{\nu \vec{k} \sigma} \epsilon_\nu(\vec{k}) a_{\nu \vec{k} \sigma}^\dagger a_{\nu \vec{k} \sigma} + \sum_{i\sigma} E b_{i\sigma}^\dagger b_{i\sigma}, \qquad (1)$$

where $a_{\nu \vec{k} \sigma}^\dagger$ creates an electron in state $\vec{k}$, band ν, with spin σ, and $b_{i\sigma}^\dagger$ creates a hole with spin σ at site i. The energies $\epsilon_\nu(\vec{k})$ and E are positive definite and such that

$$\Delta \equiv \min[E + \epsilon_\nu(\vec{k})] > 0 \qquad (2)$$

is the energy gap for the formation of an electron-hole pair. We further assume that the quasiparticle interaction is screened, and its range short enough so that only intra-atomic terms need be considered. In this case the interaction

APPENDIX VI

PHYSICAL REVIEW VOLUME 180, NUMBER 2 10 APRIL 1969

Tunable Far-Infrared Radiation Generated from the Difference Frequency between Two Ruby Lasers

D. W. FARIES*
Department of Physics, University of California, Berkeley, California 94720

AND

K. A. GEHRING,† P. L. RICHARDS, AND Y. R. SHEN*‡
Inorganic Materials Research Division, Lawrence Radiation Laboratory, Department of Physics, University of California, Berkeley, California 94720

(Received 20 December 1968)

Far-infrared radiation generated from the difference frequency between two temperature-tuned ruby lasers has been observed over the frequency range from 1.2 to 8.1 cm^{-1}. Lithium niobate and quartz were used as mixing crystals. The conversion efficiency was measured as a function of angle around the phase-matched direction. The expected spectral content and frequency of the far-infrared radiation has been verified using a far-infrared Fabry-Perot interferometer.

SOON after optical second-harmonic generation was discovered, it was suggested by several persons[1] that difference frequency generation in a nonlinear crystal using two temperature-tuned lasers would provide a tunable source of coherent far-infrared radiation. In this paper we describe the first observation of this tunable narrow-band far-infrared radiation. Fixed-frequency far-infrared radiation has been reported by two groups: Zernike and Berman[2] detected broadband radiation near 100 cm^{-1} resulting from the mixing of an unknown number of modes from a pulsed neodymium-glass laser. Yajima and Inoue[3] used the R_1 and R_2 lines of a single ruby laser to generate a fixed difference frequency, $\nu = 29$ cm^{-1}. In neither case was a spectral analysis reported. We have used two, simultaneously Q-switched, temperature-tuned ruby lasers to generate radiation between 1.2 and 8.1 cm^{-1}. By using sum-frequency generation to normalize the pulse-to-pulse variations, we have measured the far-infrared frequency directly and found it to be in agreement with the known temperature coefficient[4] of the ruby-laser frequency. We have also measured the variation of the far-infrared power with orientation of the $LiNbO_3$ crystal near the phase-matching angle. Difference-frequency generation was observed in quartz and $LiNbO_3$ and a comparison is made of their electro-optical coefficients as calculated from their relative efficiencies.

Consider two cylindrically symmetric beams of finite transverse radius a traversing a crystal of length l. The field intensities of the beams ($i = 1, 2$) are

$$\mathbf{E}_i(\mathbf{r},t) = \tfrac{1}{2}[\mathcal{E}_i \exp(ik_i z - i\omega_i t) + \text{c.c.}].$$

A nonlinear polarization of frequency $\omega = \omega_1 - \omega_2$ will be produced in the cylinder of length l and radius a by the interaction of the two electric fields with the medium.

$$\mathbf{P}(\mathbf{r},t) = \tfrac{1}{2}(\chi^{(2)}\mathcal{E}_1\mathcal{E}_2^* e^{i(k+\Delta k)z - i\omega t} + \text{c.c.}),$$

where $k_1 - k_2 = k + \Delta k = (\omega/c)n + \Delta k$ and where n is the index of refraction at the difference frequency ω. By integrating over the contributions of the cylindrical polarization wave in the far-field approximation, we obtain the total far-infrared power W collected in the detection system. We neglect the effect of the boundary by assuming that the detector is buried in the dielectric medium.

$$W = \frac{n\omega^4}{4c^3}|\chi^{(2)}|^2|\mathcal{E}_1|^2|\mathcal{E}_2|^2 l^2(\pi a^2)^2 \times \int_{\phi=0}^{\phi_m} \sin\phi\, d\phi \left[\frac{\sin\eta}{\eta}\right]^2\left[\frac{2J_1(\zeta)}{\zeta}\right]^2, \quad (1)$$

where $\eta = \frac{1}{2}kl(1 + \Delta k/k - \cos\phi)$, $\zeta = ka\sin\phi$, ϕ is the angle between the incoming beam and the generated radiation, and ϕ_m is the maximum angle collected in the detection system.

Equation (1) is valid for single-mode lasers. A beam with divergence Ω and area A contains $N = A\Omega/\lambda^2$ modes. Under the condition of small difference frequencies and limited collection angle (which existed in our experiments), the measured signal arises only from each mode of one laser interacting with one mode from the other laser. Therefore, the detected power is reduced by a factor of $1/N$ from that predicted by Eq. (1).

In our experiment, the two lasers were simultaneously Q-switched by using the same rotating mirror in both optical cavities.[5] The mode purity was controlled by using a resonant reflector as the output mirror and by

* Research supported by the Office of Naval Research under Contract No. Nonr-3656(32).
† Present address: The Clarendon Laboratory, Oxford, England.
‡ A. P. Sloan Research Fellow.
[1] See, for example, D. C. Laine, Nature 191, 795 (1961); J. R. Fontana and R. H. Pantell, Proc. IRE 50, 1796 (1962).
[2] F. Zernike, Jr., and P. R. Berman, Phys. Rev. Letters 15, 999 (1965).
[3] T. Yajima and K. Inoue, Phys. Letters 26A, 281 (1968); IEEE J. Quantum Electron. (to be published).
[4] I. D. Abella and H. Z. Cummins, J. Appl. Phys. 32, 1177 (1961).
[5] D. W. Faries and Y. R. Shen (to be published).

using a saturable dyecell (Eastman 10220). One of the lasers was cooled by circulating ethyl alcohol at $T \geq -40°C$ and the other was operated at room temperature. The two laser beams were made coincident and accurately parallel (within 1 min of arc) by careful adjustment of a beam splitter. No focusing lens was used. The polarizations of the lasers were made accurately perpendicular (vertical and horizontal) by the use of external polarizers. Each laser typically delivers a power of 1 MW over an area of 0.2 cm^2 with an angular divergence of 1.5 mrad and a pulse duration of 3×10^{-8} sec. The power is usually distributed into two frequency modes separated by 0.2 cm^{-1}.

The far-infrared signal was detected using a crystal of n-type InSb (Putley[6] detector) at $T=1.3°K$ in a magnetic field of 5500 Oe. It was biased with a constant voltage of 0.25 V and the current was measured using an operational amplifier with a feedback resistor $R_F=205$ kΩ. The response time of this system is 2 μS. The sensitivity of the detector was measured using a blackbody at 200°C and a filter passing 0–50 cm^{-1}. This showed the average noise equivalent power in a 5×10^5-Hz bandwidth to be 10^{-6} W. However, since the sensitivity is certainly not uniform in this energy region[6] and since there are inevitable local system resonances at these long wavelengths, the absolute values of the infrared power may be in error by more than an order of magnitude. For this reason, emphasis was on relative powers in our measurements.

The nonlinear crystal was mounted on a rotatable table directly in front of the light pipe leading to the detector. A black polyethylene filter was used to reject unwanted radiation.

The infrared power generated is proportional to the integrated overlap in space and time of the two laser beams. Since this overlap varies from shot to shot, it is desirable to obtain an independent measurement of it for use as normalization.[7] This was done by monitoring the intensity of the sum frequency generated in a crystal of potassium dihydrogen phosphate (KDP). The discrimination of the sum frequency from the second-harmonic signal was achieved by using the scheme of Maier *et al.*[8] and Armstrong.[9] A discrimination factor better than 50 against second-harmonic radiation was obtained. Because of the small k vector of the far-infrared radiation, fluctuations in beam alignment and angular-mode distribution are expected to be more critical for difference-frequency than for sum-frequency generation. The far-infrared difference-frequency signals were found to be proportional to the sum-frequency signal within a factor of 2.

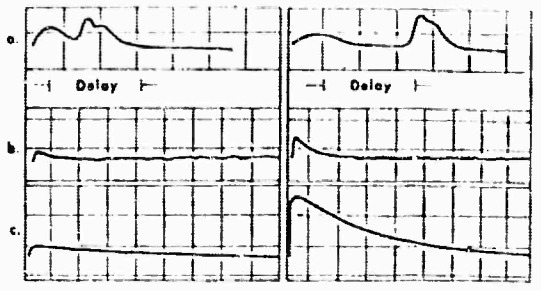

FIG. 1. Typical oscilloscope traces showing correlation between the time overlap of laser pulses and the strength of sum- and difference-frequency signals. The laser signals are displayed on a single trace (a) at a sweep rate of 50 nsec/div, with the cooled laser signal delayed by 125 nsec. Difference-frequency signals (b) and sum-frequency signals (c) are displayed at a sweep rate of 5 μsec/div. The pulse widths of (b) and (c) are characteristic of the time response of the detectors used. When there is considerable time overlap (as on the right), the sum- and difference-frequency signals are clearly much larger.

Typical infrared signals are shown in Fig. 1, where they are compared with the sum-frequency signal and the signals from the individual lasers. Satisfactory correlation is observed between the difference-frequency signal, the sum-frequency signal, and the laser timing.

The variation of the far-infrared power as the 1.5-cm $LiNbO_3$ crystal is rotated through the phase-matched direction is shown in Fig. 2. The experimental points are compared with the theoretical curve plotted assuming that the output of each laser is split equally between two frequencies separated by 0.2 cm^{-1}. The position of the peak in Fig. 2 agrees within experimental accuracy with the phase-matching angle of 0.5° from the optic axis computed using $n_e=2.189$ and $n_0=2.273$ (at the laser frequencies)[10] and $n_0=6.55$ (at 8.1 cm^{-1}).[11]

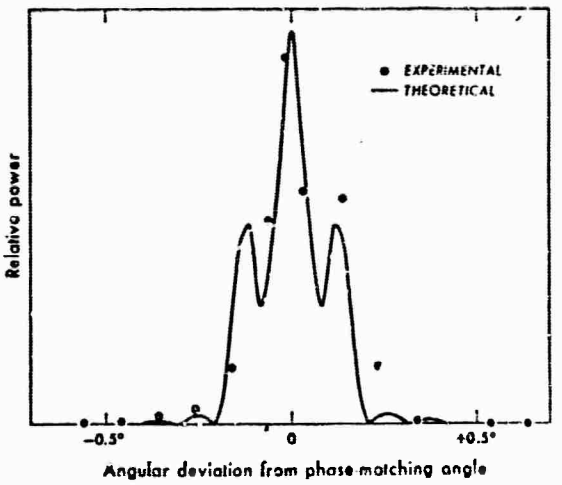

FIG. 2. Variation of the power of the difference-frequency signal as a function of the angular deviation from the phase-matched angle. The angles refer to the inside of the 1.5-cm $LiNbO_3$ crystal used.

[6] E. H. Putley and D. H. Martin, in *Spectroscopic Techniques*, edited by D. H. Martin (North-Holland Publishing Co., Amsterdam, 1967), p. 113.
[7] J. Ducuing and N. Bloembergen, Phys. Rev. 133, A1493 (1964).
[8] M. Maier, W. Kaiser, and J. A. Giordmaine, Phys. Rev. Letters 17, 1275 (1966).
[9] J. A. Armstrong, Appl. Phys. Letters 10, 16 (1967).
[10] G. D. Boyd, R. C. Miller, K. Nassau, W. L. Bond, and A. Savage, Appl. Phys. Letters 5, 234 (1964).
[11] J. D. Axe and D. F. O'Kane, Appl. Phys. Letters 9, 58 (1966).

The measured far-infrared power from a 0.047-cm $LiNbO_3$ crystal at the phase-matching peak is about 1 mW. This is in order-of-magnitude agreement with the value calculated from Eq. (1) with a collection half-angle of 30°. For the 1.5-cm crystal, the measured peak power is 2×10^{-2} W, which is two orders of magnitude lower than what is expected. This discrepancy is most likely due to crystal inhomogeneity,[12] which would reduce the efficiency of optical mixing in long crystals. All the long crystals we used suffered damage after several hundred shots. The validity of quantitative comparisons with Eq. (1) is also limited by the unrealistic boundary conditions used in its derivation. Neglected effects include radiation from the edges of the crystal and multiple reflections at the faces.

The far-infrared wavelength was measured using a Fabry-Perot interferometer with electroformed metal mesh mirrors.[13] Typical transmission curves are shown in Fig. 3. The solid curve is obtained from the Airy formula by integrating over the finite collection angle so as to fit the decrease in Q with increasing order number. The wavelengths used were 3% [Fig. 3(a)] and 5% [Fig. 3(b)] smaller than those predicted from the known temperature dependence of the ruby-laser frequency. The finesse was computed from the geometry of the mesh. The fit shows unambiguously that we are observing a difference frequency with a bandwidth less than the ~1 cm^{-1} resolution of our interferometer. The linewidth of the two frequency modes (separated by 0.2 cm^{-1}) from each laser is less than 0.02 cm^{-1}, leading to a predicted linewidth of less than 0.04 cm^{-1} for each of the three far-infrared frequencies produced.

We also compare the far-infrared power generated from a 0.047-cm-thick crystal of $LiNbO_3$ with that from a 1-cm-thick crystal of quartz. Using Eq. (1), the ratio of the electro-optic coefficients $r_{22}(LiNbO_3)/r_{62}(\text{quartz})$ is estimated to be 8.5. According to other measurements,[14] the ratio is 3.7. Because of the uncertainties in our measurement, this agreement must be considered satisfactory.

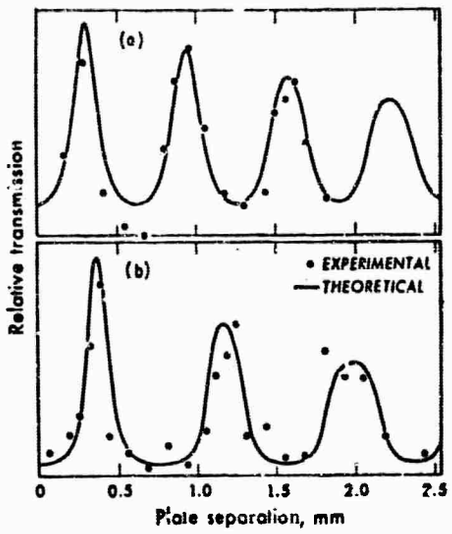

FIG. 3. Fabry-Perot scan of the difference-frequency output. The upper scan (a) is for a temperature difference $\Delta T=60$°C of the two lasers. For the lower scan (b), $\Delta T=47$°C. The theoretical curves are Airy functions calculated from the geometrical properties of the Fabry-Perot reflectors and averaged to account for the 30° collection half-angle.

The tuning range was limited to frequencies less than 8.1 cm^{-1} by the cooling system used. This range could be extended to ~20 cm^{-1} by using liquid nitrogen as a coolant. If the warmer laser were operated on the R_2 line, then the range could be extended to ~50 cm^{-1}. The use of a tunable dye laser, stimulated Raman radiation, or parametric sources would, of course, extend this range throughout the infrared.

We would like to thank D. Woody for computing the theoretical interferometer curves and Dr. E. Washwell for furnishing samples of $LiNbO_3$.

[12] A. Ashkin, G. D. Boyd, J. M. Dziedzic, R. G. Smith, A. A. Ballman, J. J. Levinstein, and K. Nassau, Appl. Phys. Letters 9, 72 (1966).

[13] R. Ulrich, K. F. Renk, and L. Genzel, IEEE Trans. Microwave Theory Tech. MTT-11, 363 (1963).

[14] A. Yariv, *Quantum Electronics* (Wiley-Interscience, Inc., New York, 1967), p. 351.

BLANK PAGE

VOLUME 19, NUMBER 20 PHYSICAL REVIEW LETTERS 13 NOVEMBER 1967

THEORY OF SELF-TRAPPED FILAMENTS OF LIGHT

Y. R. Shen,*† M. Y. Au Yang,‡ and Marvin L. Cohen†‡
Department of Physics, University of California, Berkeley, California
(Received 30 August 1967)

We present a calculation modeled after the theory of phase transitions to explain the observations on self-trapped filaments of laser light in liquids. The resulting state is shown to be similar to the Abrikosov vortex state in superconductors.

Self-focusing and self-trapping of intense light beams have recently become one of the most important and interesting subjects in nonlinear optics. While self-focusing as a result of intensity-dependent changes of the refractive index is now more or less understood both theoretically[1] and experimentally,[2] the formation of intense filaments arising from self-trapping[3] still remains a mystery. It is believed that the filament formation is also a consequence of the change of refractive index with intensity.[3] However, experimental results indicate that the change in the refractive index of a filament, calculated from the observed intensity in the filament under Kerr effect assumptions, is not sufficient to account for the observed filament size.[4] In addition, a number of other experimental facts have received no satisfactory explanation.

In this paper, we present a calculation which enables us to explain most of the experimental observations on self-trapped filaments. The calculation is based on the assumption of a field-induced phase transition in the medium and is similar to that of vortex formation in Type-II superconductors. Preliminary results of the calculation yield the following predictions: (1) The splitting of an intense beam into small-scale circular filaments is energetically favorable; (2) aside from fluctuations, all filaments have the same size and the same power density; (3) the filament size and the power contained in each filament are characteristics of the medium independent of the input beam intensity. In the calculation, we will assume that a critical field exists and that aside from the intensity-dependent dielectric constant $\epsilon(\omega) = \epsilon_0(\omega) + \epsilon_2(\omega)|E(\omega)|^2$, to produce this field, other nonlinear optical processes can be neglected before the filaments are formed.

Grob and Wagner[5] have also suggested the analog of vortex lines in superconductors to the filaments in this problem. However, they assume that the filament formation is a result of coupling between light fields and density fluctuations in the medium. Their results are essentially the same as those obtained by Chiao, Gamire, and Townes.[3]

Our calculation is modeled after the theory of phase transitions and the theory of vortex formation in superconductivity.[6] We assume that the molecules in a liquid are correlated, and at temperature T, the state of the liquid can be described by a dielectric function. We further assume that in the presence of an intense optical field greater than the critical field E_c, the molecular interactions in the liquid can be changed, and the system can experience a phase transition. (Field-induced phase transitions have been observed in ferroelectrics.)

We shall begin by discussing the energy of an arbitrary two-phase configuration of the liquid and then go on to discuss a liquid with trapped light filaments. In both cases we as-

sume that the system can exist in two states described by the dielectric constants ϵ_a and ϵ_b. As will be clearer later, the states a and b will be analogous to the superconducting and normal states, respectively. The energy difference between these states (or the condensation energy) is $\Delta\epsilon|E_c|^2/8\pi$, where $\Delta\epsilon=\epsilon_b-\epsilon_a$. We now consider the case of a light beam of uniform intensity $c|E_0|^2/8\pi$ propagating into the liquid medium where both a and phases exist simultaneously. After the light beam has traveled some distance along the $\hat{z}$ direction, the field distribution in the beam should become stable and invariant with respect to z. We can then conclude that from the minimization of the Gibbs free energy, the fields will concentrate in the high-dielectric-constant b region with field penetration of distance λ into the a region. For simplicity, we assume that the field E_b is constant in the b region and the λ penetration region.[7] The free energy of the system is (assuming a dispersionless medium),

$$F=F_0+(8\pi)^{-1}\{A_b(E_c^2\Delta\epsilon+|E_b|^2\epsilon_{b0}+\tfrac{1}{2}|E_b|^4\epsilon_{b2}) +\lambda l_b(|E_b|^2\epsilon_{a0}+\tfrac{1}{2}|E_b|^4\epsilon_{a2}) +\xi l_b(E_c^2\Delta\epsilon+|E_b|^2\Delta\epsilon)\}, \quad (1)$$

with

$$(A_b+\lambda l_b)|E_b|^2=A|E_0|^2,$$

where F_0 is the free energy arising from all sources other than those we are considering, A_b and A are the cross-sectional areas of the b region and of the beam, respectively, l_b is the perimeter length of the ϵ_b region, ξ is the characteristic length over which the transition from ϵ_a to ϵ_b takes place,[7] and it is assumed for simplicity that $\epsilon_{a2}\approx\epsilon_{b2}\equiv\epsilon_2$. Comparison of Eq. (1) with the free energy for a uniphase in A shows that a two-phase system is energetically favorable if $|E_0|>E_c$ and $\lambda>\xi$. The medium wants to form new walls between the phases. From arguments similar to those used to describe the formation of vortex lines in superconductivity,[8] it is energetically favorable to form circular filaments of radius ξ (field filaments of radius λ).

For the case of n filaments, the free energy of the system can be written as

$$F=F_0+(8\pi)^{-1}\{n\pi\lambda^2(|E_b|^2\epsilon_{a0}+\tfrac{1}{2}|E_b|^4\epsilon_2) +n\pi\xi^2(|E_b|^2\Delta\epsilon+E_c^2\Delta\epsilon)\}, \quad (2)$$

with the constraint $n\pi\lambda^2|E_b|^2=A|E_0|^2$, where E_b is the field in the filament. For a given $|E_0|^2$, the above free energy can be minimized to yield the number of filaments. Thus, $\partial F/\partial n=0$, and we find that

$$n=\frac{A|E_0|^2\epsilon_2^{1/2}}{\pi\lambda\xi E_c(2\Delta\epsilon)^{1/2}}. \quad (3)$$

Note that the minimum n we can have is at $E_0=E_c$. From Eq. (3), the field intensity in each filament can be obtained:

$$\frac{c|E_b|^2}{8\pi}=\frac{c\xi E_c(2\Delta\epsilon)^{1/2}}{8\pi\lambda\epsilon_2^{1/2}}, \quad (4)$$

which is independent of the applied field if λ is only dependent on the characteristics of the medium. The total power contained in each filament is a constant:

$$Q=\frac{c\lambda\xi E_c(2\Delta\epsilon)^{1/2}}{8\epsilon_2^{1/2}}. \quad (5)$$

The above equations relate the field in a filament to the size of the filament, and these can be solved if the quantity $\xi E_c(\Delta\epsilon)^{1/2}$ is known. This quantity is a characteristic of the phase transition in the medium. It is possible to obtain a numerical estimate of $\xi E_c(\Delta\epsilon)^{1/2}$ by making the simplifying assumption that the phase transition we are considering is a second-order phase transition. This allows the use of the Landau-Ginzburg equation,[8]

$$(N/2m)[(\hbar/i)\nabla-(e^*/c)\vec{\mathbf{A}}]^2\psi+\alpha\psi+\beta|\psi|^2\psi=0, \quad (6)$$

where ψ is a complex, position-dependent order parameter describing the additional induced correlated polarization responsible for the $\Delta\epsilon$ change. We assume that the induced polarization arises from electronic interactions and N, m, and e^* refer to the density, mass, and effective charge of the electron (assuming one interacting electron per molecule). In deriving Eq. (2) we assume a square well approximation for ψ and E_b; $\psi=1$ for $r>\xi$, $\psi<\xi$,[8] and $E=E_b$ for $r<\lambda$, where r is the radial position measured from the center of the filament.

From the equilibrium condition in the absence of the fields, we find[8] that

$$\alpha=-\beta=-E_c^2\Delta\epsilon/4\pi. \quad (7)$$

If the fields are independent of z, then ψ is also independent of z, and both the fields and ψ can be taken to have cylindrical symmetry.

We can use Eq. (6) to give the characteristic relaxation length ξ to describe the variation of ψ from zero at the center of the filament to unity outside:

$$\xi \approx [2\pi\hbar^2 N/m\Delta\epsilon E_c^2]^{1/2}. \quad (8)$$

For CS_2, $N \approx 10^{22}$ cm^{-3} and we find that $\xi E_c(\Delta\epsilon)^{1/2} = 8.7\times10^{-3}$ esu. Using this value and the experimental values $\lambda \approx 2$ μ and $\epsilon_2 = 1.8\times10^{-11}$ esu in Eqs. (4) and (5) gives the field intensity $c|E_b|^2/8\pi = 1.8\times10^9$ W/cm^2, and the power contained in each filament, $Q = 220$ W. These estimates agree well with experiment.[4] To find ξ, E_c, and $\Delta\epsilon$ separately, a microscopic calculation which considers the molecular interactions in detail is necessary.

It is possible to compute $\Delta\epsilon$ if λ is known by using the Maxwell wave equation

$$\{\nabla_r^2 - k_z^2 + (\omega^2/c^2)[\epsilon_{b0} - \Delta\epsilon\langle|\psi|^2\rangle_{Av} + \epsilon_2|E|^2]\}E(r) = 0, \quad (9)$$

where $\langle|\psi|^2\rangle_{Av}$ represents the average value of $|\psi(r)|^2$. If we made the simplification $\langle|\psi(r)|^2\rangle_{Av} = \psi_0^2$ for $r < \xi$, $\langle|\psi(r)|^2\rangle_{Av} = 1$ for $r > \xi$, and $E(r) = E_b$ for $r < \xi$ (since the macroscopic field will not vary appreciably over a dimension less than a wavelength),

$$k_z = (\omega/c)(\epsilon_{b0} - \Delta\epsilon\psi_0^2 + \epsilon_2|E_b|^2)^{1/2}. \quad (10)$$

For $\epsilon_0 \gg \epsilon_2|E|^2$, $\epsilon_2|E|^2$ can be neglected in Eqs. (9) and (10) in first order. The solution of Eq. (9) for $r > \xi$ is the zeroth-order modified Bessel function $K_0(r/\lambda)$, with a characteristic decay length

$$\lambda = (c/\omega)[\Delta\epsilon(1-\psi_0^2)]^{-1/2}. \quad (11)$$

For CS_2, $\lambda \approx 2$ μ, and at ruby laser frequency we estimate that typically $\Delta\epsilon > 3\times10^{-3}$, which is much larger than $\epsilon_2|E_b|^2 (\approx 2\times10^{-4})$. We expect that typical values should be $\Delta\epsilon \sim 10^{-2}$, $E_c \sim 2\times10^3$ esu, and $\xi \sim 0.4$ μ. A more rigorous treatment of this problem should account for the variation of E and ψ across the phase boundary by solving the coupled equations (6) and (9). This should yield a functional representation for the n stable filaments as obtained from energy considerations. This would be equivalent to the Abrikosov calculation for vortex lines in superconductors.[9]

In the above discussion, the dynamic process to reach the final stable field distribution in the beam has not been considered. It is clearly not important as far as the stable configuration of filaments is concerned. This is analogous to the growing of a crystal, where we are only interested in the final crystal structure and not in the dynamic process of crystal formation. In actual experiments, the incoming beam intensity is often much less than E_c. However, through self-focusing, the beam cross section reduces and the field intensity finally exceeds E_c. The field distribution in the beam then becomes unstable, and filaments would be nucleated by fluctuations in the medium. The intensity in each filament is so high that stimulated scattering processes set in and deplete the laser power in the filament very rapidly.[4] Fluctuation and stimulated scattering processes would probably prevent the field distribution from reaching a stable configuration of filaments, but each filament already formed should have the characteristics of filaments in the final-state configuration.

We would like to thank Professor G. Rochlin for helpful discussions.

---

*Research supported by the joint sponsorship of the Advanced Research Projects Agency and the Office of Naval Research under Contract Nonr-3656(32).

†Alfred P. Sloan Foundation Fellow.

‡Supported by the National Science Foundation.

[1]P. L. Kelley, Phys. Rev. Letters 15, 1005 (1965); V. I. Talanov, Zh. Eksperim. i Teor. Fiz.—Pis'ma Redakt. 2, 218 (1965) [translation: JETP Letters 2, 138 (1966)]; S. A. Akhmanov, A. P. Sukhorukov, and R. V. Khokhlov, Zh. Eksperim. i Teor. Fiz. 50, 1537 (1966) [translation: Soviet Phys.—JETP 23, 1025 (1966)].

[2]Y. R. Shen and Y. J. Shaham, Phys. Rev. Letters 14, 1008 (1965); P. Lallemand and N. Bloembergen, Phys. Rev. Letters 14, 1010 (1965); G. Mayer and G. Hauchecorne, Compt. Rend. 261, 4014 (1965).

[3]R. Y. Chiao, E. Garmire, and C. H. Townes, Phys. Rev. Letters 13, 479 (1964).

[4]E. Garmire, R. Y. Chiao, and C. H. Townes, Phys. Rev. Letters 16, 347 (1966); R. Y. Chiao, M. A. Johnson, S. Krinsky, H. A. Smith, C. H. Townes, and E. Garmire, IEEE J. Quantum Electron. QE-2, 467 (1966); D. H. Close, C. R. Guiliano, R. W. Hellwarth, L. D. Hess, F. J. McClung, and W. G. Wagner, IEEE J. Quantum Electron. QE-2, 553 (1966); R. Brewer and L. Lifshitz, Phys. Letters 23, 79 (1966).

[5]K. Grob and M. Wagner, Phys. Rev. Letters 17, 819 (1966).

[6]See, for example, P. G. deGennes, Superconductivity of Metals and Alloys (W. A. Benjamin, Inc., New York, 1966); L. Landau and E. M. Lifshitz, Statistical Physics, (Pergamon Press, London, 1958).

[7]See, for example, C. Kittel, Introduction to Solid State Physics (John Wiley & Sons, Inc., New York, 1966), 3rd ed., Fig. 27, p. 367.
[8]V. L. Ginzburg and I. D. Landau, Zh. Eksperim. i Teor. Fiz. 20, 1064 (1950).
[9]A. A. Abrikosov, Zh. Eksperim. i Teor. Fiz. 32, 1442 (1957) [translation: Soviet Phys.—JETP 5, 1174 (1957)].

APPENDIX VIII

Reprinted from THE PHYSICAL REVIEW, Vol. 141, No. 1, 298–305, January 1966
Printed in U. S. A.

Optical Nonlinearities of a Plasma*

N. BLOEMBERGEN† AND Y. R. SHEN
Department of Physics, University of California, Berkeley, California
(Received 6 August 1965)

Second-harmonic generation and stimulated Raman effects for a plasma are calculated by the same methods that have been used for bound electrons. The nonlinear susceptibility describing the stimulated Raman effect in a gaseous or metallic plasma is 6 to 10 orders of magnitude smaller than the corresponding effect in liquids. This process in a plasma can also be described as the parametric interaction between a damped plasma wave and two light waves. The second-harmonic generation from a plasma boundary is dominated by a surface term which originates from the discontinuity in the normal component of the electric field. It is shown that the observed second-harmonic generation from metallic silver probably stems from bound ion cores in the surface layer rather than from a plasma surface term.

I. INTRODUCTION

THE basic nonlinearity in the interaction between a free electron and an electromagnetic wave is caused by the Lorentz force. Additional nonlinearities may result from convective density fluctuations in the plasma. The nonlinearities in gaseous plasmas have been studied extensively in the microwave region of the electromagnetic spectrum.[1,2] Recently much attention has been given to optical nonlinearities of a plasma, although they are by their very nature rather small.[3–11] In this paper hydrodynamic terms and convection will be ignored.

The same basic formalism can be used to describe the nonlinearities for bound and free electrons. This is particularly evident in the formulation of Cheng and Miller[5] and of Pine,[12] who emphasized the self-consistent-field description of the nonlinear susceptibilities. In Sec. II of this paper, the second-harmonic volume polarization for a plasma is rederived. The self-consistent-field correction on this longitudinal polarization is explicitly exhibited in the same manner as has been done by Ehrenreich and Cohen[13] for the longitudinal linear dielectric constant. In Sec. III, it is shown that surface terms are actually more important than the volume effect for the second-harmonic generation (SHG) from a metallic surface. Jha[14] has first called attention to these plasma surface terms. Our results are somewhat different from Jha's and in better agreement with recent experimental observations. We show furthermore that the dominant contribution to the SHG may come from bound electrons in the ion cores at the surface rather than from the conduction electrons.

The next higher order nonlinearity describes the Raman-type effects in a plasma. If, for example, a laser beam at frequency ω_L is incident on a plasma, the plasma will present exponential gain for a light beam

* This research was supported by the U. S. Office of Naval Research. An abbreviated version of this work was presented at the Physics of Quantum Electronics Conference, Puerto Rico, 1965 (unpublished).
† On leave from Harvard University.
[1] P. A. Sturrock, Thermonucl. Res. (GB) 2, 158 (1961).
[2] R. F. Whitmer and E. B. Barrett, Phys. Rev. 121, 661 (1961); *ibid.* 125, 1478 (1962).
[3] N. Bloembergen, Proc. IEEE 51, 124 (1963).
[4] R. Kronig and J. I. Poukema, Proc. Koninkl. Ned. Akad. Wetenschap. 66B, 8 (1963).
[5] H. Cheng and P. B. Miller, Phys. Rev. 134, A683 (1964).
[6] P. M. Platzman, S. J. Buchsbaum, and N. Tzoar, Phys. Rev. Letters 12, 573 (1964); P. M. Platzman and N. Tzoar, Phys. Rev. 136, A11 (1964).
[7] D. F. Dubois and V. Gilinsky, Phys. Rev. 135, A995 (1964).
[8] N. Kroll, A. Ron, and N. Rostoker, Phys. Rev. Letters 13, 83 (1964).
[9] H. Cheng and Y. C. Lee, Phys. Rev. Letters 14, 426 (1965).
[10] D. F. Dubois, Phys. Rev. Letters 14, 818 (1965).
[11] Various authors in *Proceedings of the Conference on the Physics of Quantum Electronics, Puerto Rico* (McGraw-Hill Book Company, Inc., New York, 1965).
[12] A. Pine, Phys. Rev. 139, A901 (1965). The authors are indebted to Dr. Pine for making his manuscript available before publication.
[13] H. Ehrenreich and M. H. Cohen, Phys. Rev. 115, 786 (1959).
[14] S. S. Jha, Phys. Rev. 140, A2020 (1965). The authors are indebted to Dr. Jha for receiving a copy of this paper prior to publication.

at $\omega_s=\omega_L-\omega_{p,q_L-q_s}$ where ω_{p,q_L-q_s} is the frequency of a plasma wave with wave vector $\mathbf{q}_L-\mathbf{q}_s$. If both beams at ω_L and ω_s are incident, generation of the antistokes frequency at $2\omega_L-\omega_s$ is possible, etc. All these effects are derived in a straightforward manner in Sec. IV by a simple extension of the SHG calculation of Sec. II. The same numerical results are obtained as from more complex calculations.[7–11] The stimulated Raman effect is so small that it will be of little use as a probe for gaseous plasmas, although the Raman-type nonlinearity may be important in semiconductor plasmas in the far infrared. In Sec. V the same Raman effect is described as the parametric interaction between two light waves and a plasma wave. This illustrates again the parallel treatment for free and bound electrons. The Raman effect in a plasma is quite analogous to the Raman effect in liquids and solids,[15] if the optical phonons are replaced by plasmons.

II. SELF-CONSISTENT-FIELD CALCULATION OF THE LONGITUDINAL SECOND-HARMONIC POLARIZATION IN A PLASMA

General expressions for the lowest order nonlinear susceptibility have been given by Cheng and Miller [Eq. (13) of Ref. 5] and by Pine [Eq. (18) of Ref. 12]. Their results are valid for Bloch one-electron wave functions in a periodic lattice potential and can be specialized for the case of free electrons. Because of the complexity of the expressions, it seems worthwhile to rederive the result for free electrons in a special gauge, which will clearly and explicitly exhibit the self-consistent-field corrections. Ehrenreich and Cohen first utilized this method to get physical insight in the linear self-consistent dielectric constant. They also pointed out that the one-electron Hamiltonian approach is equivalent to the random-phase approximation in the exact many-body problem.

The zero-order or equilibrium density matrix for an ensemble of free electrons with eigenstates,

$$|\mathbf{k}\rangle=\Omega^{-1/2}\exp(i\mathbf{k}\cdot\mathbf{r}),$$

where Ω is a volume of normalization, is given by

$$\rho^{(0)}|\mathbf{k}\rangle=f_0(\epsilon_\mathbf{k})|\mathbf{k}\rangle.$$

Here f_0 is the Fermi-Dirac distribution function and $\epsilon_\mathbf{k}=\hbar^2k^2/2m$ is the unperturbed (kinetic) energy in the state $|\mathbf{k}\rangle$. The equation of motion for the density matrix must now be solved in successive approximation, when the perturbation by the transverse electromagnetic wave and the self-consistent Coulomb screening potential is admitted. Since general expressions have already appeared elsewhere,[16] here only the physically dominant terms will be retained. The perturbation may be written as

$$\mathcal{H}_{\text{pert}}=(e^2/2mc^2)\mathbf{A}^2+e\varphi_s. \tag{1}$$

It can be shown by explicit calculation that for free electrons the contributions from the linear term, $-(e/2mc)\{\mathbf{p}\cdot\mathbf{A}+\mathbf{A}\cdot\mathbf{p}\}$, are smaller by a factor $(\hbar\omega/mc^2)$, where ω is the light frequency. The transverse vector potential $\mathbf{A}$ describes the light wave *inside* the plasma. It is *not* the incident field, but the transmitted wave into the plasma,

$$\mathbf{A}=\mathbf{A}_0\exp(i\mathbf{q}\cdot\mathbf{r}-i\omega t)+\mathbf{A}_0^*\exp(-i\mathbf{q}\cdot\mathbf{r}+i\omega t). \tag{2}$$

The complex amplitude $\mathbf{A}_0$ has twice the value of the more conventional definition.

With the perturbation given by Eqs. (1) and (2), the lowest order nonvanishing density-matrix elements at the harmonic frequency 2ω are given by

$$\begin{aligned}-(2\hbar\omega)\langle\mathbf{k}|\rho^{(2\omega)}|\mathbf{k}-2\mathbf{q}\rangle&=(\epsilon_\mathbf{k}-\epsilon_{\mathbf{k}-2\mathbf{q}})\langle\mathbf{k}|\rho^{(2\omega)}|\mathbf{k}-2\mathbf{q}\rangle\\&+\langle\mathbf{k}|(e^2/2mc^2)\mathbf{A}^2+e\varphi_s|\mathbf{k}-2\mathbf{q}\rangle\{f_0(\epsilon_\mathbf{k})-f_0(\epsilon_{\mathbf{k}-2\mathbf{q}})\}\\&+i\Gamma\langle\mathbf{k}|\rho^{(2\omega)}|\mathbf{k}-2\mathbf{q}\rangle.\end{aligned} \tag{3}$$

The last term is a phenomenological damping term to represent the effect of collisions and Landau damping. The screening potential is related to the induced charge density by Poisson's equation. Using the Fourier series expansion for the screening potential,

$$\varphi_s(\mathbf{r})=\textstyle\sum_{\mathbf{q}'}\varphi_{s,\mathbf{q}'}e^{+i\mathbf{q}'\cdot\mathbf{r}},$$

and for the charge density,

$$n^{(2\omega)}e=e\textstyle\sum_{\mathbf{q}'}e^{+i\mathbf{q}'\cdot\mathbf{r}}\sum_{\mathbf{k}'}\langle\mathbf{k}'|\rho^{(2\omega)}|\mathbf{k}'-\mathbf{q}'\rangle,$$

one finds

$$\begin{aligned}&\langle\mathbf{k}|e\varphi_s^{(2\omega)}|\mathbf{k}-2\mathbf{q}\rangle\\&\qquad=(4\pi e^2/4q^2)\textstyle\sum_{\mathbf{k}'}\langle\mathbf{k}'|\rho^{(2\omega)}|\mathbf{k}'-2\mathbf{q}\rangle.\end{aligned} \tag{4}$$

When Eq. (4) is substituted back into Eq. (3), the solution can, after some manipulation, be written in the form

$$\begin{aligned}&\langle\mathbf{k}|\rho^{(2\omega)}|\mathbf{k}-2\mathbf{q}\rangle\\&\qquad=\frac{f_0(\epsilon_{\mathbf{k}-2\mathbf{q}})-f_0(\epsilon_\mathbf{k})}{\epsilon_{\mathbf{k}-2\mathbf{q}}-\epsilon_\mathbf{k}+2\hbar\omega+i\Gamma}\frac{e^2A_0^2}{2mc^2}\frac{1}{\epsilon_{\text{SCF}}(2\omega,2\mathbf{q})},\end{aligned} \tag{5}$$

where $\epsilon_{\text{SCF}}(2\omega,2\mathbf{q})$ is the longitudinal, frequency- and wave-vector-dependent, self-consistent linear dielectric constant calculated by Ehrenreich and Cohen,

$$\epsilon_{\text{SCF}}(\omega,\mathbf{q})=1-\frac{4\pi e^2}{q^2}\sum_{\mathbf{k}'}\frac{f_0(\epsilon_{\mathbf{k}-\mathbf{q}})-f_0(\epsilon_\mathbf{k})}{\epsilon_{\mathbf{k}-\mathbf{q}}-\epsilon_\mathbf{k}+\hbar\omega+i\Gamma}. \tag{6}$$

The Fourier transforms of the current density operator are given by

$$\begin{aligned}\mathbf{j}^{(0)}(\mathbf{q},0)&=(he/2im)e^{-i\mathbf{q}\cdot\mathbf{r}}(-i\mathbf{q}+2\nabla),\\\mathbf{j}^{(1)}(\mathbf{q},\omega)&=-(e^2/mc)\mathbf{A}_0.\end{aligned}$$

[15] Y. R. Shen and N. Bloembergen, Phys. Rev. 137, 1787 (1965).
[16] See, for example, Refs. 5 and 12, or N. Bloembergen, *Nonlinear Optics* (W. A. Benjamin, Inc., New York, 1965).

The expectation value of the nonlinear second-harmonic current density is

$$\langle j(2\omega,2\mathbf{q})\rangle=\sum_{\mathbf{k}}\langle\mathbf{k}-2\mathbf{q}|j^{(0)}|\mathbf{k}\rangle\langle\mathbf{k}|\rho^{(2\omega)}|\mathbf{k}-2\mathbf{q}\rangle$$
$$=(he/m)\sum_{\mathbf{k}}(\mathbf{k}-\mathbf{q})\langle\mathbf{k}|\rho^{(2\omega)}|\mathbf{k}-2\mathbf{q}\rangle. \quad (7)$$

The nonlinear current density given by Eqs. (5) and (7) creates the second-harmonic field. At optical frequencies the change in electron energy and the damping rate are small compared to the photon energy. If the denominator in Eq. (5) is thus approximated by $2\hbar\omega$, one finds immediately from the relations $\sum\mathbf{k}f(\epsilon_{\mathbf{k}})=0$, $\sum\mathbf{q}f(\epsilon_{\mathbf{k}})=N\mathbf{q}$, where N is the number of electrons per unit volume, that the current density is given by

$$\mathbf{j}^{\mathrm{NL}}(\mathbf{r},t)=[Ne^3\mathbf{q}A_0^2/2m^2\omega c^2\epsilon_{\mathrm{SCF}}(2\omega,2\mathbf{q})]$$
$$\times\exp(2i\mathbf{q}\cdot\mathbf{r}-2i\omega t).$$

The corresponding nonlinear susceptibility is obtained by replacing $\mathbf{j}(2\omega)$ by $-2i\omega\mathbf{P}(2\omega)$ and the vector potential $\mathbf{A}$ by $(ic/\omega)\mathbf{E}$. One finds

$$\mathbf{P}^{\mathrm{NLS}}=\chi^{\mathrm{NL}}(2\omega):\mathbf{E}^2=[-iNe^3E_0^2\mathbf{q}/4m^2\omega^4\epsilon_{\mathrm{SCF}}(2\omega,2\mathbf{q})]$$
$$\times\exp(2i\mathbf{q}\cdot\mathbf{r}-2i\omega t). \quad (8)$$

This result for the longitudinal second-harmonic polarization could also have been obtained more directly from the relation that the divergence of this polarization equals the second-harmonic charge density:

$$\mathrm{div}\,\mathbf{P}(2\omega)=e\sum_{\mathbf{k}}\langle\mathbf{k}|\rho^{(2\omega)}|\mathbf{k}-2\mathbf{q}\rangle$$
$$\mathbf{P}^{\mathrm{NLS}}=[2ie\mathbf{q}/(2q)^2]\sum_{\mathbf{k}}\langle\mathbf{k}|\rho^{(2\omega)}|\mathbf{k}-2\mathbf{q}\rangle.$$

Substitution of Eq. (5) and expansion of its denominator in the approximation, $\hbar^2/2m\{2\mathbf{k}\cdot(2\mathbf{q})+(2\mathbf{q})^2\}\ll 2\hbar\omega$, again yields Eq. (8). In the limit of low electron density, $2\omega\gg\omega_p$ and $\epsilon_{\mathrm{SCF}}\sim 1$, and substituting $q/\omega=c^{-1}$, one fines the same nonlinear susceptibility $(-iNe^3/4m^2c\omega^3)$ as was first found by very elementary considerations.[17] The occurrence of ϵ_{SCF} in the denominator was not explicitly noted before, but its physical origin is evident from the present calculation. Since the polarization is longitudinal there is no second-harmonic power radiated in the plasma. There is, however, a reflected harmonic wave with the electric vector in the plane of reflection. The reflected-harmonic amplitude has been expressed in terms of the nonlinear volume polarization by Bloembergen and Pershan.[18] Equation (4.12) or (4.13) of their paper with $\alpha=0$ gives,

$$E_{R,\mathrm{vol}}(2\omega)=\frac{4\pi P^{\mathrm{NLS}}\epsilon^{-1/2}(\omega)\sin\theta_i}{\epsilon^{1/2}(2\omega)\{1-\epsilon^{-1}(2\omega)\sin^2\theta_i\}^{1/2}+\epsilon(2\omega)\cos\theta_i}. \quad (9)$$

Here θ_i is the angle of incidence of the fundamental wave on the plane plasma boundary, $\epsilon(\omega)$ is the transverse linear dielectric constant of the plasma. P^{NLS} is given by Eq. (8) and it should be remembered that E_0 in that expression is the electric field after refraction just inside the plasma. This E_0 should be computed from the incident amplitude with the appropriate linear Fresnel equation. For a metallic reflector this implies a considerable reduction in its numerical value. A quantitative discussion will be postponed until the next section. There it will be shown that there are surface terms which may contribute more than the volume polarization. This is perhaps not too surprising, since the volume term is essentially a magnetic dipole term which vanishes, for constant ω, in the limit $q\to 0$.

When the incident electric vector is normal to the plane of incidence, there is, however, no surface contribution. In this case the reflected amplitude $E_R(2\omega)$ from Eqs. (8) and (9) and Fresnel's equation may be expressed in terms of the incident amplitude $E^{(i)}$ as follows:

$$E_R(2\omega)=\frac{-4\pi iNe^3}{4m^2c\omega^3(1-\frac{1}{4}x^2)}\times\frac{\sin\theta_i}{[(\cos^2\theta_i-\frac{1}{4}x^2)^{1/2}+(1-\frac{1}{4}x^2)\cos\theta_i]}\times\frac{4\cos^2\theta_i}{[\cos\theta_i+(\cos^2\theta_i-x^2)^{1/2}]^2}(E_i^{(i)})^2. \quad (10)$$

Here $x=\omega_p/\omega$, and $\omega_p^2=4\pi Ne^2/m$ is the plasma frequency. The dielectric constants have been taken in the limit $q\to 0$,

$$\epsilon(\omega)=1-\omega_p^2/\omega^2,$$
$$\epsilon(2\omega)=\epsilon_{\mathrm{SCF}}(2\omega,0)=1-\omega_p^2/4\omega^2.$$

Except for the factor $\epsilon_{\mathrm{SCF}}^{-1}$, noted above, this result agrees with a calculation by Jha[19] on the basis of the Boltzmann transport equation for a free-electron gas.

III. THE SECOND-HARMONIC SURFACE POLARIZATION

Jha called attention to the importance of surface terms which are connected with the discontinuity of the normal component of the electric field at the boundary. For these terms it is essential that the incident field has a component in the plane of incidence. Choose a coordinate system where this plane is the xz plane and let $\hat{z}$ be the direction normal to the boundary. According to the macroscopic equations the discontinuity in the normal component is described by

$$\partial E_z/\partial z=[1-\epsilon^{-1}(\omega)]E_{z=+0}\delta(z),$$

[17] See Ref. 3, or N. Bloembergen, *Nonlinear Optics* (W. A. Benjamin and Company, New York, 1965).

[18] N. Bloembergen and P. S. Pershan, Phys. Rev. 128, 606 (1962). There is a misprint in Eq. (4.12) of this paper. The denominator of the last term should read "$\epsilon_T^{1/2}\epsilon_R^{1/2}\cos\theta_T+\epsilon_T\cos\theta_R$" instead of "$\epsilon_T^{1/2}\epsilon_S^{1/2}\cos\theta_T+\epsilon_T\cos\theta_R$."

[19] See Ref. 4. The authors are indebted to Dr. Jha for a helpful discussion.

where $E_{z=+0}$ is the normal component of the transmitted wave just outside the plasma. It consists of the sum of the normal components of the incident and reflected waves and is $\epsilon(\omega)$ times larger than the normal component just inside the plasma.

In a microscopic picture there is of course no strict discontinuity. The normal component E_z varies rapidly over about one Thomas-Fermi screening length in the case of a metal. In the case of semiconductors, insulators or any other medium one can still expect that the field component changes rapidly over about one interatomic distance. For a detailed calculation a precise knowledge of the surface potential and the surface-state wave function would be required.

Fortunately, the radiation field of a thin slab of polarization, $0 \leq z \ll \lambda$, does not depend sensitively on the distribution of the polarization as a function of z, but only on the integral $\int P dz$. The second-harmonic surface polarization may therefore be calculated in the following manner: The discontinuity in the normal component of the fundamental frequency induces a free charge density at the surface

$$\rho(\mathbf{r},\omega) = (1/4\pi e)[1-\epsilon^{-1}(\omega)]E_{z=+0}\delta(z)e^{ik_x x - i\omega t}. \quad (11)$$

For a free-electron gas the current density induced by a field $A(\mathbf{r},\omega)$ for an electron density $\rho^{(0)}(\mathbf{r}) = N$ is

$$\langle \mathbf{j}^{(1)}(\mathbf{r},\omega)\rangle = \mathbf{j}^{(1)}(r,\omega)\rho^{(0)} = (Ne^2/mc)\mathbf{A}(\mathbf{r},\omega) = (Ne^2/im\omega)\mathbf{E}(\mathbf{r},\omega).$$

In the same manner the second-harmonic current density corresponding to the oscillating free charge density (11) at the surface is

$$\langle \mathbf{j}^{(\mathrm{surf})}(2\omega)\rangle = (e/4\pi i m\omega)[1-\epsilon^{-1}(\omega)] \times \mathbf{E}(\omega)E_{z=+0}(\omega)\exp(2ik_x x). \quad (12)$$

For the normal component of this surface current density there is some ambiguity in Eq. (12) whether one should take the normal component of $\mathbf{E}(\omega)$ just outside or inside the plasma. If one takes half the sum of these values, the normal surface current density becomes

$$j_z^{(\mathrm{surf})}(\mathbf{r},2\omega) = (e/4\pi i m\omega)[1-\epsilon^{-1}(\omega)] \times [\tfrac{1}{2}+\tfrac{1}{2}\epsilon^{-1}(\omega)][E_{z=+0}(\omega)]^2\exp(2ik_x x). \quad (13)$$

It should be noted that this normal component will make the dominant contribution to the reflected harmonic intensity from highly reflecting materials. It follows from the Fresnel equations that the tangential components of the incident and reflected waves at ω nearly cancel each other, while the normal component just outside the surface is almost twice the normal component of the incident field. The normal component $E_{z=+0}$ is expressed in terms of the incident electric field amplitude $E^{(i)}$ which makes an angle φ with the plane of incidence and the direction of the incident beam makes an angle of incidence θ_i with the normal,

$$E_{z=+0}(\omega) = \frac{2\cos\theta_i \sin\theta_i}{\cos\theta_i + \epsilon^{-1/2}(\omega)(1-\epsilon^{-1}(\omega)\sin^2\theta_i)^{1/2}} E_i^{(i)}\cos\varphi. \quad (14)$$

From Eqs. (13) and (14) it follows that the second-harmonic intensity generated by this surface term is proportional to $\cos^4\varphi$. This dependence has recently been observed by Brown and co-workers[20] for second-harmonic generation from metallic silver. It is therefore of interest to compare the intensity produced by the surface term with the volume terms of the preceding section. The radiation from a thin slab-source distribution has been given by Bloembergen and Pershan.[21] Their Eq. (6.22) may be used with the following substitutions, $-2i\omega P^{\mathrm{NLS}}d = j_s^{\mathrm{surf}}$, $\alpha = \pi - \theta_s$, $\epsilon_T = \epsilon(2\omega)$, $\epsilon_M^{-1/2}\sin\theta_M = \sin\theta_i$, $\epsilon_M = \epsilon(\omega)$. The result is

$$E_R^{\mathrm{surf}}(2\omega) = \frac{2\pi\epsilon^{-1}(\omega)\sin\theta_i c^{-1}}{\cos\theta_i + \epsilon^{-1/2}(2\omega)(1-\epsilon^{-1}(2\omega)\sin\theta_i)^{1/2}} \times j_s^{\mathrm{surf}}(2\omega). \quad (15)$$

When θ_i approaches zero, this field rapidly becomes very small, because $j_s(2\omega)$ itself approaches zero, as well as the factor $\sin\theta_i$. In that case the tangential components of the surface source in Eq. (12) should be taken into account. The radiation field can quite generally be calculated with Eqs. (6.12) and (6.22) of Ref. 18. The resulting harmonic amplitudes should be added to those obtained from the volume polarization and subsequently squared to obtain the second-harmonic intensity. The resulting equations for arbitrary polarization direction φ and arbitrary angle of incidence θ_i of the fundamental field are cumbersome and will not be reproduced here. The detailed results are essentially the same as those of Jha.[21]

It is, however, of interest to compare the order of magnitude of the volume term given by Eqs. (8) and (9) with the surface term given by Eqs. (12), (14), and (15) near angles $\theta_i = \varphi = \pi/4$, where the angular factors do not have zero's. Leaving out all angular factors, the ratio of the second-harmonic amplitudes resulting from the surface contribution given by Eq. (15) and the volume contribution given by Eq. (10) has the order of magnitude $(c^2/\omega_p^2)\epsilon(\omega)$, or about unity for $\omega < \omega_p$. On the basis of these calculations, it is doubtful that the observed SHG from metallic silver by Brown *et al.* has its origin in a plasma effect. When the experimental value[22] $\omega_p/\omega = 2.2$, instead of 5, is used in Jha's equations, an observable volume effect should remain, when

[20] F. Brown, R. E. Parks, and A. M. Sleeper, Phys. Rev. Letters 14, 1029 (1965).

[21] S. S. Jha, Phys. Rev. Letters 15, 412 (1965). This paper appeared after our manuscript had been submitted. The experimental points should be compared with a theoretical calculation for $\omega_p/\omega = 2.2$ rather than 5.

[22] H. Ehrenreich and H. R. Phillip, Phys. Rev. 128, 1622 (1962).

the incident field is polarized normal to the plane of incidence.

It has been suggested that the silver ion cores[23] of the surface layer play a dominant role in the SHG. Further support that one does not deal with a plasma effect comes from the observation by Bloembergen and Chang[23] that silicon, germanium and other insulating material with bulk inversion symmetry also show a reflected second-harmonic intensity with a $\cos^4\varphi$ dependence on the angle between the incident electric field and the plane of incidence. The atoms in the surface layer are not at positions of inversion symmetry, and if the incident electric field has a component normal to the surface, large harmonic dipole moments can be induced in these atoms.

The dominant term for these bound electrons in the interaction Hamiltonian is the term

$$\mathcal{H}^{(1)} = -(e/2mc)(\mathbf{p}\cdot\mathbf{A}+\mathbf{p}\cdot\mathbf{A}) \approx -(eh/2imc)(\partial A_z/\partial z + 2\mathbf{A}\cdot\nabla).$$

It should be kept in mind that A_z varies rapidly in the first atomic layer and that $\partial A_z/\partial z$ there is so large that the "quadrupole-like" contribution from this term has the same order of magnitude as an electric dipole contribution. The detailed matrix elements of $\mathcal{H}^{(1)}$, which is very inhomogeneous over the surface orbital function ψ_z, are difficult to evaluate. Because both $\mathcal{H}^{(1)}$ and ψ_z have even and odd terms in z, the following nonlinear current density is induced in the surface atoms,

$$\mathbf{j}_{\text{bound}}(2\omega,\mathbf{r}) = N_0 \sum_{n,n'} \frac{\langle\psi_z(\mathbf{r}_0)|\mathbf{j}^{(0)}(\mathbf{r})|n(\mathbf{r}_0)\rangle\langle n|\mathcal{H}^{(1)}|n'\rangle\langle n'|\mathcal{H}^{(1)}|\psi_z\rangle}{(W_z-W_n+\hbar\omega)(W_z-W_{n'}+2\hbar\omega)} + \text{other terms which differ in the order of the operators and in the frequency denominators.} \quad (16)$$

The number of atoms per unit volume is N_0. The current density operator is defined by

$$\mathbf{j}^{(0)}(\mathbf{r}) = \delta(\mathbf{r}-\mathbf{r}_0)\cdot(he/2im)\nabla + (he/2im)\nabla\delta(\mathbf{r}-\mathbf{r}_0). \quad (17)$$

For media with inversion symmetry, the second harmonic source density given by Eq. (16) is appreciable only in a surface layer of thickness d, where d is about one interatomic distance, or the Thomas-Fermi screening distance in a metal.

A rough estimate of the bound surface states can be obtained as follows. It is known that the core polarizability of silver ions contributes appreciably to the dielectric constant of the metal in the near ultraviolet.[24] It is therefore not unreasonable to assume the same nonlinear polarizability for a silver ion at the surface as for a GaSb or InAs molecule in the bulk of those piezoelectric crystals. The current density integrated over a layer of thickness d gives therefore a surface source $2i\omega\chi^{\text{NL}}dE_{z=+0}^2$, where $\chi^{\text{NL}}\sim 10^{-6}$ esu as for GaSb, and $d\sim 2\times 10^{-8}$ cm. This should be compared with the plasma-surface source of magnitude $(e/4\pi m\omega)\times E_{z=+0}^2$ according to Eq. (13). One finds for the ratio of bound-surface to plasma-surface contribution $8\pi m\omega^2\times\chi^{\text{NL}}de^{-1}\approx 8$ in our numerical example. For the second-harmonic intensity this ratio must be squared, and the bound electron in the surface layer could easily contribute one or two orders of magnitude more than the total plasma contribution. For the bound-surface electrons the same symmetry considerations hold as for the plasma effect. The surface layer is amorphous and essentially isotropic for directions in the plane of the boundary. The current density has tangential component j_x proportional to E_xE_z and j_y proportional to E_yE_z. The normal component j_z proportional to E_z^2 will be dominant for good reflectors since the normal component E_z is much larger than the tangential components in that case. The second-harmonic intensity is consequently proportional to j_z^2 or $\cos^4\varphi$, and the electric field $E_R(2\omega)$ should lie in the plane of reflection. The effect should occur quite generally at the surface of dense polarizable media, including liquids. The SHG should not depend strongly on the plasma density. The available observations on silver, silicon, and germanium are in agreement with this picture.

IV. THE RAMAN SUSCEPTIBILITY OF A PLASMA

The next higher order nonlinearities may be calculated in a similar manner. In principle, again volume and surface terms should be considered. The most important case is the volume effect, which occurs when two electromagnetic waves traverse the plasma, with a difference in frequency close to the plasma frequency. The vector potential in Eq. (2) now consists of four terms with amplitudes A_L, A_L^*, A_z, and A_z^* and frequencies ω_L, $-\omega_L$, ω_z, and $-\omega_z$, respectively. The dominant term in the density-matrix quadratic in the field amplitudes results from the resonance which occurs when $\omega_L-\omega_z$ is near the plasma frequency. In analogy with Eq. (5) one finds immediately,

$$\langle\mathbf{k}|\rho^{(\omega_z-\omega_L)}|\mathbf{k}+\mathbf{q}_z-\mathbf{q}_L\rangle = \frac{f_0(\epsilon_{\mathbf{k}+\mathbf{q}_z-\mathbf{q}_L})-f_0(\epsilon_{\mathbf{k}})}{\epsilon_{\mathbf{k}+\mathbf{q}_z-\mathbf{q}_L}-\epsilon_{\mathbf{k}}+\hbar(\omega_z+\omega_L)+i\Gamma}\,\frac{2e^2A_zA_L^*}{2mc^2} \times\epsilon_{\text{SCF}}(\omega_L-\omega_z,\,\mathbf{q}_L-\mathbf{q}_z).$$

For $\omega_L-\omega_z\sim\omega_p$, $\text{Re}\,\epsilon_{\text{SCF}}\approx 0$, a resonance occurs. Large density fluctuations are induced at the difference frequency, which beat again with the incident laser field at ω_L. In this manner a current density at the Stokes frequency ω is induced, which is cubic in the field

[23] See paper by N. Bloembergen and R. K. Chang in Ref. 11.
[24] See Ref. 22.

amplitudes,

$$\mathbf{j}_{\text{Raman}}(\omega_s,\mathbf{q}_s)=\sum_{\mathbf{k}}\langle\mathbf{k}|\rho^{+(\omega_s-\omega_L)}|\mathbf{k}+\mathbf{q}_s-\mathbf{q}_L\rangle\langle\mathbf{k}+\mathbf{q}_s-\mathbf{q}_L|-(e^2/mc)A_L|\mathbf{k}+\mathbf{q}_s\rangle$$
$$=\frac{-e^4|A_L|^2A_s}{m^2c^3\epsilon_{\text{SCF}}^*(\omega_L-\omega_s,\,\mathbf{q}_L-\mathbf{q}_s)}\times\sum_{\mathbf{k}}\frac{f_0(\epsilon_{\mathbf{k}+\mathbf{q}_s-\mathbf{q}_L})-f_0(\epsilon_{\mathbf{k}})}{\epsilon_{\mathbf{k}+\mathbf{q}_s-\mathbf{q}_L}-\epsilon_{\mathbf{k}}+\hbar(\omega_s-\omega_L)-i\hbar\Gamma}. \quad (18)$$

When the plasmon energy is considered to be the leading term in the denominator, $\hbar(\omega_L-\omega_s)\gg(\hbar^2/2m)\times(\mathbf{q}_L-\mathbf{q}_s)\cdot\mathbf{k}_F$ and $\omega_L-\omega_s>\Gamma$, an expansion of the denominator yields for Eq. (18) the simple expression,

$$\mathbf{j}_{\text{Raman}}(\omega_s,\mathbf{q}_s)=\frac{-Ne^4|A_L|^2\mathbf{A}_s}{m^3c^5\epsilon_{\text{SCF}}^*(\omega_L-\omega_s,\,\mathbf{q}_L-\mathbf{q}_s)}\frac{(\mathbf{q}_L-\mathbf{q}_s)^2}{(\omega_L-\omega_s)^2}. \quad (19)$$

For forward Raman scattering the last factor may be replaced by c^{-2}. It should be noted that the picture of resonance with a plasma wave only has validity for $|\mathbf{q}_L-\mathbf{q}_s|\ll L_D^{-1}$ where L_D is the Debye length of the plasma. For larger values the real part of $\epsilon_{\text{SCF}}(\omega,\mathbf{q}_L-\mathbf{q}_s)$ cannot be made equal to zero. For gaseous plasmas, the resonance occurs only near the forward direction. At the plasma resonance ϵ_{SCF}^* is negative imaginary and has a value $-i(\omega_p\tau)^{-1}$, where the decay time for the power is determined by the Landau damping rate and the collision rate $\tau^{-1}=\tau_{\text{Landau}}^{-1}+\tau_{\text{coll}}^{-1}$. One may again replace the current density by an equivalent polarization and the vector potentials by the corresponding electric field amplitudes. In this manner the Raman susceptibility for a plasma is introduced. For resonant scattering in the forward direction one finds

$$\mathbf{P}(\omega_s,\mathbf{q}_s)=\chi_{\text{Raman}}|E_L|^2\mathbf{E}_s=\frac{-iNe^4}{\omega_s^2\omega_L^2m^3c^5(\omega_p\tau)}|E_L|^2\mathbf{E}_s. \quad (20)$$

Off resonance, where $\epsilon_{\text{SCF}}\sim1$, one should replace $i\omega_p\tau$ by unity in Eq. (20). In that case the same formula could have been obtained from a very elementary independent electron model.

The Raman polarization given by Eq. (20) is 90° out of phase with the Stokes field $\mathbf{E}_s$. The susceptibility is negative imaginary and produces an exponential gain at the frequency ω_s. If one takes a plasma characterized by the same parameters as the case considered by Kroll, Ron, and Rostoker,[25] $n_0=10^{14}$ cm^{-3}, $\omega_p\tau=10^3$, and $\omega_L=\omega_s+\omega_p=2\pi(4\times10^{14})^{-1}$, one finds $\chi_{\text{Raman}}^{\text{plasma}}\approx10^{-22}$ esu. This is about ten orders of magnitude smaller than the Raman susceptibility of liquids ordinarily used in Raman lasers. Since the plasma frequency is very small compared to the light frequency in this example, the susceptibility can be considerably enhanced by introducing a small angle between the Stokes and the laser beam. In that case one should return to the more general expression Eq. (19). The optimum value of

$$[\epsilon_{\text{SCF}}''(\omega_L-\omega_s,\,\mathbf{q}_L-\mathbf{q}_s)]^{-1}(\mathbf{q}_L-\mathbf{q}_s)^2(\omega_L-\omega_s)^{-2}$$

can be made about a factor 10^4 larger in this example than $(\omega_p\tau)c^{-2}$ which it assumes in the forward direction. The nonlinear susceptibility for this optimum direction, occurring at angle of about 10^{-2} radian between the two light beams, is still six orders of magnitude smaller than that in ordinary Raman liquids. It is doubtful that the stimulated Raman effect in a plasma will lead to observable effects.

Since Kroll and co-workers arrived at a more optimistic conclusion, it is of interest to show that our result can be reconciled numerically with their equation for a scattering cross section per unit solid angle. They, and other workers, considered a scattering process involving four light quanta with frequencies ω_1, ω_2, ω_3, and ω_4, satisfying the energy and momentum conservation relationships $\omega_4-\omega_3=\omega_2-\omega_1=\omega_p$, and $\mathbf{q}_4-\mathbf{q}_3=\mathbf{q}_2-\mathbf{q}_1$. Although the calculation for this cross section is considerably more complicated in scattering theory than the calculation of an inelastic Raman scattering involving only the two quanta ω_L and ω_s, the calculation of the corresponding complex nonlinear susceptibility is straightforward and essentially the same as for the Raman process. The complex susceptibilities automatically take account of all questions of phase coherence and elastic and inelastic scattering processes. In direct analogy to Eq. (20), one finds a polarization at ω_4,

$$P^{\text{NL}}(\omega_4=\omega_2+\omega_3-\omega_1)=\frac{-n_0e^4(\mathbf{q}_2-\mathbf{q}_1)^2}{\omega_1\omega_2\omega_3\omega_4m^3(\omega_2-\omega_1)^2\epsilon_{\text{SCF}}^*(\omega_2-\omega_1,\,\mathbf{q}_2-\mathbf{q}_1)}E_2E_3E_1^*. \quad (21)$$

For $\omega_2=\omega_3=\omega_L$, ω_4 represents, of course, the anti-Stokes frequency.

Consider a homogeneous interaction region in the plasma of volume $V=Al$, where A is the cross-sectional area of the three beams E_1, E_2, and E_3 and l is the length. The field strength E_4 of the phase matched wave at ω_4, which is parametrically generated in the volume V, is given by[26]

$$E_4=4\pi P^{\text{NL}}(\omega_4=\omega_2+\omega_3-\omega_1)\omega_4c^{-1}l. \quad (23)$$

The total power radiated at ω_4 is

$$I_4=\frac{c}{2\pi}A|E_4|^2=\frac{8\pi n_0^2e^8|E_1|^2|E_2|^3|E_3|^2}{m^6c^5\omega_1^2\omega_2^2\omega_3^2|\epsilon_{\text{SCF}}|^2}Al^2. \quad (23)$$

[25] See Ref. 8.

[26] See Ref. 17.

A factor 2π rather than 8π is used in the denominator of the Poynting vector because our amplitudes are defined in Eq. (2) as twice the conventional ones. In this form the result may be compared with the scattering cross section per electron for a four-photon collision, $\omega_3+\omega_2\rightarrow\omega_1+\omega_4$, given by Kroll, Ron, and Rostoker,

$$\frac{d\sigma}{d\Omega}=\frac{(e^2/mc^2)^2k^4|E_1|^2|E_2|^2}{32(2\pi)^3m^2n_0\omega_1^2\omega_2^2|\epsilon_{\rm SCF}|^2}\delta(\mathbf{k}-\Delta\mathbf{k}), \quad (24)$$

where $k^2=\omega_p^2/c^2=4\pi n_0e^2/mc^2$ and $\delta(\mathbf{k}-\Delta\mathbf{k})\approx V$, and the amplitudes now have the conventional definition. The total cross section for the volume V, integrated over the solid angle $d\Omega$, which is determined by the diffraction limit from an area A, $d\Omega=(4\pi^2c^2/\omega_3\omega_4)A^{-1}$, is obtained by multiplying Eq. (24) by $n_0Ald\Omega$,

$$\sigma_{\rm total}=\frac{\pi n_0^2e^8A^2|E_1|^2|E_2|^2}{m^6c^6\omega_1^2\omega_2^2\omega_4\omega_3|\epsilon_{\rm SCF}|^2}. \quad (25)$$

The number of incident quanta in the beam at ω_3 per second is $c|E_3|^2A/8\pi\hbar\omega_3$. The number of scattered quanta at ω_4 is

$$c|E_3|^2\sigma_{\rm total}/8\pi\hbar\omega_3$$

and the total scattered intensity at ω_4 is

$$I_4=(\omega_4/\omega_3)c|E_3|^2\sigma_{\rm total}/8\pi. \quad (26)$$

When Eq. (25) is substituted into Eq. (26), a result is obtained that is a factor 2^6 smaller than given by Eq. (23). This difference may be ascribed to the difference in definition of the field amplitudes. The amplitudes defined by Eq. (2) and used in Eq. (23) are a factor 2 smaller than the conventional amplitudes used in Eqs. (24–26).

Although there is formal agreement between the two results, the rather more optimistic estimate of detectability by Kroll and co-workers can be traced to their use of the scattering cross section per unit solid angle. For a diffraction limited beam the total available solid angle is quite small, and the total scattered intensity is probably more significant from an experimental point of view. Baym and Hellwarth have independently arrived at a similar conclusion.[27]

In a metal plasma the electron density can be higher by eight orders of magnitude than in the preceding example, while the quality factor $\omega_p\tau$ of the plasma resonance in silver can be taken as 10^2. The nonlinear susceptibiliby for two ultraviolet beams could thus be substantially higher than a gaseous plasma. Unfortunately the transparency of metals for frequencies $\omega>\omega_p$ is far from perfect due to excitation of core electrons. The absorption from powerful ultraviolet beams, if these were available, would probably be prohibitive. The best possibility to detect the stimulated Raman effect in a plasma would appear to be for infrared beams in a semiconductor plasma. Spontaneous inelastic or Raman scattering should be easier to detect than the stimulated effects.

V. THE INTERACTION BETWEEN TWO LIGHT WAVES AND A PLASMA WAVE

The Raman and Brillouin effect in liquids and solids can be described as the parametric interaction between two light waves and a vibrational wave. When the optical or acoustical phonon wave is heavily damped, this description is equivalent to one in terms of Raman susceptibilities.[28] In this section the Raman effect in a plasma will be described in terms of a parametric interaction between two light waves and a plasma wave. An equivalent discussion with detailed numerical examples has independently been given by Cosimar.[29]

Consider a small volume element at the point $\mathbf{r}$. Let the average deviation of the electrons from their equilibrium position in this volume element be $\mathbf{u}(\mathbf{r})$. Introduce normal coordinates Q_k as the Fourier transform of this average deviation or local strain of the electron gas,

$$\mathbf{Q}_k=\int\mathbf{u}(\mathbf{r})e^{-i\mathbf{k}\cdot\mathbf{r}}d^3r.$$

The canonical conjugate to this variable is $\mathbf{P}_k$. The Hamiltonian density for the plasma waves then takes the form,[30]

$$\mathcal{H}_{\rm plasma}=\tfrac{1}{2}\sum_k((1/Nm)\mathbf{P}_k\cdot\mathbf{P}_{-k}+\alpha k^2\mathbf{Q}_k\cdot\mathbf{Q}_{-k}+4\pi N^2e^2\mathbf{Q}_k\cdot\mathbf{Q}_{-k}). \quad (27)$$

Here N is the average number of electrons per unit volume and α is the bulk modulus of the electron gas. The fluctuation in the electron density from the average due to the presence of plasma waves is

$$\delta\rho(\mathbf{r})=N\,\mathrm{div}\mathbf{u}=iN\sum_k\mathbf{k}\cdot\mathbf{Q}_ke^{i\mathbf{k}\cdot\mathbf{r}}.$$

The change in the interaction of the two light waves with the electrons in a unit volume due to the presence of the plasma waves is consequently

$$\mathcal{H}_{\rm int}=(e^2/2mc^2)\mathbf{A}^2\delta\rho(\mathbf{r}),$$

where

$$\mathbf{A}=\mathbf{A}_Le^{i\mathbf{q}_L\cdot\mathbf{r}-i\omega_Lt}+\mathbf{A}_se^{i\mathbf{q}_s\cdot\mathbf{r}-i\omega_st}+\text{c.c.}$$

When all nonresonant perturbations are truncated, the interaction Hamiltonian density between the two linear parallel polarized light waves and the longitudinal plasma waves ($\mathbf{Q}\|\mathbf{k}$) becomes,

$$\mathcal{H}_{\rm int}=(iNe^2/mc^2)\sum_k kA_LA_s^*Q_k^*e^{i(\mathbf{q}_L-\mathbf{q}_s-\mathbf{k})\cdot\mathbf{r}}+\text{c.c.} \quad (28)$$

[27] Paper by G. Baym and R. W. Hellwarth in Ref. 11.

[28] See Ref. 15.

[29] G. C. Cosimar (private communication). The authors are indebted to Dr. Cosimar for receiving a copy of a forthcoming paper.

[30] See, for example, C. Kittel, *Quantum Theory of Solids* (John Wiley & Sons, Inc., New York, 1963) p. 35.

The equations of motion for the plasma coordinate are

$$\dot{P}_k = -\partial(\mathcal{H}_{\text{plasma}}+\mathcal{H}_{\text{int}})/\partial Q_k,$$
$$\dot{Q}_k = +\partial(\mathcal{H}_{\text{plasma}}+\mathcal{H}_{\text{int}})/\partial P_k.$$

These equations of motion can be combined into a wave equation for Q_k. Because of the presence of $\mathcal{H}_{\text{int}}$ a driving term proportional to the light amplitudes $A_L A_s^*$ is added to the plasma wave equation. Landau damping and damping by collisions may be taken into account by a phenomenological damping term,

$$\ddot{Q}_k+\alpha\nabla^2\dot{Q}_k+\omega_p^2 Q_k = (ie^2k/m^2c^2)A_L A_s^*+(2i\omega_k/\tau')Q_k. \quad (29)$$

The exponential factor

$$\exp\{i(\mathbf{q}_L-\mathbf{q}_s-\mathbf{k})\cdot\mathbf{r}-i(\omega_L-\omega_s-\omega_k)t\}$$

can be dropped from the inhomogeneous driving term, because the effect of coupling between the light waves and plasma wave will be small unless the conditions of conservation of energy and momentum are satisfied, $\omega_L-\omega_s=\omega_k$ and $\mathbf{q}_L-\mathbf{q}_s=\mathbf{k}$. The plasma wave concept only has validity, if its wavelength is long compared to the characteristic Debye length. For the most important case of forward scattering with parallel laser and stokes beams this condition will usually be satisfied. One may then write $k=q_L-q_s=\omega_p/c$, because the dispersion in the plasma frequency will then be negligible since $(\alpha/Nm)(q_L-q_s)^2\ll\omega_p^2$. The characteristic time τ' in Eq. (29) refers to the decay time for the amplitude. The decay rate for the power is related to the imaginary part of the longitudinal dielectric constant by $2\tau'^{-1}=\epsilon_{SCF}''\omega_p$.

The wave equations for the light amplitudes A_L and A_s are also augmented by a nonlinear term, because the interaction Hamiltonian gives rise to a nonlinear current density,

$$j^{NL}(\omega_s) = -c\partial\mathcal{H}_{\text{int}}/\partial A_L^* = (+iNe^2/mc)kA_L Q_k^* \quad (30)$$

and a similar expression for $j^{NL}(\omega_L)$. The wave equations for the two light waves become, consequently,

$$-\ddot{A}_L+c^2\nabla^2 = (4\pi iNe^2/m)kA_s Q_k, \quad (31)$$
$$-\ddot{A}_s+c^2\nabla^2 = (4\pi iNe^2/m)kA_L Q_k^*. \quad (32)$$

The set of three coupled nonlinear wave equations is familiar from the Brillouin and Raman effect in other media. If the laser amplitude can be taken as a constant parameter, a set of two linear coupled equations (29) and (32) for A_s and Q results. An exact solution can readily be written down, but the following approximate solution will be adequate for our purposes. Since the plasma wave is heavily damped its amplitude is essentially the driven steady state value, when the right-hand side of Eq. (29) is separately put equal to zero. When the value of Q so obtained is substituted back into Eq. (30), one obtains for forward scattering,

$$j^{NL}(\omega_s) = \frac{Nc^4k^2}{m^3c^3\omega_p^2\epsilon_{SCF}''}|A_L|^2A_s = \frac{Nc^4}{m^3c^5\epsilon_{SCF}''}|A_L|^2A_s. \quad (33)$$

This is identical to the result of Eq. (19) taken at resonance, $\epsilon_{SCF}'=0$. The equivalence of the two different ways to describe the interaction between photons and plasmons is thus established. When the value of Q is substituted into the wave equation (32), one obtains the exponential gain at the Stokes frequency. Coupling with anti-Stokes waves in the plasma, etc., can of course be treated in the same manner.

VI. CONCLUSION

The optical nonlinearities of a plasma can be treated by the same methods that have been used to describe the nonlinear optical properties of other media. The nonlinearities of the plasmas are generally smaller by many orders of magnitude, because they would vanish altogether for free electrons in the electric dipole approximation.

Although spontaneous nonlinear scattering processes in certain plasmas may be detectable, stimulated Raman effects would hardly be accessible to experimental observation at optical frequencies. The situation is of course much more favorable in the far infrared and microwave region. Even the lower order nonlinear process of second-harmonic generation from a plasma has not been established experimentally at optical frequencies. The second-harmonic radiation observed from a silver surface is shown to have its origin in the nonlinearity of bound electrons in the ion cores of a monatomic surface layer.

Reprinted from THE PHYSICAL REVIEW, Vol. 145, No. 1, 390, 6 May 1966
Printed in U. S. A.

Optical Nonlinearities in a Plasma, N. BLOEMBERGEN AND Y. R. SHEN [Phys. Rev. **141**, 298 (1966)]. The factor $\epsilon_{SCF}^{-1}=(1-\frac{1}{4}x^2)^{-1}$ should be omitted from the right-hand side of Eq. (10). Although the straightforward substitution of Eq. (8) into Eq. (9) includes this factor, this procedure is incorrect. The reason is that the self-consistent nonlinear longitudinal polarization given by Eq. (8) includes a part corresponding to the linear polarization induced by the self-consistent longitudinal component of the field. This part must be subtracted before the substitution into Eq. (9), derived by Bloembergen and Pershan, is made. In their derivation of Eq. (9) a different gauge, with $\phi_s=0$, was used, while Eq. (8) in this paper is derived in a gauge with a nonvanishing ϕ_s. The result is that the factor ϵ_{SCF}^{-1} must be dropped and our Eq. (10) becomes identical with the volume term derived by Jha. The authors are indebted to Dr. S. S. Jha and Dr. A. Pine for clarifying discussions.

The name in Ref. 29 is misspelled. Reference 29 should now read: G. C. Comisar, Phys. Rev. **141**, 200 (1966).

APPENDIX IX

Reprinted from THE PHYSICAL REVIEW, Vol. 143, No. 2, 372-384, 11 March 1966
Printed in U. S. A.

Interaction between Light Waves and Spin Waves*

Y. R. SHEN
Department of Physics, University of California, Berkeley, California
AND
N. BLOEMBERGEN†
Department of Electrical Engineering, University of California, Berkeley, California
(Received 1 September 1965)

The coupling of photons and magnons can be treated by the same methods developed for the coupling between photons and phonons. The coupled wave equations are derived directly from the Hamiltonian density for the quantized fields with the density-matrix formalism. The similarity between the spin Raman effect and the vibrational Raman effect is emphasized and it is shown that the spin Raman effect will usually be one or two orders of magnitude smaller than the vibrational effect in Raman liquids. The possibility of exiciting spin-wave modes by light in ferro-, ferri-, and antiferromagnetic materials is discussed. The combined coupling of magnetic, vibrational, and light waves is also analyzed and a magnon excitation may be induced by the stimulated Brillouin effect on a magnetoelastic mode.

I. INTRODUCTION

THE Raman effect can be described as a second-order inelastic scattering of light, in which the scattering system makes a transition to an excited state.[1] Originally the spontaneous Raman scattering was almost exclusively employed to study vibrational and rotational excitations of molecules.[2] Loudon[3] suggested that electronic excitations of transition-metal ions should be observable in the Raman effect. Hougen and Singh[4] independently succeeded in finding this purely electronic Raman effect for Pr^{3+} ions in LaF_3.

It is also possible for the excitation to be of a purely

* This research was supported by the U. S. Office of Naval Research.

† On leave from Harvard University.

[1] P. A. M. Dirac, Proc. Roy. Soc. (London) A114, 710 (1927).

[2] See, for example, G. Placzek, *Marx Handbuch der Radiologie*, edited by E. Marx (Academische Verlagsgesellschaft, Leipzig, Germany, 1934), 2nd ed., Vol. VI, part II, p. 209.

[3] R. J. Elliott and R. Loudon, Phys. Letters 3, 189 (1964); R. Loudon, Advan. Phys. 13, 423 (1964).

[4] J. T. Hougen and S. Singh, Phys. Rev. Letters 10, 406 (1963).

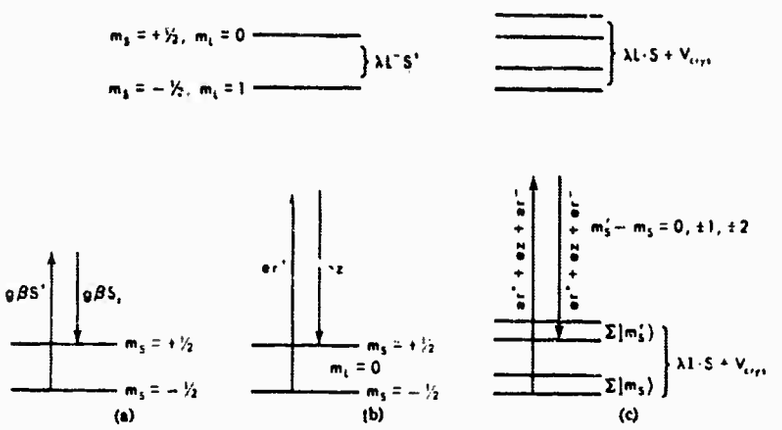

FIG. 1. Energy diagrams showing the spin-Raman processes. (a) Magnetic-dipole Raman transitions in a two-level spin system; (b) electric-dipole Raman transitions in a system with negligible crystalline field; (c) electric-dipole Raman transitions in a system with an appreciable crystalline field.

magnetic nature. In this case the excited state differs from the ground state in the spin magnetic quantum number. Such two-photon processes are well known in magnetic resonance.[5] The Raman susceptibility for the purely magnetic dipole transitions in a two-level system [Fig. 1(a)] has been reviewed by the present authors.[6] The final state with a different magnetic quantum number may also be reached with electric dipole transitions via a virtual electronic excited state, as shown in Fig. 1(b). It is of course necessary in this case to invoke spin-orbit coupling to change the spin quantum number. This process was also suggested by Loudon.[3] In the simplest case, the transition from the state $m_s = -\frac{1}{2}$ to $m_s = +\frac{1}{2}$ in a Kramers ground-state doublet of a ${}^2S_{1/2}$ ion would take place with a virtual optical transition to the ${}^2P_{3/2}$ or ${}^2P_{1/2}$ manifold. Although the optical electric dipole matrix elements cannot change the spin magnetic quantum number, it is possible to reach the final state with $\Delta m_s = \pm 1$ by invoking the spin-orbit coupling, as indicated in Fig. 1(b). More generally, for transition metal ions with spin-orbit coupling in crystalline fields of arbitrary strength, different magnetic sublevels of the ground-state multiplet could be reached via a two-photon process with electric dipole matrix elements, provided the initial and final states have components whose magnetic quantum numbers differ by $\Delta m_s = 0$, ± 1 or ± 2, as shown in Fig. 1(c).

In ferro-, ferri-, and antiferromagnetic materials, the spin excitation is not localized and the elementary excitation is described as a spin wave. It is the purpose of this paper to present the formalism which describes the coupling of light waves to these spin-wave excitations and to discuss the possibility of observing the stimulated spin Raman effect in magnetic media.

The same formalism that was developed[7,8] to describe the coupling of light waves with acoustical waves (stimulated Brillouin effect) and with optical phonons (stimulated Raman effect) can be adapted to the case of magnetic excitations. In Sec. II, the general quantum mechanical formulation for coupled boson fields is applied to the coupling of electromagnetic fields and vibrations. The wave equations for the expectation values of the fields and the nonlinear coupling constants are derived directly from a Hamiltonian. Although localized electronic states are used, as would be appropriate for insulators, the considerations could readily be extended to conductors by using itinerant Bloch wave functions.

In Sec. III this same procedure is applied to magnons. The exponential gain for the Stokes wave in the spin Raman effect is derived from the coupled wave equations. The result reduces to that derived from a spin Raman susceptibility for isolated magnetic ions, which would be appropriate in the paramagnetic case.

The possibility of detecting the spin Raman effect in various magnetic systems is discussed in Sec. IV. Some explicit equations are given for the two-sublattice model for ferri- and antiferromagnetic materials. The spin Raman effect is roughly 1 or 2 orders of magnitude smaller than the ordinary Raman effect in liquids, because the oscillator strengths of the electronic transitions involved in the magnetic ions are smaller than those involved in the molecules. In Sec. V, the general case of coupling between laser, Stokes, and infrared electromagnetic waves with phonon and magnon waves is discussed. A magnetic excitation could be induced by the combination of the stimulated Brillouin and the spin Raman effect.

II. COUPLING OF LIGHT WITH PHONONS

A detailed calculation of the ordinary stimulated Raman and Brillouin scattering has been given earlier.[8] In this section, a brief review of the subject is given in order to develop notations convenient for the later discussion of coupling of light with magnons. This also affords the opportunity to generalize the formalism so

[5] A. Javan, J. Phys. Radium 19, 836 (1958); J. M. Winter, *ibid.* 19, 834 (1958).
[6] N. Bloembergen and Y. R. Shen, Phys. Rev. 133, A37 (1964).
[7] E. Garmire, F. Pandarese, and C. H. Townes, Phys. Rev. Letters 11, 160 (1963); R. W. Hellwarth, Current Sci. India 33, 129 (1964).
[8] N. Bloembergen and Y. R. Shen, Phys. Rev. Letters 12, 504 (1964). Y. R. Shen and N. Bloembergen, Phys. Rev. 137, A1787 (1965).

that both the light and the other coupled boson fields are quantized. The wave equations together with the coupling constants are derived directly from the total Hamiltonian of the system

$$\mathcal{H}=\mathcal{H}_{\rm rad}+\mathcal{H}_{\rm phonon}+\mathcal{H}_{\rm e-e}+\mathcal{H}_{\rm int}. \tag{1}$$

The Hamiltonian for the radiation field can be quantized in the usual way,[9] as well as the phonon Hamiltonian in its harmonic approximation.[10]

$$\mathcal{H}_{\rm rad}=\sum_{\mathbf{k},i}\hbar\omega_{\mathbf{k},i}(\alpha_{\mathbf{k}i}^{\dagger}\alpha_{\mathbf{k}i}+\tfrac{1}{2}),$$
$$\mathcal{H}_{\rm phonon}=\sum_{\mathbf{q},j}\hbar\omega_{\mathbf{q},j}(a_{\mathbf{q}j}^{\dagger}a_{\mathbf{q}j}+\tfrac{1}{2}). \tag{2}$$

α, $\alpha^{\dagger}$ and a, $a^{\dagger}$ are the annihilation and creation operators for photons and phonons, respectively. Their operations on the number states yield $\alpha|n)=n^{1/2}|n-1\rangle$ and $\alpha^{\dagger}|n)=(n+1)^{1/2}|n+1)$. The photon and the phonon wave vectors are indicated by $\mathbf{k}$ and $\mathbf{q}$, respectively. The particular phonon branch under consideration is labeled by j.

The interaction Hamiltonian consists of two parts, the electron-phonon interaction and the electron-radiation interaction, which may be written in the form

$$\mathcal{H}_{\rm int}=\mathcal{H}_{e\text{-}p}+\mathcal{H}_{e\text{-}r}, \tag{3}$$

with

$$\mathcal{H}_{e\text{-}r}=-\sum_{m,b}(e\mathbf{r})_{mb}\cdot\mathbf{E}_{mb},$$
$$\mathcal{H}_{e\text{-}p}=\sum_{m,b}\sqrt{M_{mb}}\mathbf{U}_{mb}\cdot\mathbf{f}_{mb}. \tag{4}$$

In a nonpolar medium the phonon-radiation interaction can be neglected. The Raman effect in polar media has been discussed elsewhere.[11] In Eq. (4), $e\mathbf{r}$, $\mathbf{E}$, M, $\mathbf{U}$, and $\mathbf{f}$ are the electric dipole, the electric field, the atomic mass, the atomic displacement, and the generalized force on the atom, respectively. The indices m and b refer to the bth atom in the mth unit cell of the lattice. Both operators $\mathbf{E}$ and $\mathbf{U}$ can be expanded in terms of annihilation and creation operators. In the Schrödinger representation,

$$\mathbf{E}_{mb}=\textstyle\sum_{\mathbf{k}}[\mathbf{E}^{+}(\mathbf{k})e^{i\mathbf{k}\cdot\mathbf{R}_m}+\mathbf{E}^{-}(\mathbf{k})e^{-i\mathbf{k}\cdot\mathbf{R}_m}],$$
$$\mathbf{E}^{+}(\mathbf{k})=i(2\pi\hbar\omega_{\mathbf{k}}/V)^{1/2}\hat{\epsilon}\alpha_{\mathbf{k}}, \tag{5a}$$
$$\mathbf{E}^{-}(\mathbf{k})=i(2\pi\hbar\omega_{\mathbf{k}}/V)^{1/2}\hat{\epsilon}^{*}\alpha_{\mathbf{k}}^{\dagger},$$

where the fields are normalized with respect to a volume V;

$$\mathbf{U}_{mb}=\sum_{q,j}[\mathbf{U}^{+}(\mathbf{q},b,j)e^{i\mathbf{q}\cdot\mathbf{R}_m}+\mathbf{U}^{-}(\mathbf{q},b,j)e^{-i\mathbf{q}\cdot\mathbf{R}_m}],$$
$$\mathbf{U}^{+}(\mathbf{q},b,j)=(\hbar/2M_bN\omega_{qj})^{1/2}\mathbf{e}(\mathbf{q},b,j)a_{qj}, \tag{5b}$$
$$\mathbf{U}^{-}(\mathbf{q},b,j)=(\hbar/2M_bN\omega_{qj})^{1/2}\mathbf{e}^{*}(\mathbf{q},b,j)a_{qj}^{\dagger},$$
$$\{\mathbf{e}(\mathbf{q},b,j)\}\cdot\{\mathbf{e}(\mathbf{q},b,j)\}^{\dagger}\equiv\textstyle\sum_b\mathbf{e}(\mathbf{q},b,j)\cdot\mathbf{e}^{*}(\mathbf{q},b,j)=1.$$

Here N is the number of unit cells in the lattice, $\mathbf{R}_m$ the position of the mth unit cell, $\hat{\epsilon}$ the unit vector indicating polarization of the E field, and $\{e\}$ a set of b vectors with $\mathbf{e}(\mathbf{q},b,j)$ denoting the relative displacement of the bth atom in a unit cell corresponding to the phonon mode specified by $\mathbf{q}$ and j.

The wave equations for photons and phonons can be derived using the density-matrix formalism. Let ρ be the density-matrix operator for the entire system. The density-matrix operator for the radiation system alone is obtained by taking the trace over electron and phonon systems, such that $\rho_r=\mathrm{Tr}_{(e,p)}\rho$. From the equation of motion for ρ, we find

$$\left(\frac{\partial^2}{\partial t^2}+\omega_{\mathbf{k}}^2\right)\langle(n+1)_{\mathbf{k}}|\rho_r(t)|n_{\mathbf{k}}\rangle$$
$$=\left(\frac{\partial}{\partial t}-i\omega_{\mathbf{k}}\right)$$
$$\times(1/i\hbar)\,\mathrm{Tr}_{(e\text{-}p)}\langle(n+1)_{\mathbf{k}}|[\mathcal{H}_{e\text{-}r},\rho(t)]|n_{\mathbf{k}}\rangle, \tag{6}$$

where $(n_{\mathbf{k}}|$ is the photon number state for n photons in the mode $\mathbf{k}$. With $\langle\mathbf{E}_{\mathbf{k}}(\mathbf{R},t)\rangle=\mathrm{Tr}\rho(t)\mathbf{E}^{+}(\mathbf{k})\exp(i\mathbf{k}\cdot\mathbf{R})$ and $\omega_{\mathbf{k}}=kc$, and with the aid of Eqs. (2)–(5), the above equation yields the wave equation for $\langle\mathbf{E}_{\mathbf{k}}(\mathbf{R},t)\rangle$. In first approximation with $\rho(t)=\rho_r(t)\rho_{e,p}(t)$, one finds

$$\left(\frac{1}{c^2}\frac{\partial^2}{\partial t^2}+k^2\right)\langle\mathbf{E}_{\mathbf{k}}(\mathbf{R},t)\rangle=-\frac{4\pi}{c^2}\frac{\partial^2}{\partial t^2}\langle\mathbf{P}_{\mathbf{k}}(\mathbf{R},t)\rangle, \tag{7}$$

where $\langle\mathbf{P}_{\mathbf{k}}(\mathbf{R},t)\rangle=\mathrm{Tr}\rho(t)e\mathbf{r}$ is proportional to $\exp(i\mathbf{k}\cdot\mathbf{R}-i\omega_{\mathbf{k}}t)$. In summing over all Fourier components, one can replace the factor k^2 by $-\nabla^2$; Eq. (7) then reduces to the classical wave equation for $\langle\mathbf{E}(\mathbf{R},t)\rangle$.

The radiation density as measured by photosensitive detectors is, however, proportional to $\langle|E^2|\rangle=\mathrm{Tr}\rho\mathbf{E}^{+}\mathbf{E}^{-}$. The differential equation for $\langle|E^2|\rangle$ can also be readily derived from the equation of motion for ρ. As expected, the spontaneous emission noise, if present will turn out in this full quantum-mechanical treatment. The noise problem in parametric quantum oscillators and amplifiers has been discussed by other authors in the Heisenberg representation.[12] In the classical treatment, the spontaneous emission noise can usually be taken into account in an *ad hoc* manner by inserting in the field amplitude equation a noise term with a random phase. In the following discussion, we are mainly interested in the parametric amplification of a coherent input field. The spontaneous noise will not be considered. The radiation fields will be treated classically, since the quantized field treatment yields exactly the same results as long as the approximation $\rho(t)=\rho_r(t)\rho_{e,p}(t)$ is made.

[9] See, for example, W. Heitler, *Quantum Theory of Radiation* (Oxford University Press, New York, 1954).
[10] See, for example, J. M. Ziman, *Electrons and Phonons* (Clarendon Press, Oxford, 1960).
[11] Y. R. Shen, Phys. Rev. 137, A1741 (1965).
[12] W. H. Louisell, A. Yariv, and A. E. Siegman, Phys. Rev. 124, 1646 (1961).

We shall assume the presence of only two em modes, such that

$$\mathbf{E}(\mathbf{R},t)=\boldsymbol{\varepsilon}_I \exp[i\mathbf{k}_I\cdot\mathbf{R}-i\omega_I t]+\boldsymbol{\varepsilon}_S \exp[i\mathbf{k}_S\cdot\mathbf{R}-i\omega_S t] + \text{complex conjugate}.$$

The phonon wave equation can be obtained from the equation of motion for ρ_{ep}. For simplicity, we assume only two electronic states for each atom, the ground state $\langle g|_{ma}$ and the excited state $\langle i|_{mb}$. Let $\langle G| = \prod_{m,b}\langle g_{mb}|$. The equation of motion for ρ_{ep} yields

$$\left(\frac{\partial^2}{\partial t^2}+2\Gamma\frac{\partial}{\partial t}+\omega_q^2\right)\langle (n+1)_q, G|\rho_{ep}^{(\omega)}|n_q,G\rangle e^{-i\omega t}=(-1/\hbar)\left(\omega_q+i\frac{\partial}{\partial t}\right)\langle (n+1)_q, G|[\mathcal{H}_{e-r},\rho_{ep}]^{(\omega)}|n_q,G\rangle e^{-i\omega t}, \quad (8)$$

where $\omega=\omega_I-\omega_S$, n_q denotes the number of phonons with wave vector $\mathbf{q}$ and frequency ω_q, and Γ is the phenomenological damping constant. The matrix element of $[\mathcal{H}_{e-r},\rho_{ep}]$ can be calculated by a perturbation expansion. The lowest order nonvanishing result is

$$\langle (n+1)_q, G|[\mathcal{H}_{e-r},\rho_{er}]^{(\omega)}|n_q,G\rangle=\sum_{m,I}\left[\frac{\langle (n+1)_q, g|\sum_b(er)_b\cdot\boldsymbol{\varepsilon}_S^*|I\rangle\langle I|\sum_b(er)_b\cdot\boldsymbol{\varepsilon}_I|n_q,g\rangle}{\hbar(\omega_I-\omega_{I,gn_q})}\right.$$
$$\left.-\frac{\langle (n+1)_q, g|\sum_b(er)_b\cdot\boldsymbol{\varepsilon}_I|I\rangle\langle I|\sum_b(er)_b\cdot\boldsymbol{\varepsilon}_S^*|n_q,g\rangle}{\hbar(\omega_S+\omega_{I,gn_q})}\right](\rho_{n_q}^0-\rho_{(n+1)_q}^0)\exp[i(\mathbf{k}_I-\mathbf{k}_S)\cdot\mathbf{R}_m]. \quad (9)$$

Here $(\rho_{n_q}^0-\rho_{(n+1)_q}^0)$ is the average population difference between the phonon number states $\langle n_q|$ and $\langle (n+1)_q|$ at an arbitrary temperature and $\langle I|$ is the intermediate state with arbitrary mixing of electronic and vibrational character. The states $\langle (n+1)_q|$ and $|n_q\rangle$ in the square bracket yield a factor $\exp(-i\mathbf{q}\cdot\mathbf{R}_m)$ in the explicit calculation. The above matrix element is therefore nonvanishing only if the momentum matching condition $\mathbf{q}=\mathbf{k}_I-\mathbf{k}_S$ is satisfied, since otherwise $\sum_m \exp[i(\mathbf{k}_I-\mathbf{k}_S-\mathbf{q})\cdot\mathbf{R}_m]=0$. The matrix element would vanish if the electron-phonon interaction were absent, as the electron-radiation interaction cannot change the occupation number of phonons.

In the long-wavelength limit, the dispersion of the phonon modes has the form

$$\omega_q^2=\omega_0^2+\beta q^2.$$

For acoustic phonons, β is positive and $\omega_0=0$. The phonon wave of wave vector $\mathbf{q}$ attached to the ground electronic state $\langle g|$ can be defined in terms of a dimensionless normal coordinate,

$$\langle \mathbf{Q}_q(\mathbf{g},\mathbf{R},t)\rangle=\langle G|\sum_b(2M_g\omega_q/\hbar)^{1/2}\,\mathrm{Tr}_{(g)}\rho_{ep}^{(\omega)}\mathbf{U}^+(q,b)\exp(i\mathbf{q}\cdot\mathbf{R}-i\omega t)|G\rangle$$
$$=\langle \mathbf{Q}(\mathbf{q},\omega)\rangle\exp(i\mathbf{q}\cdot\mathbf{R}-i\omega t). \quad (10)$$

Equations (9) and (10) lead to the phonon wave equation

$$\left[\frac{\partial^2}{\partial t^2}+2\Gamma\frac{\partial}{\partial t}+\omega_0^2-\beta\nabla^2\right]\langle Q_q(g,\mathbf{R},t)\rangle=\boldsymbol{\lambda}:\mathbf{E}_I\mathbf{E}_S^*\exp(i\mathbf{q}\cdot\mathbf{R}-i\omega t),$$

where $\boldsymbol{\lambda}$ is a third-rank tensor:

$$\boldsymbol{\lambda}=(2\omega_q/\hbar)\sum_{n_q}(n+1)_q\xi(\rho_{n_q}^0-\rho_{(n+1)_q}^0),$$

$$\xi=\{\mathbf{e}(\mathbf{q},b)\}(1/\hbar)\sum_I(n+1)_q^{-1/2}N^{1/2}\left[\frac{\langle (n+1)_q, g|\sum_b(er)_{bs}|I\rangle\langle I|\sum_b(er)_{bi}|n_q,g\rangle}{\omega_I-\omega_{I,gn_q}}\right.$$
$$\left.-\frac{\langle (n+1)_q, g|\sum_b(er)_{bi}|I\rangle\langle I|\sum_b(er)_{bs}|n_q,g\rangle}{\omega_S+\omega_{I,gn_q}}\right]\exp(i\mathbf{q}\cdot\mathbf{R}_m). \quad (11)$$

The square bracket in the expression for ξ is likely to be proportional to $(n+1)_q^{1/2}$, since the states $\langle (n+1)_q|$ and $|n_q\rangle$ must be connected implicitly by the operator $U^+(q,b)$ or a_q. The factor $N^{1/2}$ in ξ arises as a normalization factor attached to the states $\langle (n+1)_q|$ and $|n_q\rangle$ because of the definition of $U_\pm(q,b)$ in Eq. (5). The quantity ξ, which has the dimension of an atomic polarizability, is then independent of n_q, and since

$$\sum_{n_q}(n+1)_q(\rho_{n_q}^0-\rho_{(n+1)_q}^0)=\sum_{n_q}\rho_{n_q}^0=1,$$

Eq. (11) gives

$$\boldsymbol{\lambda}=(2\omega_q/\hbar)\xi. \quad (11a)$$

This can be shown explicitly for the case where the electron-phonon interaction is small so that it can be treated as a small perturbation, mixing the states. The intermediate state can be written as $\langle I| = \langle (n+1)_q, i|$, and

$$\langle (n+1)_q, i|er|n_q, g\rangle = \frac{\langle i|er|g\rangle}{h\omega_q}[\langle (n+1)_q, i|\mathcal{H}_{e\text{-}p}|n_q, i\rangle - \langle (n+1)_q, g|\mathcal{H}_{e\text{-}p}|n_q, g\rangle],$$
$$\langle (n+1)_q, g|er|n_q, i\rangle = \frac{\langle g|er|i\rangle}{-h\omega_q}[\langle (n+1)_q, i|\mathcal{H}_{e\text{-}p}|n_q, i\rangle - \langle (n+1)_q, g|\mathcal{H}_{e\text{-}p}|n_q, g\rangle]. \tag{12}$$

With $\mathcal{H}_{e\text{-}p}$ given by Eq. (4), and substituting the above expression into Eq. (11), one finds

$$\xi = \{e(q,b)\}(1/\hbar)[\langle g|\sum_b (er)_{bS}|i\rangle\langle i|\sum_b (er)_{bI}|g\rangle(\langle i|\sum_b (\mathbf{f}\cdot\hat{e}^*)_b|i\rangle - \langle g|\sum_b (\mathbf{f}\cdot\hat{e}^*)_b|g\rangle)](A/\omega_q), \tag{13}$$
$$A = [(\omega_S-\omega_{n_q})^{-1} - (\omega_I-\omega_{n_q})^{-1} + (\omega_S+\omega_{n_q})^{-1} - (\omega_I+\omega_{n_q})^{-1}]/\hbar,$$

where $\mathbf{f}$ is the generalized force in Eq. (4). The phonon wave is coupled to the laser and Stokes fields $\langle \mathbf{E}_I\rangle$ and $\langle \mathbf{E}_S\rangle$ to give rise to the stimulated Raman and Brillouin effects. The wave equation for $\langle \mathbf{E}_I\rangle$ and $\langle \mathbf{E}_S\rangle$ is

$$\nabla^2\langle \mathbf{E}_{I,S}\rangle + (\omega_{I,S}^2\varepsilon_{I,S}/c^2)\langle \mathbf{E}_{I,S}\rangle = -(4\pi\omega_{I,S}^2/c^2)\langle \mathbf{P}_{I,S}{}^{NL}\rangle, \tag{14}$$

where $\langle \mathbf{P}_{I,S}{}^{NL}\rangle$ is obtained from the usual iterative procedure in the density matrix formalism. In particular,

$$\langle \mathbf{P}_S{}^{NL}(\mathbf{R},t)\rangle = \mathfrak{N}\xi^\dagger\varepsilon_I\langle \mathbf{Q}_q(g\mathbf{R},t)\rangle, \tag{15}$$

where $\mathfrak{N}$ is the number of unit cells per unit volume. The Boltzmann factors $\rho_n{}^0$ disappear in the nonlinear coupling terms of both Eq. (11) and Eq. (15). Therefore, the stimulated Raman gain, obtained from the solution of the coupled wave equations for $\langle \mathbf{E}_S\rangle$ and $\langle \mathbf{Q}_q\rangle$ would be independent of the average thermal excitations of phonons.

For acoustic phonons the harmonic approximation on which the linear expression for the displacement operator U is based, is nearly always valid. The effect of anharmonic terms may be taken into account as a damping term, caused by collisions between the acoustic waves. The temperature dependence of the stimulated Brillouin effect is entirely contained in the temperature dependence of the damping constant Γ. Even though the concept of elementary excitations breaks down at high temperature, the classical acoustic wave can still be described in the same manner, even in liquids.

The situation is different for optical phonons. In this case the anharmonicity of the molecular vibrations limits the validity of the harmonic collective excitations to the low-temperature regime, where the probability to have an excitation at a particular localized site is small compared to unity.

The dispersion law for optical phonons is very different from that of acoustic phonons. The contribution of the collective motion to the wavelength-dependent part of the energy is small and the damping is relatively large, $\beta q^2 \ll \omega_q\Gamma$. Under these circumstances it is appropriate to consider the localized vibrational excitations of individual molecules.[8] Since the vibrations are strongly anharmonic, only the ground state and the first vibrational level need be considered. It is a well-known result for this case of individual molecules that the Raman susceptibility is proportional to the population difference in these two states, $\rho_0{}^0 - \rho_1{}^0$. This temperature dependence through the Boltzmann factors does not appear in the calculation with collective elementary excitation waves, which is strictly valid only at absolute zero. The case of optical phonons derived for a lattice array of molecules with two vibrational levels is analogous to the case of spin waves derived from a lattice of spins with $S=\frac{1}{2}$. The representation by elementary excitations with boson characteristics is a low-temperature approximation.

The formalism of the coupling of light with optical phonons may be taken over to the case of spin waves. The coupling of light with plasma waves has been discussed elsewhere.[13]

III. COUPLING OF LIGHT WITH MAGNONS

The electronic Hamiltonian for a magnetic system consists of spin and orbital parts. The spin part, with exchange interaction among spins, forms the magnon system. The radiation field is treated classically and is again assumed to consist of two waves, E_I and E_S. The total Hamiltonian is written as

$$\mathcal{H} = \mathcal{H}_{\text{magnon}} + \mathcal{H}_{\text{orb}} + \mathcal{H}_{\text{int}}. \tag{16}$$

The nuclear vibrational part is omitted in this section. The interaction Hamiltonian consists of spin-orbit, spin-radiation, and orbit-radiation interactions,

$$\mathcal{H}_{\text{int}} = \mathcal{H}_{S\text{-}L} + \mathcal{H}_{L\text{-}r} + \mathcal{H}_{S\text{-}r}. \tag{17}$$

These interactions have the familiar bilinear form

$$\mathcal{H}_{S\text{-}L} = \sum_{m,b}\lambda_{mb}\mathbf{L}_{mb}\cdot\mathbf{S}_{mb},$$
$$\mathcal{H}_{L\text{-}r} = -\sum_{m,b}[e\mathbf{r}_{mb}\cdot\mathbf{E}_{mb} + \mu\mathbf{L}_{mb}\cdot\mathbf{H}_{mb}], \tag{18}$$
$$\mathcal{H}_{S\text{-}r} = -\sum_{m,b}2\mu\mathbf{S}_{mb}\cdot\mathbf{H}_{mb},$$

[13] N. Bloembergen and Y. R. Shen, Phys. Rev., 141, 298 (1966).

where λ and μ are the spin-orbit coupling constant and the Bohr magneton, respectively. The electric and magnetic fields of the radiation at the bth atom in the mth unit cell are designated by E_{mb} and H_{mb}. The terms $\mu\mathbf{L}\cdot\mathbf{H}$ and $2\mu\mathbf{S}\cdot\mathbf{H}$ correspond to magnetic-dipole transitions. Javan and Winter first suggested the stimulated Raman maser action in a paramagnetic two-level spin system [compare Fig. 1(a)]. In the optical spin Raman transitions, shown in Figs. 1(b) and 1(c), the intermediate states can be connected by the electric-dipole interaction $e\mathbf{r}\cdot\mathbf{E}$. The magnetic-dipole terms $\mu\mathbf{L}\cdot\mathbf{H}$ and $2\mu\mathbf{S}\cdot\mathbf{H}$ are negligible in comparison. The interaction Hamiltonian reduces in these cases to a form similar to the one in the previous section. The role of $\mathcal{H}_{e\text{-}p}$ is taken over by $\mathcal{H}_{S\text{-}L}$.

The magnon Hamiltonian is

$$\mathcal{H}_{\text{magnon}}=-\sum_{\substack{m,m'\\ b,b'}} J_{mb-m'b'}\mathbf{S}_{mb}\cdot\mathbf{S}_{m'b'}-2\mu\mathbf{H}_0\cdot\sum_{m,b}\mathbf{S}_{mb}, \quad (19)$$

where J is the exchange coupling constant and $\mathbf{H}_0$ the dc magnetic field. In the harmonic approximation, $\mathcal{H}_{\text{magnon}}$ can be quantized as[14]

$$\mathcal{H}_{\text{magnon}}=\sum_{\mathbf{q},j}\hbar\omega_{\mathbf{q},j}(a_{\mathbf{q},j}^{\dagger}a_{\mathbf{q},j}+\tfrac{1}{2}). \quad (20)$$

The spin component is expressed in terms of creation and annihilation operators $a_{\mathbf{q},j}^{\dagger}$, $a_{\mathbf{q},j}$ from the linearized Holstein-Primakoff transformation[15]

$$S_{mb}^{+}=(S_{mb})_x+i(S_{mb})_y=(2S_b/N)^{1/2}\sum_{\mathbf{q},j}e(\mathbf{q},b,j)a_{\mathbf{q},j}\exp(i\mathbf{q}\cdot\mathbf{R}_m)$$

$$=\sum_{\mathbf{q},j}S(\mathbf{q},j)\exp(i\mathbf{q}\cdot\mathbf{R}_m), \quad (21)$$

$$(S_{mb})^2=S_b(S_b+1).$$

The magnon modes $\omega_{\mathbf{q},j}$ are obtained by solving the set of linearized Bloch equations of motion for S_{mb}^{+} for the magnetically inequivalent atoms in a unit cell,[16] just as in the case of phonons. The number of magnon branches is of course equal to the number of magnetically inequivalent atoms in each unit cell. In the long-wavelength limit,

$$\omega_{\mathbf{q},j}=\omega_0(\mathbf{H}_0,J)+\beta(J)q^2. \quad (22)$$

In particular, when there is only one magnetic sublattice with one magnetic atom per unit cell, there is only one magnon branch with $\omega_0=2\mu H_0$ and $\beta=JSa^2$, where a is the lattice constant.

The magnon wave equation can now be derived from the density matrix formalism. Let ρ be the density matrix operator for the material system. We shall again assume only two states for the orbital part of each atom, $\langle i|_{mb}$ and $\langle g|_{mb}$ and $\langle G|=\prod_{m,b}\langle g|_{mb}$. Consider the equation for $\langle(n+1)_{\mathbf{q}},G|\rho|n_{\mathbf{q}},G\rangle$, where $\langle n_{\mathbf{q}}|$ denotes the excitation of the magnon wavelength wave vector $\mathbf{q}=\mathbf{k}_I-\mathbf{k}_S$. From the equation of motion for ρ and Eqs. (16)–(20), we find

$$\left(i\frac{\partial}{\partial t}-\omega_{\mathbf{q}}+i\Gamma\right)\langle(n+1)_{\mathbf{q}},G|\rho^{(\omega)}|n_{\mathbf{q}},G\rangle e^{-i\omega t}=\frac{1}{\hbar}\langle(n+1)_{\mathbf{q}},G|[\mathcal{H}_{e\text{-}r},\rho]^{(\omega)}|n_{\mathbf{q}},G\rangle e^{-i\omega t}, \quad (23)$$

where $\omega=\omega_I-\omega_S$. The lowest order nonvanishing result in the perturbation expansion of $[\mathcal{H}_{e\text{-}r},\rho]^{(\omega)}$ gives

$$\langle(n+1)_{\mathbf{q}},G|[\mathcal{H},\rho]^{(\omega)}|n_{\mathbf{q}},G\rangle=\sum_{m,I}\left[\frac{\langle(n+1)_{\mathbf{q}},g|\sum_b(e\mathbf{r}\cdot\boldsymbol{\mathcal{E}}_S^{*})_b|I\rangle\langle I|\sum_b(e\mathbf{r}\cdot\boldsymbol{\mathcal{E}}_I)_b|n_{\mathbf{q}},g\rangle}{\hbar(\omega_I-\omega_{I,gn})}\right.$$

$$\left.-\frac{\langle(n+1)_{\mathbf{q}},g|\sum_b(e\mathbf{r}\cdot\boldsymbol{\mathcal{E}}_I)_b|I\rangle\langle I|\sum_b(e\mathbf{r}\cdot\boldsymbol{\mathcal{E}}_S^{*})_b|n_{\mathbf{q}},g\rangle}{\hbar(\omega_S+\omega_{I,gn})}\right](\rho_{n_{\mathbf{q}}}{}^{0}-\rho_{(n+1)_{\mathbf{q}}}{}^{0})\exp(i\mathbf{q}\cdot\mathbf{R}_m). \quad (24)$$

Here, the intermediate state with arbitrary mixing of spin and orbital character is denoted by $\langle I|$, and $\omega_{I,gn}$ is the frequency separation between $\langle I|$ and $\langle n_{\mathbf{q}},g|$. Since $\mathcal{H}_{e\text{-}r}$ cannot change the occupation number of magnons, Eq. (24) would vanish if the spin-orbit interaction $\mathcal{H}_{S\text{-}L}$ were not present. When $\mathcal{H}_{S\text{-}L}$ is small, it can be treated as a perturba-

[14] See, for example, C. Kittel, *Quantum Theory of Solids* (John Wiley & Sons, Inc., New York, 1964).
[15] T. Holstein and H. Primakoff, Phys. Rev. 58, 1098 (1940).
[16] See, for example, B. Harris, Phys. Rev. 132, 2398 (1963).

tion in mixing the states. With the intermediate state written as $\langle I| = \langle n_q, i|$, one finds

$$\langle (n+1)_q, i|er|n_q, g\rangle = \sum_{i'} \left[\frac{\langle (n+1)_q, i|\mathcal{H}_{S\text{-}L}|n_q, i'\rangle\langle n_q, i'|er|n_q, g\rangle}{\hbar\omega_{i(n+1),i'n}} + \frac{\langle (n+1)_q, i|er|(n+1)_q i'\rangle\langle (n+1)_q, i'|\mathcal{H}_{S\text{-}L}|n_q, g\rangle}{\hbar\omega_{gn,i'(n+1)}} \right],$$

$$\langle (n+1)_q, g|er|n_q, i\rangle = \sum_{i'} \left[\frac{\langle (n+1)_q, g|er|(n+1)_q, i'\rangle\langle (n+1)_q, i'|\mathcal{H}_{S\text{-}L}|n_q, i\rangle}{\hbar\omega_{in,i'(n+1)}} + \frac{\langle (n+1)_q, g|\mathcal{H}_{S\text{-}L}|n_q, i'\rangle\langle n_q, i'|er|n_q, i\rangle}{\hbar\omega_{g(n+1),i'n}} \right]. \tag{25}$$

These equations may apply for certain iron-group ions. If $\langle g|$ and $\langle i|$ denote eigenstates in the crystalline field potential, the quenching of the orbital angular momentum implies that the diagonal elements of the spin-orbit interaction vanish

$$\langle (n+1)_q, i|\mathcal{H}_{S\text{-}L}|n_q, i\rangle = \langle (n+1)_q, g|\mathcal{H}_{S\text{-}L}|n_q, g\rangle = 0.$$

This is different from the phonon case described by Eq. (12).

The spin wave is defined as

$$\langle S_q(R,t)\rangle = \langle G|\mathrm{Tr}\sum_b (1/2S_b)^{1/2}\rho S_b^{+}(\mathbf{q},\omega)|G\rangle \exp(i\mathbf{q}\cdot\mathbf{R} - i\omega t). \tag{26}$$

Equation (23) then leads to the equation for the spin wave

$$\left[\frac{\partial}{\partial t} - \omega_0 + i\Gamma + \beta\nabla^2\right]\langle S_q(\mathbf{R},t)\rangle = \lambda_S : \mathcal{E}_I\mathcal{E}_S^{*}\exp(i\mathbf{q}\cdot\mathbf{R} - i\omega t),$$

$$\lambda_S = \hbar^{-1}\sum_{n_q}(n+1)_q\xi_S(\rho_{n_q}{}^0 - \rho_{(n+1)_q}{}^0),$$

$$\xi_S = (1/\hbar)\{e(\mathbf{q},b)\}\sum_I N^{1/2}(n+1)_q^{-1/2}\left[\frac{\langle (n+1)_q, g|\sum_b (er)_{bS}|I\rangle\langle I|\sum_b (er)_{bI}|n_q, g\rangle}{\omega_I - \omega_{I,gn}} - \frac{\langle (n+1)_q, g|\sum_b (er)_{bI}|I\rangle\langle I|\sum_b (er)_{bS}|n_q, g\rangle}{\omega_S + \omega_{I,gn}}\right]\exp(i\mathbf{q}\cdot\mathbf{R}_m). \tag{27}$$

Note the similarity of this expression and the corresponding Eq. (11) for the phonon case. The expression in square brackets can be evaluated explicitly in the case of weak spin-orbit coupling with Eq. (25). It is seen to be proportional to $(n+1)_q^{1/2}$. This result has probably more general validity, as the term in square brackets connects two boson eigenstates differing by one unit of excitation. The factor $N^{1/2}$ in the expression again arises as a normalization factor attached to the states $\langle (n+1)_q|$ and $|n_q\rangle$. The expression for λ_S is independent of the $\rho_{n_q}{}^0$ in this case by the same arguments which led to Eq. (11a) and, in fact $\lambda_S = \xi_S/\hbar$. The coupling constant is therefore independent of temperature in this harmonic approximation. This result can only be expected to have validity for temperatures well below the Curie or Néel temperature. When T becomes an appreciable fraction of T_c higher order terms in the spin-wave variables can no longer be ignored in the Holstein-Primakoff transformation. This is the usual restriction on the validity of spin-wave theories.

The spin wave is coupled to the two light waves $\mathbf{E}_I$ and $\mathbf{E}_S$ to give rise to the spin-Raman effect. The wave equation for the Stokes wave is

$$\nabla^2\mathbf{E}_S(\mathbf{R},t) + (\omega_S^2\epsilon_S/c^2)\mathbf{E}_S(\mathbf{R},t) = -(4\pi\omega_S^2/c^2)\langle \mathbf{P}_S^{NL}(\mathbf{R},t)\rangle. \tag{28}$$

The nonlinear polarization in Eq. (28) can be found by the usual perturbation calculation,

$$\mathbf{P}_S^{NL}(R,t) = \mathfrak{N}\xi_S^{\dagger}\mathcal{E}_I\langle S(\mathbf{q},\omega)\rangle^{*}\exp(i\mathbf{q}\cdot\mathbf{R} - i\omega t), \tag{29}$$

where $\mathfrak{N}$ is the number of unit spin cells per unit volume.

The above derivation is very similar to that in the coupled photon-phonon case. If the spin-orbit coupling and the crystalline-field interaction are large, a pure spin wave of course does not exist. The formal derivation remains valid in this case, which is represented by Fig. 1(c).

The gain coefficient for the stimulated spin Raman effect[6,8] can now be solved from the set of coupled wave equations (27) and (28) with λ_S replaced by ξ_S. For

infinite plane waves with linear polarization in a medium of plane boundaries, the Stokes wave vector is found to be

$$\mathbf{k}_{S\pm}=\mathbf{k}_S{}^0+\hat{z}\left\{\frac{1}{2}(i\alpha_S-D/2\beta q_z{}^0)\right.$$
$$\left.\pm\frac{1}{2}\left[\left(\frac{D^*}{2\beta q_z{}^0}+i\alpha_S\right)^2-\frac{2\mathfrak{N}\pi\omega_S{}^2\xi_S{}^2|\mathcal{E}_l|^2}{c^2\beta k_{Sz}{}^0 q_z{}^0 h}\right]^{1/2}\right\}, \quad (30)$$

where

$$k_S{}^0=\omega_S{}^2\epsilon_S'/c^2,$$
$$\alpha_S=\omega_S{}^2\epsilon_S''/2c^2k_{Sz}{}^0,$$
$$D^*=\omega-\omega_0-\beta q^{02}-i\Gamma_S, \quad (31)$$
$$\mathbf{q}^0=\mathbf{k}_l-\mathbf{k}_S{}^0,$$
$$\mathbf{q}'=\mathbf{k}_l'-\mathbf{k}_S' \quad \text{and} \quad k_S''=q''.$$

The laser field $\mathcal{E}_l$ is assumed to be a constant parameter and the unit vector $\hat{z}$ is normal to the boundaries of the Raman cell. The imaginary part of k_S is the gain or loss coefficient. The corresponding waves are given by

$$E_S=[C_{S+}\exp(i\mathbf{k}_{S+}\cdot\mathbf{r})+C_{S-}\exp(i\mathbf{k}_{S-}\cdot\mathbf{r})]e^{-i\omega_S t},$$
$$\langle S\rangle=[C_{S+}'\exp(i\mathbf{q}_+\cdot\mathbf{r})+C_{S-}'\exp(i\mathbf{q}_-\cdot\mathbf{r})]e^{-i\omega t},$$
$$C_{S\pm}/C_{S\pm}'=\mathfrak{N}(\pi\omega_S{}^2/c^2k_{Sz}{}^0)\xi_S\mathcal{E}_l/(k_S-k_S{}^0+i\alpha).$$

If the spin wave is highly damped, such that

$$(D^*/2\beta q_z{}^0+i\alpha_S)^2\gg 2\mathfrak{N}\pi\omega_S{}^2\xi_S{}^2|\mathcal{E}_l|^2/c^2\beta q_z{}^0k_{Sz}{}^0h,$$

the square root in Eq. (30) can be expanded into a power series to give a gain coefficient

$$\mathrm{Im}k_{S+}=\alpha_S+\mathrm{Im}\left\{\frac{2\mathfrak{N}\pi\omega_S{}^2\xi_S{}^2|\mathcal{E}_l|^2}{c^2k_{Sz}{}^0D^*h}\right\}. \quad (32)$$

The gain is a maximum when both linear momentum and energy matching conditions are satisfied, i.e.,

$$\mathbf{k}_l=\mathbf{k}_S{}^0+\mathbf{q}^0 \quad \text{and} \quad \omega_l=\omega_S+\omega.$$

This is indicated by the resonance point R in Fig. 2. Curves 2 and 3 in this figure are given by

$$q^0=|\mathbf{k}_l-\mathbf{k}_S{}^0|=[\omega_l(n_l\hat{k}_l-n_S\hat{k}_S{}^0)\cdot\hat{q}^0+\omega_S n_S\hat{k}_S{}^0\cdot\hat{q}^0]/c$$

for the forward and backward scattering, respectively. Here, n's are the indices of refraction, and $\hat{k}$'s the unit vectors. The Raman susceptibility corresponding to the Raman gain of Eq. (32) assumes the very simple form,[8]

$$\chi_{\text{Raman}}{}^{\text{spin}}=\mathfrak{N}\xi_S{}^2/\hbar\Gamma_S, \quad (33)$$

where ξ_S is given by Eq. (27) and has the dimension of an atomic polarizability, and Γ_S is the damping constant for the spin wave.

When the probability for spin excitation at a localized site is not very small compared to unity, this harmonic approximation of the spin waves loses its validity. In the opposite limit of very high temperature, above the Curie or Néel point, it is clearly more appropriate to consider the energy levels of localized spins. In this paramagnetic case, the Boltzmann factor $\rho_0{}^0-\rho_1{}^0$ appears. The effect is proportional to the difference in population of the two magnetic levels concerned. If these levels form a Kramer's doublet, the temperature dependence is the same as the paramagnetic magnetization arising from these two levels. This suggests that the temperature dependence of the spin Raman transitions in a ferromagnet is similar to, although not necessarily identical to, the temperature dependence of the magnetization $M(T)$.

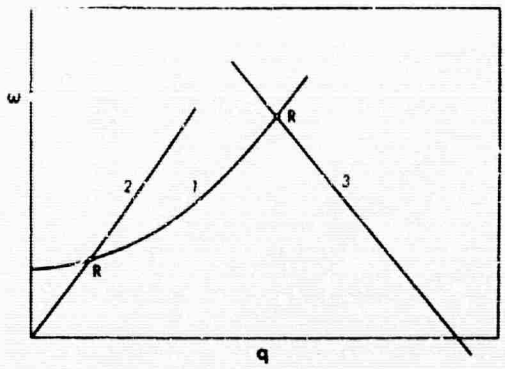

FIG. 2. Dispersion curves describing the spin Raman effect. Curve 1 is the dispersion curve for an acoustic magnon wave. Curves 2 and 3 describe the linear-momentum and energy-matching condition given by

$$q^0=|\mathbf{k}_l-\mathbf{k}_S{}^0|=[\omega_l(n_l\hat{k}_l-n_S\hat{k}_S{}^0)\cdot\hat{q}^0+\omega n_S\hat{k}_S{}^0\cdot\hat{q}^0]/c$$

for the forward and backward Stokes scattering, respectively. The resonant points are denoted by R.

IV. THE SPIN RAMAN EFFECT IN PARA-, FERRO-, FERRI-, AND ANTIFERROMAGNETIC MATERIALS

The possibility of observing the Raman effect in magnetic systems was described in the introduction. Hough and Singh[4] observed the spontaneous Raman transitions between two electronic levels of Pr^{3+} in a LaF_3 crystal. The Raman scattering due to spin excitations, however, has not yet been observed.

Both the spontaneous and the stimulated Raman scattering depend on the coupling constant ξ_S. The Raman transition probability increases as $|\xi_S|$ increases. As shown in Eq. (27), the magnitude of ξ_S becomes large if (1) the frequency ω_l or ω_S (or both) approaches a resonance, and (2) the matrix elements are large. In some simple cases, there are also selection rules governing the Raman transitions.

Consider first a paramagnetic system with a small crystalline field, so that m is still a good magnetic quantum number. The localized spin model applies to this case. The Raman transition probability is proportional to $\mathfrak{N}|\xi_S|^2|\mathcal{E}_l|^2(\rho_0{}^0-\rho_1{}^0)/\Gamma$, where ξ_S is given by Eq. (27) with the magnon states replaced by the local paramagnetic states. The degeneracy of the mag-

netic states is of course lifted by the applied dc magnetic field. In order to have the initial and the final magnetic states, $\langle g|$ and $\langle f|$, in the normal Raman transitions connected by the electric-dipole operator, the magnetic quantum number must change by $\Delta m = m_f - m_i = 1$ or 2. With $\Delta m = 1$ [see Fig. 1(b)] the selection rule requires the laser polarization to have a circular component around, and the Stokes polarization to have a linear component along, the magnetic field, or vice versa. The exciting beam propagating along the magnetic field cannot excite Stokes scattering in the forward direction. In the spontaneous Raman emission, one observes preferably at right angles to the incoming beam. One would find a linearly polarized Stokes light if the exciting beam is propagating in the direction of the magnetization, and a circularly polarized Stokes light if the exciting beam is propagating in the direction perpendicular to the magnetization. In the stimulated Raman effect, it is best to have the laser and the Stokes parallel to each other. They may then propagate at 45° with respect to the magnetic field. The geometry used by Dennis and Tennanwald[17] with the laser beam at an angle to the Stokes beam would also be possible. With $\Delta m = 2$, the selection rules require the polarizations of the laser and the Stokes to have components circulating in the same sense around the magnetic field. Again, the polarization properties depend in an interesting way on the direction of the magnetization and on the directions of propagation of the two beams. If the crystalline field is so large that m is no longer a good quantum number, the above selection rules in general break down.

Consider next a simple ferromagnet with a single sublattice, and assume the spin waves originating from individual ion states with pure magnetic quantum numbers $m = \pm\frac{1}{2}$. Only the acoustic magnon branch exists. The states corresponding to zero- and one-magnon excitation can be written as

$$\begin{aligned} \langle 0_q| &= \prod_i \langle +|_i, \\ \langle 1_q| &= (1/N)^{1/2} \sum_j (\langle -|_j \prod_{i\neq j} \langle +|_i) \exp(i\mathbf{q}\cdot\mathbf{R}_j), \end{aligned} \tag{34}$$

where $\langle +|_i$ and $\langle -|_i$ are the two spin states for the ith spin. Substituting Eq. (34) into Eq. (27), one finds that ξ_S is nonvanishing only if the product of matrix elements of the type $\langle g, -|er|I\rangle\langle I|er|g, +\rangle$ is different from zero. This requires that the magnetic quantum numbers of the initial and the final states in the Raman transitions differ by $\Delta m = 1$. The selection rule governing the polarization properties for the laser and the Stokes discussed previously for the paramagnetic case again applies. If the crystalline field is large, the spin wave is no longer composed of pure spin states. Then, in general, the selection rule breaks down.

[17] J. H. Dennis and P. E. Tannenwald, Appl. Phys. Letters **5**, 58 (1964).

In ferromagnets with more than one sublattice, and in ferri- and antiferromagnets, the sublattices are coupled together through exchange coupling to give different magnon branches. The eigenmodes and the eigenvectors are obtained from the coupled Bloch equations for the magnetizations of the sublattices. Assume a ferrite with two sublattices A and B, the corresponding spins being S_A and S_B, respectively, with pure spin states $\langle \pm\frac{1}{2}|$ for each spin. Since the spins are pointing in opposite directions, we write $S_{Az} = S_a$ and $S_{Bz} = -S_b$, and $S_A^{\pm}|\pm\rangle_A = |\pm\rangle_A$ and $S_B^{\pm}|\pm\rangle_B = |\mp\rangle_B$. Also assume that the exchange coupling exists only between spins on different sublattices. The coupled Bloch equations for $S_A^{\pm}$ and $S_B^{\pm}$ yield the magnon exchange eigenfrequency, or optical magnon mode at $\mathbf{q} = 0$[18]

$$\begin{aligned} \omega_0 = \tfrac{1}{2}(\omega_{eB} + \omega_{aA} - \omega_{eA} - \omega_{aB}) + \tfrac{1}{2}[(\omega_{eA} + \omega_{eB} \\ + \omega_{aA} + \omega_{aB})^2 - 4\omega_{eA}\omega_{eB}]^{1/2}, \\ (\omega_{eB} + \omega_{eA}) \geqq (\omega_{eA} + \omega_{aB}), \end{aligned} \tag{35}$$

where ω_{eA}, ω_{eB}, ω_{aA}, and ω_{aB} are the exchange and anisotropic frequencies for the two spins, respectively. The corresponding eigenmode is

$$\begin{aligned} &\langle S_A^+\rangle/\langle S_B^+\rangle = -\alpha_1/\alpha_2, \\ &\alpha_1 = \omega_{eA}/D, \\ &\alpha_2 = (\omega_{eB} + \omega_{eA} - \omega_0)/D, \\ &D = [\omega_{eA}^2 + (\omega_{eB} + \omega_{aA} - \omega_0)^2]^{1/2}. \end{aligned} \tag{36}$$

The states with zero- and one-magnon excitation can be written as

$$\begin{aligned} \langle 0_q| &= \prod_i \langle -, +|_i, \\ \langle 1_q| &= (1/N)^{1/2} \sum_j [(\alpha_1\langle +, +|_j - \alpha_2\langle -, -|_j) \\ &\quad \times \prod_{i\neq j} \langle -, +|_i] \exp(i\mathbf{q}\cdot\mathbf{R}_j), \end{aligned} \tag{37}$$

where $\langle \pm, \pm|_j$ are the combined spin states for the spins in the jth unit cell. We have $S_{Aj}|-+\rangle_j = |++\rangle_j$ and $S_{Bj}|-+\rangle_j = |--\rangle_j$. A typical term in Eq. (2.1) which contributes to the value of ξ_S is

$$\begin{aligned} &\alpha_1\langle g, +, +|(er_A^+ + er_B^+)|I\rangle\langle I|(er_A^z + er_B^z)|g, -, +\rangle \\ &\quad - \alpha_2\langle g, -, -|(er_A^+ + er_B^+)|I\rangle \\ &\quad \times \langle I|(er_A^z + er_B^z)|g, -, +\rangle, \end{aligned} \tag{38}$$

or with the superscripts $+$ and Z interchanged. This again requires that the polarization of one beam, the laser or the Stokes, has a circular component around and the polarization of the other beam has a linear component along the direction of magnetization. The situation here is very similar to that in the direct infrared excitation discussed by Tinkham for the case of rare-earth garnets.[19] There, the absorption coefficient is

[18] T. Nagamiya, K. Yosida, and R. Kubo, Advan. Phys. **4**, 14 (1955).

[19] M. Tinkham, Phys. Rev. **124**, 311 (1961); A. J. Sievers and M. Tinkham, *ibid.* **124**, 321 (1961).

proportional to the square of the matrix elements

$$[\alpha_1\langle g,+,+|(M_A^+ + M_B^+)|g,-,+\rangle - \alpha_2\langle g,-,-|(M_A^+ + M_B^+)|g,-,+\rangle].$$

Because of the antiparallel exchange coupling between the two sublattices, the two terms tend to cancel each other, so that the infrared absorption coefficient (and the Raman transition probability) becomes smaller when the exchange coupling increases relative to the anisotropy energy. The above analysis also applies to the case of antiferromagnets if one puts $S_a = S_b$, $\omega_{aA} = \omega_{bB}$, and $\omega_{aA} = \omega_{aB}$. The direct far-infrared excitation of magnons in the antiferromagnet FeF_2 has also been investigated by Tinkham.[20] The eigenfrequencies and the eigenmodes given in Eqs. (35) and (36) should be slightly modified in the presence of a dc applied magnetic field. If the crystalline field is large, the selection rule governing the polarizations of the beams again breaks down.

The magnitude of the spin Raman effect may be estimated as follows. Comparison of Eqs. (15) and (27) shows that the two coupling constants ξ and ξ_S are comparable in magnitude. In the case of optical phonons, ξ would be zero if the electron-phonon interaction were absent, it therefore suffers a reduction factor $\mathcal{H}_{e\text{-}p}/(\text{vibrational energy})$. In the case of magnons, ξ_S would be zero if there were no spin-orbit interaction; the reduction factor is $\mathcal{H}_{LS}/(\text{crystal field})$. The two coupling constants would be of the same order of magnitude if the matrix elements involved were the same. In practice, the ultraviolet oscillator strength for organic molecules is close to 1, but for magnetic ions it is usually less than 0.1.[21] If the reduction factors and the damping constants for the two cases are approximately the same, the spin Raman effect would be about 2 orders of magnitude smaller than the ordinary Raman process in liquids. The linewidth of the spin excitation at low temperatures seem to be comparable to the optical phonon linewidth which is about 1 cm^{-1}. For example, the antiferromagnetic resonance in FeF_2 has a width of 0.1 cm^{-1} at 1°K which increases with temperature as T^4.[20] The damping constant for the ferromagnetic spin excitations at room temperature, lies in the range $\Gamma_S \sim 10^9 - 10^{11}$ sec^{-1}. The narrowest ferromagnetic linewidth in a garnet is about 0.5 G or $\Gamma_S \sim 10^7$ sec^{-1} at low temperatures.[19]

An alternative way to estimate the order of magnitude of the spin Raman effect is by comparison with the optical rotatory power of the magnetic system.[22,23] Physically, the spin Raman effect and the Faraday rotation are closely related magneto-optical effects. The former is derivable from a thermodynamical potential connected with the coupling between light waves and a spin wave. The coupling energy per ion is $\xi_S E_i E_S^* \langle S(\omega - \omega_S)\rangle^*$. The Faraday rotation is derivable from a potential that gives the difference in coupling energy of a right-circular- and a left-circular-polarized light wave with a longitudinal dc magnetization. This time-averaged energy per ion is $\xi_{Far}\{|E_l^+|^2 - |E_l^-|^2\} \times \langle S(0)\rangle$, where $2\xi_{Far}$ is the difference of the right and the left circular polarizabilities. Both effects would vanish in the absence of spin-orbit coupling, and the coupling constants in the two cases are quite similar. The constant ξ_S has the same order of magnitude as the circular polarizability, and so has ξ_{Far}, if the two circular polarizabilities do not accidentally cancel each other. This is the case of some iron-group ions, such as Mn^{2+}, etc. Such a relationship was also noted by Pershan and coworkers.[24] They were only concerned with light polarizations perpendicular to the magnetization. Thus, only $\Delta m = 0$ or $\Delta m = \pm 2$ Raman transitions occur in their geometry. For the excitation of magnetic spin waves, the $\Delta m = \pm 1$ transitions are significant. They require the presence of a light component parallel to the magnetization. The ratio ξ_{Far}/ξ_S depends of course on the detailed geometry, crystal field splitting and mixing of the magnetic states.

The rotary power at magnetic saturation is related to the Faraday susceptibility by[25]

$$\phi = 4\pi \mathfrak{N} \xi_{Far}(\omega/nc) \text{ rad/cm},$$

where $\mathfrak{N}$ is the number of magnetic ions per cc and n is the index of refraction. For Eu^{2+} the rotary power per ion has been determined experimentally.[25] For light at the ruby wavelength one finds $\xi_{Far} = 5 \times 10^{-27}$ esu.

If we take $\mathfrak{N} = 5 \times 10^{22}$ in Eq. (33) and $\Gamma_S \approx 10^{11}$ sec^{-1} for a typical ferromagnet, one finds $\chi_{Raman}^{spin} \approx 10^{-14}$ esu. This is about two orders of magnitude smaller than the Raman susceptibility of several liquids in which stimulated Raman emission has been observed.

In principle, all magnon branches can be excited through the Raman process. In a spin Raman laser, however, the mode with the highest gain would be dominant. The stimulated Raman process would also have to compete with the ordinary stimulated Raman and Brillouin scattering.

For a single magnetic lattice, the acoustic ferromagnetic spin wave is of course the only magnon mode. It is interesting to compare the Raman excitation of this magnon mode with the Brillouin scattering. In both cases, the dispersion of the mode frequency is quite strong so that the Stokes radiation in different directions has different frequencies. The Stokes radiation in the spin Raman scattering can also go in the forward direction. If a strong dc magnetic field is applied, the mode frequency for $q = 0$ is still different from zero. The frequency of the spin waves in the forward direction would

[20] R. C. Ohlmann and M. Tinkham, Phys. Rev. 123, 425 (1961).
[21] Estimated from optical absorption data in rare-earth and iron-group ions. See, for example, B. R. Judd, Phys. Rev. 127, 750 (1962).
[22] Y. R. Shen, Phys. Rev. 133, A511 (1964).
[23] A. M. Clogston, J. Phys. Radium 20, 151 (1959).
[24] J. P. van der Ziel, P. S. Pershan, and L. D. Malmstrom, Phys. Rev. Letters 15, 190 (1965).
[25] Y. R. Shen and N. Bloembergen, Phys. Rev. 133, A515 (1964).

be low in small external fields. The momentum-matching condition becomes unimportant if the length of the sample l is so small that $ql<1$, as the uncertainty in the wave vector $\sim 1/l$ exceeds the wave vector q itself.

Since stimulated Brillouin scattering has a threshold which is comparable to that of the ordinary Raman effect in liquids, it will often dominate the spin Raman effect. The dispersion law is more favorable for spin waves in the forward direction. Note that the frequency of the magnon mode can also be tuned by the applied dc magnetic field.

In using giant-pulse lasers, one may still use the steady-state solution of the coupled wave equations, if the group velocity (or $\beta^{1/2}$) is small. This is the case for ordinary Raman effect and should also be valid for optical spin waves (or exchange modes) and for acoustic spin waves in very high fields. Otherwise, the transient solution of the type developed by Kroll[26] for the Brillouin case must be used.

The more interesting aspect of the spin Raman effect lies in the optical magnon branches. This includes the antiferromagnetic spin waves. Polarization properties of the beams should be investigated to see whether the simple selection rules break down or not. Experiments on FeF_2 with a Stokes shift of 55 cm^{-1} would be quite interesting. The large Stokes shift makes optical detection relatively easy. Various garnets are also suitable for investigation, especially yttrium iron garnet which is quite transparent in the near infrared.

In paramagnetic materials, the spin Raman effect arises from isolated ions. The Raman effect between two magnetic sublevels of the ground state and the Raman effect between two electronic levels have these same nature. The latter process was found by Hougen and Singh[4] in $LaF_3:Pr^{3+}$. Their experimental results give assurance that the spin Raman process and the Brillouin process might have the same order of magnitude. Although the concentration of magnetic ions in paramagnetic salts would be low, the linewidth could be as narrow as 10^{-2} or even 10^{-4} cm^{-1}, corresponding to a few gauss. The gain is proportional to the average population difference between the magnetic sublevels. If only these two sublevels are populated, the paramagnetic spin Raman gain would be proportional to the magnetization. This effect could be observed in the forward direction and could be tuned by the dc magnetic field, as distinguished from the Brillouin effect.

It appears worthwhile to search experimentally both for the spontaneous and the stimulated spin Raman effect. For the former, a gas laser focused into crystals at low temperature would be appropriate to observe a scattered radiation with a small Stokes shift.[27] For the latter, a resonant cavity with a different feedback factor for spin Stokes and Brillouin-shifted radiation would be useful.

[26] N. Kroll, J. Appl. Phys. 36, 34 (1965).
[27] R. Y. Chiao and B. P. Stoicheff, J. Opt. Soc. Am. 54, 1286 (1964); T. C. Daman, R. C. C. Leits, and S. P. S. Porto, Phys. Rev. Letters 14, 9 (1965).

V. COUPLING OF LIGHT WITH PHONONS AND MAGNONS

In discussing the spin Raman effect, we have neglected the term $\mu(\mathbf{L}+2\mathbf{S})\cdot\mathbf{H}$ in the Hamiltonian. This term would add to each electric-dipole matrix element a magnetic-dipole counterpart. In addition, if the em mode at the magnon frequency is present, there is a direct coupling between this em wave and the spin wave. It is this direct coupling that gives rise to magnetic resonance and far-infrared magnon excitation. We have also neglected the nuclear motion which is responsible for the phonon waves.

In principle, all waves existing in the medium can be coupled together either linearly or nonlinearly. The coupling is, however, effective only when both linear momentum and energy matching conditions are satisfied. Consider the case where five waves are present in the medium, the laser and the Stokes waves at ω_l and ω_S, and the infrared (or micro-) wave, the acoustic magnon wave, and the acoustic phonon wave at ω with $\omega=\omega_l-\omega_S$. The laser and the Stokes waves can be coupled to the phonon and the magnon waves through the nonlinear Raman-type coupling, and to the infrared (or micro-) wave through a nonlinear susceptibility of mixed electric and magnetic dipole character. This coupling constant is given by λ_2 or λ_4 in Eqs. (39) and (40). The magnon wave can be coupled linearly to the phonon wave through the magnetoelastic coupling,[28] and to the infrared (or micro-) wave magnetic field through the magnetic-dipole interaction. The coupling constants λ_8 and λ_9 between the acoustic phonon and the infrared (or micro-) wave is negligibly small since the waves cannot be matched simultaneously in energy and momentum. If the laser field is treated as a constant parameter, the remaining four waves are linearly coupled. The coupled wave equations can be written as

$$\begin{aligned}
&\nabla^2\mathbf{E}_S+(\omega_S^2\varepsilon_S/c^2)\mathbf{E}_S=\lambda_1\mathbf{E}_l\langle S\rangle^*+\lambda_2\mathbf{E}_l\mathbf{E}_v^*+\lambda_3\mathbf{E}_l\mathbf{A}_v^*,\\
&\nabla^2\mathbf{E}_v^*+(\omega^2\varepsilon_v^*/c^2)\mathbf{E}_v^*=\lambda_4\mathbf{E}_l^*\mathbf{E}_S+\lambda_5\langle S\rangle^*+\lambda_6\mathbf{A}_v^*,\\
&\nabla^2\mathbf{A}_v^*+(\rho_a\omega^2/\mathbf{C}_a)\mathbf{A}_v^*-i(\rho_a/\mathbf{C}_a)2\omega\Gamma\mathbf{A}_v^*\\
&\qquad=\lambda_7\mathbf{E}_l^*\mathbf{E}_S+\lambda_8\langle S\rangle^*+\lambda_9\mathbf{E}_v^*,\\
&\nabla^2\langle S\rangle^*+(1/\beta)(\omega-\omega_0-i\Gamma_S)\langle S\rangle^*\\
&\qquad=\lambda_{10}\mathbf{E}_v^*+\lambda_{11}\mathbf{A}_v^*+\lambda_{12}\mathbf{E}_l^*\mathbf{E}_S,
\end{aligned}\tag{39}$$

where $\mathbf{A}_v$ denotes the acoustic vibrational wave. The coupling constants are either related to physical constants or can be derived explicitly.

$$\begin{aligned}
&\lambda_1=-\mathfrak{N}(4\pi\omega_S^2/c^2)\xi_S^{\dagger},\\
&\lambda_2\sim(4\pi\omega_S^2/c^2)\\
&\qquad\times\mathfrak{N}\frac{(e\mathbf{r})_{gn}(e\mathbf{r})_{ng'}[\mu e^{1/2}(\mathbf{L}+2\mathbf{S})\times\hat{q}]_{g'g}}{\hbar^2(\omega_{l,S}-\omega_{ng})(\omega+\omega_{g'g})}.
\end{aligned}\tag{40a}$$

This coupling between three em waves in a medium with inversion symmetry is about 4 to 6 orders of

[28] C. Kittel, Phys. Rev. 110, 836 (1958).

magnitude smaller than the coupling parameter for the second-harmonic generation in piezoelectric crystals. The magnetic-dipole term makes this term negligibly small compared to the other types of coupling.

$$\lambda_3 \sim (4\pi\omega_S^2/c^2)(-i\mathbf{q}\cdot\mathbf{p}). \tag{40b}$$

$\mathbf{p}$ is the photoelastic tensor, whose elements are of order unity

$$\lambda_4=\lambda_2,$$
$$\lambda_5=\mathcal{R}[\mu\epsilon^{1/2}(\mathbf{L}+2\mathbf{S})\times\hat{q}]_{\sigma\sigma'}\sqrt{S_b}/S_{\sigma\sigma}{}^{+}. \tag{40c}$$

This is the magnetic resonance term, that couples the magnetic field at the resonance frequency to the spin wave.

$$\lambda_6\sim 0,$$
$$\lambda_7\sim(i\mathbf{q}\cdot\mathbf{p})/\mathbf{C}_a^{-1}. \tag{40d}$$

Here p is the photoelastic tensor and $\mathbf{C}_a$ is the elastic modulus tensor;

$$\lambda_8=iqb_2/\mathbf{C}_a. \tag{40e}$$

This magnetoelastic coupling is derived from the interaction Hamiltonian

$$\mathcal{H}_{ms}=2b_2[(S_x/S)\sigma_{xz}+(S_y/S)\sigma_{yz}],$$

where

$$\sigma_{yz}=(1/2)(\partial A_y/\partial z+\partial A_z/\partial y)$$

and

$$\sigma_{xz}=(1/2)(\partial A_x/\partial x+\partial A_z/\partial z)$$

are the shear strain components. The static magnetization is along the z direction. This is the only magnetoelastic coupling term in a cubic crystal which is linear in the spin variable. For a normal ferromagnet, the magnetoelastic constant b_2 has the magnitude of the order of 5×10^{-7} erg/cm^3.[28]

$$\lambda_9\sim 0,$$
$$\lambda_{10}=-\frac{1}{\hbar}[\mu\epsilon^{1/2}(\mathbf{L}+2\mathbf{S})\times\hat{q}]_{\sigma'\sigma}S_{\sigma\sigma'}{}^{+}/\beta, \tag{40f}$$
$$\lambda_{11}=iqb_2S_0\mathfrak{v}/\hbar\mu.$$

In this elastomagnetic coupling constant $\mathfrak{v}$ is the volume of a unit cell.

$$\lambda_{12}=-\xi_S/\hbar\beta. \tag{40g}$$

λ_1 and λ_{12} are the spin-light coupling constants described in Sec. III. Here, with $E_l=\mathcal{E}_l\exp[i\mathbf{k}_l\cdot\mathbf{r}-i\omega_l t]$, a solution of the set of coupled equations (39) takes the form

$$E_S\sim\exp[i\mathbf{k}_S\cdot\mathbf{r}-i\omega_S t],$$
$$E_v,\ A_v,\ \langle S\rangle\sim\exp[i\mathbf{q}\cdot\mathbf{r}-i\omega t]. \tag{41}$$

The complex wave vectors $\mathbf{k}_S$ and $\mathbf{q}=\mathbf{k}_l-\mathbf{k}_S{}^*$ are obtained from the determinant

$$\begin{vmatrix} -(k_S{}^2-\omega_S{}^2\epsilon_S/c^2) & -\lambda_1\mathcal{E}_l & -\lambda_2\mathcal{E}_l & -\lambda_3\mathcal{E}_l \\ -\lambda_{12}\mathcal{E}_l{}^* & -q^2+(\omega-\omega_0-i\Gamma_S)/\beta & -\lambda_{10} & -\lambda_{11} \\ -\lambda_4\mathcal{E}_l{}^* & -\lambda_5 & -q^2+\omega_v{}^2\epsilon_v{}^*/c^2 & 0 \\ -\lambda_7\mathcal{E}_l{}^* & -\lambda_8 & 0 & -q^2+(\rho_a/c_a)(\omega^2-i2\omega\Gamma) \end{vmatrix}=0. \tag{42}$$

The imaginary part of k_S gives the Stokes gain.

It is quite difficult to find the solution of Eq. (42). However, the dispersion relations of the waves are such that in general only three waves can be effectively coupled, since the infrared wave E_v is always decoupled from the acoustic wave A_v.

Consider first the coupling of E_S, A_v, and $\langle S\rangle$. The problem is essentially the same as the problem of the Raman effect in a polar medium[11] where the Stokes wave is coupled to the infrared and the optical phonon waves. That calculation can be carried over to the present case. Let

$$\mathbf{k}_S=\mathbf{k}_S{}^0+(\Delta K)\hat{z},\quad (k_S{}^0)^2=\omega_S\epsilon_S'/c^2,$$
$$\mathbf{k}_l'=\mathbf{k}_S'+\mathbf{q}',\qquad k_S''=q'', \tag{43}$$
$$\mathbf{k}_l'=\mathbf{k}_S{}^0+\mathbf{q}^0.$$

We are interested in the solution $\Delta K\ll k_{Sz}{}^0, k_{lz}{}^0$. In this case Eq. (42) reduces to

$$(-\Delta K+i\alpha_S)(\Delta K+F_1/2k_{vz}{}^0)(\Delta K+F_2/2k_{vz}{}^0)$$
$$+\Lambda_1(\Delta K+F_2/2k_{vz}{}^0)-\Lambda_2(\Delta K+F_1/2k_{vz}{}^0)$$
$$+\Lambda_3(-\Delta K+i\alpha_S)-\Lambda_{123}=0, \tag{44}$$

where

$$F_1=(\omega-\omega_0-\beta(q^0)^2-i\Gamma_S)/\beta,$$
$$F_2=(\rho_a/c_a)(\omega^2-i2\omega\Gamma)-(q^0)^2,$$
$$\Lambda_1=-\lambda_1\lambda_{12}|\mathcal{E}_l|^2/4k_{Sz}{}^0q_z{}^0,$$
$$\Lambda_2=\lambda_2\lambda_7|\mathcal{E}_l|^2/4k_{Sz}{}^0q_z{}^0,$$
$$\Lambda_3=-\lambda_8\lambda_{11}/4(q_z{}^0)^2,$$
$$\Lambda_{123}=-(\lambda_1\lambda_7\lambda_{11}+\lambda_3\lambda_8\lambda_{12})|\mathcal{E}_l|^2/8k_{Sz}{}^0(q_z{}^0)^2.$$

The solution of Eq. (44) is shown diagrammatically in Fig. 3. Curves 1 and 2 are the dispersion curves for the acoustic wave A_v and the acoustic spin wave $\langle S\rangle$. The momentum-energy matching relation for E_S,

$$q=|\mathbf{k}_l-\mathbf{k}_S|=[\omega_l(n_l\hat{k}_l-n_S\hat{k}_S)\cdot\hat{q}^0+\omega n_S\hat{k}_S\cdot\hat{q}^0]/c,$$

is given by curve 3. For small coupling constants, the curves simply cross one another instead of forming gaps.[29] Two waves can be coupled effectively only near the point where the corresponding curves meet. Thus, in the parametric approximation stimulated Brillouin

[29] No gap appears at the junction of phonon and magnon dispersion curves, if $\Lambda_3\ll(\rho_a/c_a)\omega\Gamma_S/\rho_a$. See Ref. 11.

and spin Raman effects will occur essentially independently near the points R_1 and R_2, respectively,[11] where the corresponding stimulated gain would be maximum. The three waves can be effectively coupled together only when the three waves can be made to meet one another at a single point, (R_3). This can be done by selecting the Stokes direction or by tuning the magnon frequency with the applied dc magnetic field. At this point, the gain for the mixed stimulated Brillouin and spin Raman effect would be close to maximum. Thus, the magnon can be excited indirectly by the Brillouin effect or conversely, the acoustic wave can be excited indirectly by the spin Raman effect. This has practical importance in exciting the magnon wave. Individually, the spin Raman effect may have a higher threshold than the Brillouin effect. However, by coupling the magnon waves to the acoustic waves, they can now be excited with a lower threshold via the Brillouin effect. The excited magnon frequency can be tuned by the dc magnetic field, but the direction of the Stokes radiation will also be changed. The exact solution for the case of three waves tightly coupled together should be obtained directly from Eq. (44). Further algebraic details may be found with the methods of Ref. 11.

The coupling of E_S, E_v, and $\langle S\rangle$ can in principle be discussed in the same manner. The nonlinear coupling between E_S and E_v is often small in magnetic media which are nonpiezoelectric. The mixed spin and infrared

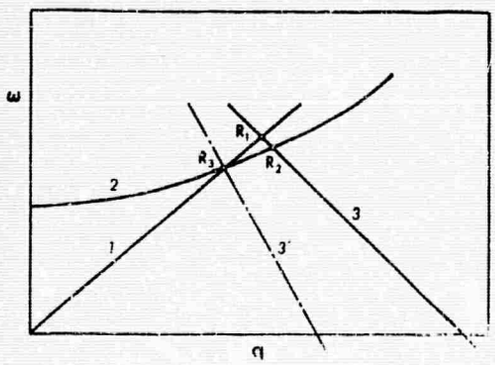

FIG. 3. Dispersion curves describing the mixed spin Raman and Brillouin effect. Curves 1 and 2 are the dispersion curves for the acoustic phonon and the acoustic magnon waves. Curves 3 and 3′ satisfy the linear momentum and energy matching condition

$$q^0=|\mathbf{k}_1-\mathbf{k}_S|=[\omega_1(n_1\hat{k}_1-n_S\hat{k}_S^0)\cdot\hat{q}^0+\omega n_S\hat{k}_S^0\cdot\hat{q}^0]/c$$

for two different directions of Stokes scattering. The resonant points R_1 and R_2 denote almost pure Brillouin effect and spin Raman effect, respectively. The resonant point R_3 corresponds to the mixed stimulated Brillouin and spin Raman effect.

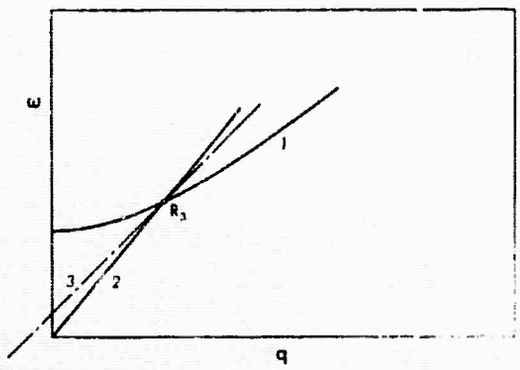

FIG. 4. Dispersion curves describing the simultaneous coupling of the acoustic magnon, the infrared, and the Stokes waves in an anisotropic medium. Curves 1 and 2 are the dispersion curves for the acoustic magnon and the infrared waves, respectively. Curve 3 describes the linear energy and momentum matching condition

$$q^0=|\mathbf{k}_1-\mathbf{k}_S|=[\omega_1(n_1\hat{k}_1-n_S\hat{k}_S^0)\cdot\hat{q}^0+\omega n_S\hat{k}_S^0\cdot\hat{q}^0]/c$$

in a particular direction of scattering. The resonant point R denotes simultaneous coupling of the three waves.

excitation is more easily excited through the spin Raman coupling. In isotropic media, the dispersion curves for the acoustic magnon and the infrared waves (curves 1 and 2, respectively, in Fig. 4) could not intersect the curve satisfying the linear momentum and energy matching relation at the same point. Therefore, the waves E_S, E_v, and $\langle S\rangle$ cannot be effectively coupled simultaneously. In anisotropic media with indices of refraction satisfying the inequality $n_1<n_S$, this is however, possible as indicated by the resonant point R in Fig. 4. The problem is similar to the Raman effect in polar media discussed by Loudon.[30]

VI. CONCLUSION

There is a close parallel between the coupling of light with optical phonons and the coupling of light with magnons. The spin Raman process appears to be two orders of magnitude smaller than the ordinary Raman process in liquids. Both the spontaneous and the stimulated spin Raman scattering may be observable in suitable magnetic substances, such as paramagnetic materials at low temperature, insulating antiferromagnets or ferrimagnetic garnets. Magnetic excitations may also be induced by light through the stimulated Brillouin effect and magnetoelastic coupling.

[30] R. Loudon, Proc. Phys. Soc. (London) A82, 393 (1963).

APPENDIX X

Reprinted from JOURNAL OF APPLIED PHYSICS, Vol. 38, No. 3, 1490-1495, 1 March 1967

Scattering of Light by Magnons*

Y. R. SHEN†
Physics Department, University of California, Berkeley, California

Scattering of light by magnons has recently been predicted by calculations, and subsequently verified by experiments. In this paper, theoretical aspects of the problem are reviewed briefly. The spin-Raman effect is treated along the same line as ordinary Raman scattering by phonons. The order of magnitude of one-magnon Raman scattering is estimated from the rotatory power of the magnetic ions. The effect is smaller in antiferromagnets because of opposite spins in different sublattices. In ferrites and antiferromagnets, two-magnon Raman scattering can occur through exchange-type interaction. Raman scattering by magnetoelastic modes should also be observable. The possibility of constructing a tunable light oscillator is discussed.

I. INTRODUCTION

A RAMAN process can be defined as a two-photon process in which one photon is absorbed and the other emitted, while the material system is either excited (the Stokes process) or de-excited (the anti-Stokes process). Raman scattering has long been a useful tool for investigating the vibrational or phonon characteristic of a medium. In principle, it should be equally useful for investigating other kinds of localized or cooperative excitations in a medium. Raman scattering in magnetic media was first suggested by Bass and Kaganov,[1] and by Elliot and Loudon,[2] and has recently been treated in detail by Shen and Bloembergen.[3] In this paper, light scattering by magnons is discussed. The problem is treated along the same line as that of scattering by phonons. Emphasis is on Raman scattering in ferro-, ferri-, and antiferromagnets. Magnetic excitations in paramagnets can be treated in the limiting sense as localized spin waves,[3] and will not be discussed. Here, it is shown that in MnF_2 and FeF_2, theoretical calculation agrees satisfactorily with experimental results recently obtained by Fleury *et al.*[4] The spin-Raman effect could also be observed on a magnetoelastic mode. In this latter case, the Raman scattering cross section may be enhanced through the combined coupling of photons, phonons, and magnons. Since the magnon frequency can be tuned by temperature and by an applied magnetic field, this leads to the possibility of constructing a tunable light oscillator.

II. SPIN RAMAN EFFECT IN FERROMAGNETS

For a Stokes process in which the material system is excited from the initial state $|i\rangle$ to the final state $|f\rangle$

* This research was supported by the U.S. Office of Naval Research under Contract Nonr 3656(32).
† Alfred P. Sloan Fellow.
[1] F. G. Bass and I. Kaganov, Zh. Eksperim. i Teor. Fiz., 37, 1390 (1959) [English transl.: Soviet Phys.—JETP 10, 986 (1960)].
[2] R. J. Elliot and R. Loudon, Phys. Letters 3, 189 (1963).
[3] Y. R. Shen and N. Bloembergen, Phys. Rev. 143, 372 (1966).
[4] P. A. Fluery, S. P. S. Porto, L. E. Cheesman, and H. J. Guggenheim, Phys. Rev. Letters 17, 84 (1966).

by absorbing a photon at frequency ω_0 and emitting a photon at ω_s, the Raman transition probability per unit volume per unit time as obtained from the second-order perturbation calculation is given by

$$W_{if}=(2\pi/\hbar)N\,|\,K\,|^2\rho_E$$

$$K=\sum_I\left\{\frac{\langle f,(n-1)_{k_0},(n+1)_{k_s}\,|\,\sum_b \mathcal{H}_{er}{}^b(\mathbf{k}_s,\omega_s)|\,I,(n-1)_{k_0},n_{k_s}\rangle\langle I,(n-1)_{k_0},n_{k_s}\,|\,\sum_b \mathcal{H}_{er}{}^b(\mathbf{k}_0,\omega_0)|\,i,n_{k_0},n_{k_s}\rangle}{\hbar(\omega_0-\omega_{Ii})}\right.$$

$$\left.-\frac{\langle f,(n-1)_{k_0},(n+1)_{k_s}\,|\,\sum_b \mathcal{H}_{er}{}^b(\mathbf{k}_0,\omega_0)|\,i,n_{k_0},(n+1)_{k_s}\rangle\langle I,n_{k_0},(n+1)_{k_s}\,|\,\sum_b \mathcal{H}_{er}{}^b(\mathbf{k}_s,\omega_s)|\,i,n_{k_0}n_{k_s}\rangle}{\hbar(\omega_s+\omega_{Ii})}\right\}$$

$$\rho_E=k_s{}^2g(\omega_s)d\Omega d\omega_s/(2\pi)^3c,$$

$$\omega_0=\omega_s+\omega_{fi}, \qquad (1)$$

where n_{k_0} and n_{k_s} are the initial numbers of photons in the incident ($\mathbf{k}_0$) and the scattered ($\mathbf{k}_s$) modes, ($n_{k_s}=0$ for spontaneous Raman scattering), N is the number of unit cells in the unit volume, $|\,I\,\rangle$ is the intermediate states of the material system, and $g(\omega_s)$, the line-shape function. The interaction between the radiation field and the bth atom in a unit cell is denoted by the Hamiltonian $\mathcal{H}_{er}{}^b$. In the electric-dipole approximation, it becomes

$$\mathcal{H}_{er}{}^b(\mathbf{k},\omega)=-e\mathbf{r}_b\cdot\mathbf{E}_b(\mathbf{k},\omega), \qquad (2)$$

the sum over electrons in the atom being omitted.

For one-phonon Stokes scattering process, one has $|\,i\,\rangle=|\,G,n_q\,\rangle$ and $|\,f\,\rangle=|\,G,(n+1)_q\,\rangle$ with $|\,G\,\rangle=\prod_b|\,g\,\rangle_b$, where $|\,g\,\rangle_b$ is the ground electronic state of the bth atom, and n_q is the number of phonons with a wave vector $\mathbf{q}=\mathbf{k}_0-\mathbf{k}_s$. It is readily seen from Eq. (1) that K would vanish if there were no electron-phonon interaction in the system, since the Hamiltonian $\mathcal{H}_{er}$ cannot connect states with different phonon occupation numbers.[5] Electron-phonon interaction $\mathcal{H}_{ep}$ operates on both ground and excited electronic states and mixes states $|\,n_q\,\rangle$ and $|\,(n+1)_q\,\rangle$. Consequently, the transition probability W_{if} no longer vanishes, but suffers a reduction factor of the order of $|\,\mathcal{H}_{ep}/\hbar\omega_q\,|^2$.

A similar situation arises in the case of the one-magnon Stokes process. Here, an eigenstate of the material system consists of spin and orbital parts. The spin part connected with the ground orbital state (which, for simplicity, is assumed to be quenched) is specified by the magnon occupation number. So, again, the initial and the final states can be written as $|\,i\,\rangle=|\,G,n_q\,\rangle$ and $|\,f\,\rangle=|\,G,(n+1)_q\,\rangle$ with $|\,G\,\rangle=\prod_b|\,g\,\rangle_b$, where $|\,g\,\rangle$ is the ground orbital state of a magnetic ion and n_q is the number of magnons with wave vector $\mathbf{q}=\mathbf{k}_0-\mathbf{k}_s$ and frequency ω_q given by the magnon dispersion relation for the magnetic medium. Also, since $\mathcal{H}_{er}$ cannot change the magnon occupation number, the Raman transition probability in Eq. (1) would be zero, if there were no spin-orbit coupling in ground and excited states. The term λL^-S^+ in the spin-orbit interaction $\mathcal{H}_{LS}$ mixes states $|\,n_q\,\rangle$ and $|\,(n+1)_q\,\rangle$, so that the transition probability W_{if} no longer vanishes, but suffers a reduction factor of the order of $|\,\mathcal{H}_{LS}/V_{crys}\,|^2$, where V_{crys} is the crystal field interaction.[3] Bass and Kaganov[2] suggested that the one-magnon Raman transition could become allowed if only the magnetic-dipole interaction is included in $\mathcal{H}_{er}$, as was first proposed by Winter and Javan[6] for the microwave Raman process in paramagnetic crystals. However, for visible frequencies, this mechanism leads to a Raman transition probability six to eight orders of magnitude smaller than the one induced by spin-orbit coupling.

There is a definite selection rule governing the one-magnon Raman transitions. In order to compensate the change of magnetic quantum number $\Delta m=1$ due to the excitation of a magnon, the incident field should have a right circular polarization around, and the scattered Stokes field a linear polarization along the magnetization, or vice versa. As a result, the Raman scattering depends in an interesting way on the relative directions of magnetization and propagation of the two beams. If the ground orbital state is not completely quenched, and the crystal field is large, the above selection rule in general breaks down.

The order of magnitude for the spin-Raman scattering cross section can be obtained by comparing with the normal Raman scattering cross section in organic liquids using Eq. (1). First, the uv oscillator strength of electric-dipole transitions for organic molecules is close to 1, but is usually less than 0.1 for magnetic ions. Then the reduction factor $|\,\mathcal{H}_{ep}/\hbar\omega_q\,|^2$ is about 10^{-2} for molecules, and $|\,\mathcal{H}_{LS}/V_{crys}\,|^2$ is about 10^{-2} to 10^{-4} for magnetic ions. Therefore, at visible frequencies, the spin-Raman effect would be about 10^{-2} to 10^{-4} times smaller than the ordinary Raman effect in liquids. Magnetic ions with unquenched orbital states should have larger spin Raman effect. For ferrites and antiferromagnets, because of opposite spins on different sublattices, the Raman scattering intensity may be reduced further (see Sec. III).

A more accurate estimate of the spin Raman effect

[5] Here, we have neglected the Hamiltonian $\mathcal{H}_{rl}$ for the interaction between radiation fields and the lattice. Inclusion of $\mathcal{H}_{rl}$ leads to two other mechanisms for one-phonon Raman scattering. See R. Loudon, Proc. Phys. Soc. (London) **82**, 393 (1963).

[6] J. M. Winter, J. Phys. Radium **19**, 834 (1958); A. Javan, *ibid.*, p. 836.

can often be obtained from the low-temperature optical rotatory power Φ of individual magnetic ions.[3]

$$\Phi=4\pi(\omega/nc)\alpha_F$$

$$\alpha_F=\tfrac{1}{2}\sum_I\{[\hbar(\omega-\omega_{Ii})]^{-1}+[\hbar(\omega+\omega_{Ii})]^{-1}\}\times[|\langle i|er_+|I\rangle|^2-|\langle i|er_-|I\rangle|^2] \quad (3)$$

For quenched orbital states, α_F would be zero if there were no spin-orbit coupling.[7] Thus, α_F^2 also suffers a reduction factor of $|\mathcal{H}_{LS}/V_{cryst}|^2$. One sees readily from Eq. (1) that α_F has the same order of magnitude as $|K|/|\langle(n-1)_{k_0}|E(\omega_0)|n_{k_0}\rangle\langle(n+1)_{k_s}|E(\omega_s)|n_{k_s}\rangle|$ in the spin Raman effect. Consequently, the differential spin Raman scattering cross section is given by $d\sigma/d\Omega\sim(\omega_0/c)^4\alpha_F^2$. As an example, Eu^{2+} in CaF_2 has a rotatory power with $\alpha_F\approx5\times10^{-26}$ in the red. This would yield $d\sigma/d\Omega\approx2.5\times10^{-32}$ cm^2/(Eu^{2+} ion)(sr) which is about three orders of magnitude smaller than that of the 992 cm^{-1} vibrational mode of benzene.[8] ($d\sigma/d\Omega=3.3\times10^{-29}$ cm^2/sr at 4880 Å). Ferromagnetic Eu^{2+} compounds could have $\alpha_F\approx10^{-24}$ in the visible[9] and hence $d\sigma/d\Omega\sim10^{-29}$ cm^2/sr. This anomalously large rotatory power and spin Raman effect of Eu^{2+} arise as a result of ω_0 approaching ω_{Ii} in the resonant denominator. It is also interesting to note that Gd^{3+}, being isoelectronic with Eu^{2+}, has nevertheless extremely small rotatory power in the visible. This is because ω_0 is so far away from ω_{Ii} that the set of excited P_J multiplets can be considered as degenerate,[10,7] and hence the net effect of spin-orbit coupling on optical rotatory power from the degenerate multiplets is zero. The same argument should also apply to spin Raman effect.

Both the Faraday effect and the spin Raman effect can be described in terms of spin Hamiltonians. From Eq. (1), with the perturbation of spin-orbit interaction, we find

$$K=\langle(n+1)_q,(n-1)_{k_0},(n+1)_{k_s}|\mathcal{H}_{int}|n_q,n_{k_0},n_{k_s}\rangle,$$

where the spin Hamiltonian for the Raman interaction is

$$\mathcal{H}_{int}=\sum_b A_b S_b^+(\omega_q)[E_b^-(\omega_0)E_b^z(\omega_s)+E_b^-(\omega_s)E_b^z(\omega_0)]+\text{adjoint}, \quad (4)$$

A_b being a coefficient independent of the spin S and the fields E. The spin Hamiltonian for the Faraday effect in the same magnetic material is found to be[3,11]

$$\mathcal{H}_F=\sum_b B_b S_b^z(0)[|E_b^+(\omega_0)|^2-|E_b^-(\omega_0)|^2]. \quad (5)$$

The coefficients A and B in Eqs. (4) and (5) have the same order of magnitude as α_F/S both vanishing in the absence of spin-orbit coupling. Selection rules for the two effects are seen explicitly from the expressions of the spin Hamiltonians.

There are n magnon branches corresponding to n magnetic ions in a unit cell.[12] For each branch in the long-wavelength limit, one has

$$\omega_q=\omega^0+\beta q^2. \quad (6)$$

Here, ω^0 and β depend upon magnetizations, anisotropy, and the applied magnetic field on different sublattices. In general, ω_q decreases as the magnetizations and anisotropy energy decrease. With increasing temperature, both magnetizations and anisotropy decrease; one would then find that the Stokes frequency shifts to the short-wavelength side. Measurements of ω_q could yield information about exchange coupling between magnetic ions and the anisotropy field in the lattice.

At finite temperatures, the integrated Stokes scattering intensity should be proportional to $\langle n_q(T)\rangle+1$, while the integrated anti-Stokes scattering intensity should be proportional to $\langle n_q(T)\rangle$. Thus, the anti-Stokes scattering intensity would grow with increasing temperature, but the Stokes scattering intensity would remain more or less unchanged until the thermal excitations of magnons become so high that $\langle n_q\rangle$ is a non-negligible fraction of 1. The linewidth, as determined by the relaxation of magnon excitations, is also a strong function of temperature. While no satisfactory theory exists for the magnon relaxation, the linewidth can possibly be accounted for by fluctuations in the molecular field.[13] Generally, the linewidth would increase strongly with temperature. The magnon spectrum disappears eventually as temperature approaches the Curie point. Above the Curie temperature, Raman scattering from individual paramagnetic ions results.

In principle, the two-magnon Raman scattering process, analogous to two-phonon Raman scattering, also exists. For ferromagnets with quenched orbital states, spin-orbit coupling has to be used twice in the perturbation in order to change the magnon occupation number by 2. The corresponding two-magnon Raman effect suffers a reduction factor of $|\mathcal{H}_{LS}/V_{cryst}|^4$. For ferrites and antiferromagnets, two-magnon Raman scattering can in fact occur without the help of spin-orbit coupling, as we shall discuss in the following section.

III. SPIN RAMAN EFFECT IN ANTIFERROMAGNETS

Recently, Fleury *et al.*[4] reported observation of Raman scattering by magnons in antiferromagnets FeF_2 and MnF_2. In this section, we shall show that their results agree satisfactorily with theoretical calculation.

Consider a ferrite with two sublattices A and B.

[7] Y. R. Shen, Phys. Rev. **133**, A511 (1964).
[8] J. G. Skinner and W. G. Nilsen, Annual Meeting of the Optical Society of America in San Francisco, 1966, Paper WE-11.
[9] J. C. Suits (private communication).
[10] L. Rosenfeld, Z. Physik **57**, 835 (1929).
[11] P. S. Pershan, J. P. van der Ziel, and L. D. Malmstrom, Phys. Rev. **143**, 574 (1966).
[12] See, for example, B. Harris, Phys. Rev. **132**, 2398 (1963).
[13] F. M. Johnson and A. H. Nethercot, Phys. Rev. **114**, 705 (1959).

Assume that exchange coupling exists only between spins on different sublattices. This gives rise to two magnon branches. The optical magnon mode at $q=0$ is[14]

$$\omega^0=\tfrac{1}{2}(\omega_{eB}+\omega_{aA}-\omega_{eA}-\omega_{aB})+\tfrac{1}{2}[(\omega_{eA}+\omega_{eB}+\omega_{aA}+\omega_{aB})^2-4\omega_{eA}\omega_{eB}]^{1/2}, \tag{7}$$

where ω_{eA}, ω_{eB}, ω_{aA}, and ω_{aB} are the exchange and anisotropic frequencies for spins in the two sublattices. The zero- and the one-magnon states are[3]

$$\begin{aligned}
&|0_q\rangle=\prod_i |-,+\rangle_i,\\
&|1_q\rangle=(1/N)^{1/2}\sum_j[(\mu_1|+,+\rangle_j-\mu_2|-,-\rangle_j)\prod_{i\neq j}|-,+\rangle_i]\exp(i\mathbf{q}\cdot\mathbf{R}_j),\\
&\mu_1=\omega_{eA}/D, \qquad \mu_2=(\omega_{eB}+\omega_{aA}-\omega^0)/D\\
&D=[\omega_{eA}^2+(\omega_{eB}+\omega_{aA}-\omega^0)^2]^{1/2},
\end{aligned} \tag{8}$$

$|\pm,\pm\rangle_j$ being the spin states for the jth unit cell. The spin operators in ferrites are defined as $S_{Az}=S_a$, $S_{Bz}=-S_b$, and $S_A^{\pm}|\mp\rangle_A=|\pm\rangle_A$ and $S_B^{\pm}|\pm\rangle_B=|\mp\rangle_B$. From Eq. (1), with the help of Eqs. (4) and (8), we find

$$K=(\mu_1A_A-\mu_2A_B)\,\langle(n-1)_{k_0},(n+1)_{k_s}|[E_b^-(\omega_0)E_b^z(\omega_s)+E_b^z(\omega_0)E_b^-(\omega_s)]|n_{k_0},n_{k_s}\rangle. \tag{9}$$

Here, A_A and A_B have the same order of magnitude as the Faraday coefficients α_F/S for ions in the two sublattices. The selection rule manifests itself in Eq. (9). Similar to the case of direct infrared excitation,[15] the one-magnon Raman transition probability for ferrites suffers a reduction factor of

$$|2(\mu_1A_A-\mu_2A_B)/(A_A+A_B)|^2$$

as compared with the case where spins on the two sublattices were aligned in the same direction.

For antiferromagnets FeF_2, MnF_2, etc., we have $A_A=A_B\sim\alpha_F$. Then, the one-magnon differential Raman scattering cross section is $d\sigma/d\Omega\sim(\mu_1-\mu_2)^2(\omega_0^4/c^4)\alpha_F^2$. In the case of FeF_2, the exchange field ω_e/γ and the anisotropy field ω_a/γ, with $\gamma=ge/2mc$, are 540 and 200 kOe respectively.[16] One gets, from Eq. (8), $\mu_1=0.905$ and $\mu_2=0.406$. If we assume that the rotatory power of Fe^{2+} is the same as that of Eu^{2+}, then the one-magnon Raman scattering in FeF_2 is $d\sigma/d\Omega\sim 6\times10^{-33}$ cm^2/sr, which is about four orders of magnitude smaller than that of benzene, and agrees with experimental observation.[4] It should be noticed that if the anisotropy field were zero, μ_1 would be equal to μ_2 and the Raman effect would disappear. In MnF_2, the anisotropy field $\omega_a/\gamma=7.2$ kOe is indeed small compared with the exchange field $\omega_e/\gamma=392$ kOe.[17] We find $\mu_1=0.771$ and $\mu_2=0.637$. In addition, the rotatory power of Mn^{2+} is perhaps at least one order of magnitude smaller than that of Eu^{2+}. Therefore, $d\sigma/d\Omega<5\times10^{-35}$ cm^2/sr. Experimentally, no one-magnon Raman scattering has been observed.[4]

The Raman scattering experiments also show that the magnon mode $\omega_{q=0}$ decreases with increasing temperature. The results agree qualitatively with the calculation by Ohlmann and Tinkham[16,18] using the molecular-field approximation. They also found a T^4 dependence of the linewidth of the magnon mode. Broadening of the Stokes component with temperature has indeed been observed,[4] although the T^4 dependence has not been checked carefully. The peak of the Stokes component should be inversely proportional to the linewidth. The anti-Stokes component was observed at temperatures above 30°.

With an external magnetic field H along the preferred axis, the degeneracy of the magnon mode is lifted[19]

$$\omega_q(H)=\omega_q(0)\pm\gamma H+O(H^2). \tag{10}$$

The splitting is about 4 cm^{-1} for $H=20$ kOe. This should be observable in Raman scattering at sufficiently low temperature.

Fleury *et al.*[4] also reported the observation of two-magnon Raman scattering in FeF_2 and MnF_2. The two-magnon lines appear to be somewhat more intense than the one-magnon line in FeF_2. This eliminates the possibility that they arise as a result of second-order perturbation of spin-orbit interaction on the states. In fact, exchange-type interaction between magnetic ions on opposite sublattices is possibly responsible for the two-magnon Raman scattering as suggested by London.[4,20] The same mechanism has been used to explain the magnon side band of optical absorption lines[21] and the two-magnon infrared absorption.[22] Here, the exchange type interaction $V_{mn}=J_{mn}S_m^+S_n^+$ be-

[14] T. Nagamiya, K. Yosida, and R. Kubo, Advan. Phys. 4, 14 (1955).
[15] M. Tinkham, Phys. Rev. **124**, 311 (1961).
[16] R. C. Ohlmann and M. Tinkham, Phys. Rev. **123**, 425 (1961).
[17] J. Kanamori and H. Minatono, J. Phys. Soc. Japan **17**, 1759 (1962).
[18] T. Oguchi, Phys. Rev. **111**, 1063 (1958). S. Foner, Phys. Rev. **107**, 683 (1957).
[19] C. Kittel, *Quantum Theory of Solids* (John Wiley & Sons, Inc., New York, 1963).
[20] R. London (unpublished).
[21] R. L. Greene, D. D. Sell, W. M. Yen, A. L. Schawlow, and R. M. White, Phys. Rev. Letters **15**, 656 (1965); P. G. Russel, D. S. McClure, and J. W. Stout, *ibid.* **16**, 176 (1966).
[22] Y. Tanabe, T. Moriya, and S. Sugano, Phys. Rev. Letters **15**, 1023 (1965). J. W. Halley and I. Silvera, *ibid.*, p. 654; S. J. Allen, R. Loudon, and P. L. Richards, *ibid.* **16**, 463 (1966).

tween ions m and n connects the states $|g_m,-;i_n,+\rangle$ and $|i_m,+;g_n,-\rangle$ and creates two magnons by flipping the spins on both ions simultaneously. The corresponding matrix element product for the Raman transitions is

$$\langle g_m,-;g_n,+|\,e\mathbf{r}_n\,|g_m,-;i_n,+\rangle \times\langle g_m,-;i_n,+|\,V_{mn}\,|i_m,+;g_n,-\rangle \times\langle i_m,-;g_n,-|\,e\mathbf{r}_m\,|g_m,+;g_n,-\rangle.$$

More generally, regardless of the detailed mechanisms, one can derive a spin Hamiltonian for the two-magnon Raman transitions

$$\mathcal{H}_{\rm int}=\sum_{m,n}(\mathbf{E}_m^{(\omega_l)}\cdot\mathbf{A}_{mn}\cdot\mathbf{E}_n^{*(\omega_s)})(S_m^+S_n^+)+\text{adjoint}. \tag{11}$$

Transformation of the above expression into momentum space yields

$$\mathcal{H}_{\rm int}=\sum_q(\mathbf{E}^{(\omega_l)}\cdot\mathbf{A}_q\cdot\mathbf{E}^{*(\omega_s)})S_{1q}^+S_{2,-q}^++\text{adjoint}, \tag{12}$$

where we assume that the wave vectors of the radiation fields are negligible compared with q. Thus, the two magnons must have approximately equal and opposite wave vectors $\pm\mathbf{q}$, and the corresponding Stokes frequency is $\omega_s=\omega_l-2\omega_q$. Not all components of $\mathbf{A}$ in Eqs. (11) and (12) are independent since the spin Hamiltonian must be invariant under the operations of the crystal symmetry group. The two-magnon Raman spectrum can then be calculated if both $\mathbf{A}$ and the magnon density of states are known. Matching of the theoretical curve to the experimental spectrum yields information about the magnitudes of $\mathbf{A}$ and the exchange coupling V_{mn} between spins. A similar approach was used by Allen, Loudon, and Richards[22] to interpret the observed two-magnon absorption spectrum. Thus, Loudon was able to explain the observed two-magnon Raman spectra in FeF_2 and MnF_2.[20] There are two peaks in both spectra.[23] The one at higher frequency arises because of the singularity in the magnon density of states at the center of the (100) face in the Brillouin zone. It has a selection rule which requires both the laser and the Stokes polarizations perpendicular to the c axis (or z axis), but at right angles to each other.[23] The one at lower frequency arises because of the singularity in the magnon density of states at the (111) corner of the Brillouin zone. The associated selection rule requires the laser polarization parallel and the Stokes polarization perpendicular to the c axis, or vice versa.[23]

The intensity ratio of two-magnon to one-magnon Raman scattering is

$$|(nV_{mn}/2\omega_q)/(\lambda\mathbf{L}\cdot\mathbf{S}/V_{\rm cryst})(\mu_1-\mu_2)|^2,$$

where n is the number of nearest neighbors. For FeF_2, $(nV_{ij}/2\omega_q)\sim(1/4S)$, $S=2$, $|\lambda\mathbf{L}\cdot\mathbf{S}/V_{\rm cryst}|\sim1/10$, and hence the intensity ratio is of the order of 1, as observed experimentally. A similar result was also found by Loudon.[20]

With an external magnetic field along the preferred axis, the degeneracy of the magnon branch is lifted as given by Eq. (10). Since the two-magnon Raman process we have described preserves the total spin magnetization along the field, the two magnons must come from the two Zeeman branches respectively.[24] Thus, to the lowest order in H, there would be no magnetic field effect on the two-magnon Raman spectrum since $\omega_q(H)+\omega_{-q}(H)=2\omega_q(0)$.[23]

The two-magnon Raman spectrum indicates that the magnon frequencies at the edges of the Brillouin zone also decrease with increasing temperature. Silvera and Halley[25] have calculated the temperature variation of $\omega_q(T)$, using the molecular field approximation of Ohlmann and Tinkham.[16] Their results agree qualitatively with experiments. From the above discussion, it is seen that the observed Raman spectra in FeF_2 and MnF_2 can indeed be described satisfactorily by the theory.

IV. RAMAN SCATTERING FROM MAGNETOELASTIC MODES

In a magnetic crystal, the spin wave can also couple linearly with the phonon wave through the magnetoelastic coupling.[26] This happens if the dispersion curves of magnons and phonons would intersect (Fig. 1). The coupling is most effective in the region near the intersection. If the coupling energy is large compared with the linewidth, there would be a splitting of the

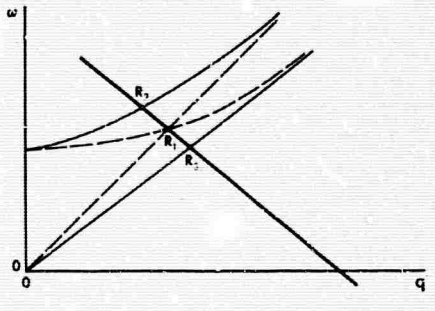

FIG. 1. Dispersion curves describing spin Raman scattering from magnetoelastic modes. The dashed and the solid curves correspond to the cases of small and large magnetoelastic coupling respectively. The heavy line describes the energy and momentum matching condition $q=|\mathbf{k}_0-\mathbf{k}_s|=[\omega_0(n_0\hat{k}_0-n_s\hat{k}_s)\cdot\hat{q}+\omega n_s\hat{k}_s\cdot\hat{q}]/c$. The intersecting points R_1, R_2, and R_3 denote the magnetoelastic modes contributing to the Raman scattering.

[22] P. A. Fleury and S. P. S. Porto, Annual Meeting of the Optical Society of America in San Francisco, 1966, Paper WE-17.

[24] Similar situation arises in the magnon side band of optical absorption and in the two-magnon infrared absorption. R. M. White (private communications).

[25] I. Silvera and W. Halley, Phys. Rev. 149, 415 (1966).

[26] C. Kittel, Phys. Rev. 110, 836 (1958).

dispersion curves at the intersection. (Fig. 1). Otherwise, no splitting exists. A new mode, with mixed character of magnons and phonons, now arises because of the coupling. This is known as the magnetoelastic mode. Both the dispersion curves and the amount of mixture in the magnetoelastic mode can be determined by solving the coupled equations of motion for magnons and phonons. Thus, the state corresponding to a single excitation of the magnetoelastic mode is

$$|1_q\rangle_{me}=\alpha_1|1_q\rangle_{\text{phonon}}+\alpha_2|1_q\rangle_{\text{magnon}}, \qquad (13)$$

where $|\alpha_1|^2+|\alpha_2|^2=1$.

Raman scattering by a magnetoelastic mode would certainly occur if the energy and momentum matching conditions can be satisfied,

$$q=|\mathbf{k}_0-\mathbf{k}_s|=[\omega_0(n_0\hat{k}_0-n_s\hat{k}_s)\cdot\hat{\mathbf{q}}+\omega_q n_s\hat{k}_s\cdot\hat{\mathbf{q}}]/c.$$

From Eqs. (1) and (13), this Raman transition probability is given by

$$W_{if}=(2\pi/\hbar)N|\alpha_1K_{\text{ph}}+\alpha_2K_{\text{mag}}|^2\rho_E, \qquad (14)$$

where K_{ph} and K_{mag} are the Raman scattering amplitudes by one phonon and one magnon at ω_q, respectively. If $|\alpha_1|\approx|\alpha_2|$, and $|K_{\text{ph}}|\gg|K_{\text{mag}}|$, then $W_{if}\approx(2\pi/\hbar)N|\alpha_1K_{\text{ph}}|^2\rho_E$. Therefore, the probability of exciting a magnon through the Raman process can be enhanced by the magnetoelastic coupling. This is particularly important in the consideration of generating magnon waves by the stimulated Raman process.[3]

Different magnetoelastic modes are excited by Stokes scattering at different angles. Since α_1/α_2 is different for different modes, it is interesting to see how the intensity and the polarization property of the Stokes change as the angle changes. The results could yield information about the magnetoelastic coupling in the crystal.

Since the magnon frequency varies with temperature T and the external magnetic field H, the intersection of the dispersion curves of phonons and magnons can be tuned over a limited range by adjusting T and H. The Stokes scattering will be changed correspondingly in a predictable way.

V. TUNABLE SPIN RAMAN OSCILLATOR

We have seen in the preceding sections that the Stokes frequency in the one-magnon Raman scattering can be tuned by temperature, by applied magnetic field, or by angle of scattering. Thus, a tunable light oscillator could be achieved if the Raman process can be made into a stimulated one.

The stimulated Raman gain can be calculated from the Raman transition probability W_{if}.[3] In particular, if the magnon damping is sufficiently strong, the gain is directly proportional to W_{if}.[27,3]

$$G(\omega_s)=(4\pi c^2/\hbar\omega_0^2\omega_s\epsilon_s^{1/2})|E_0|^2N(d\sigma/d\Omega)g(\omega_s). \qquad (15)$$

With $N=5\times10^{21}$ cm^{-3}, $d\sigma/d\Omega=10^{-31}$ cm^2, $|E_0|=450$ esu for a 100-MW/cm^2 laser beam, and a magnon linewidth of 5×10^{10} sec^{-1}, the maximum gain at resonance is $G_{\max}=2.5\times10^{-2}$ cm^{-1}. Stimulated Raman scattering can occur if $G_{\max}$ is larger than the Stokes loss per centimeter in the medium. This gain $G_{\max}$ is about two orders of magnitude smaller than that of benzene. However, the scattering cross section in some magnetic materials can be much larger, or the linewidth smaller. The gain can also be enhanced by the magnetoelastic coupling as we mentioned earlier.

Stimulated Raman scattering has been observed in benzene in a cell with or without reflecting end mirrors. In the former case, the complication of self-focusing[28] could be avoided. For the spin Raman effect, one would also expect to see stimulated scattering in such a resonant cavity if the laser intensity is sufficiently high and the loss in the medium sufficiently low. The laser and the Stokes radiation are usually made parallel to each other to achieve the maximum interaction length. However, sometimes it is more advantageous to have the laser at an angle to the Stokes radiation. Then, the cavity geometry of Dennis and Tannenwald[29] should be used. This applies to the case of Raman scattering by the magnetoelastic modes. Here, in order to obtain the maximum gain one would like to have the Stokes radiation in the direction corresponding to a mode with maximum phonon-magnon coupling. This direction changes as the mode frequency is tuned by either the temperature or the external magnetic field. The tuning range of such a light oscillator is about a few reciprocal centimeters.

---

[27] Y. R. Shen and N. Bloembergen, Phys. Rev. **137**, A1787 (1965). R. W. Hellwarth, *ibid.* **130**, 1850 (1963).

[28] See, for example, E. Garmire, R. Y. Chiao, and C. H. Townes, Phys. Rev. Letters **16**, 347 (1966).

[29] J. H. Dennis and P. E. Tannenwald, Appl. Phys. Letters **5**, 58 (1964).

APPENDIX XI

Reprinted from THE PHYSICAL REVIEW, Vol. 155, No. 3, 921-931, 15 March 1967
Printed in U. S. A.

Quantum Statistics of Nonlinear Optics*

Y. K. SHEN†
Physics Department, University of California, Berkeley, California
(Received 30 September 1966)

Nonlinear interaction of light with matter is described from the quantum-statistical point of view. The cases of two-photon absorption, Raman transition, sum-frequency generation, parametric amplification, and incoherent scattering are discussed. It is shown that the nonlinear optical effects depend strongly on the statistical properties of the light fields. The rate of nonlinear absorption, generation, and amplification is higher for chaotic than for coherent, and also higher for multimode than for single-mode pump fields. Measurements of the statistics of the output fields may yield information about the statistics of the input fields and the properties of the medium.

I. INTRODUCTION

THE quantum statistical properties of light from various sources have recently been extensively investigated.[1,2] However, the question whether interaction of light with matter would change statistical properties of light fields has seldom been raised. The purpose of this paper is to extend the quantum-statistical description to the case of light fields after interacting with a medium. Emphasis is on the effect of nonlinear interaction of light with the medium.

It is usually assumed in the literature that statistical properties of a light beam remain unchanged in traversing a medium if the response of the medium to the light fields is linear. This assumption is certainly a valid one for a nonabsorbing medium, since the linear interaction of light with the medium cannot disturb the probability distribution of photons in their number states (if the disturbance due to incoherent scattering can be neglected. See Sec. III). Only their spatial distribution is changed through the interaction. Let the vector potential be written in the usual form[3]

$$\mathbf{A}(\mathbf{r},t)=c\sum_k (2\pi\hbar/\omega_k)^{1/2} \times\{a_k\mathbf{u}_k(\mathbf{r})\exp(i\omega_k t)+a_k^\dagger\mathbf{u}_k^*(\mathbf{r})\exp(-i\omega_k t)\}, \quad (1)$$

where $a^\dagger$ and a are the creation and the annihilation operators, respectively, for the kth mode. (The subindices indicating the polarization of the fields are being omitted.) The spatial function $\mathbf{u}_k(\mathbf{r})$ is a normalized eigenfunction of the differential equation

$$[\nabla^2+\omega_k^2\epsilon_k(\mathbf{r})/c^2]\mathbf{u}_k(\mathbf{r})=0, \quad (2)$$

where $\epsilon_k(\mathbf{r})$ is the linear dielectric constant at frequency ω_k.[4] From Sturm-Louivelle theory, the orthonormality condition gives

$$\int(\epsilon_k\epsilon_l)^{1/2}\mathbf{u}_k(\mathbf{r})\mathbf{u}_l^{*}\,d\tau=\delta_{kl}. \quad (3)$$

Then, the Hamiltonian of the fields in the presence of the linear nonabsorbing medium reduces to the familiar form

$$\mathcal{H}=\sum_k \hbar\omega_k(a_k^\dagger a_k+\tfrac{1}{2}). \quad (4)$$

Thus, the photon statistics of the fields is not changed except that the spatial distribution, described by $\mathbf{u}_k(\mathbf{r})$, is now different from the vacuum case.

This is not quite true if the medium is lossy. An obvious example is the case where originally there are exactly n_k photons present in such a medium. After the absorption has been switched on for a finite length of time, the photon system has finite probabilities in the occupation number states $|n_k\rangle$, $|(n-1)_k\rangle$, $|(n-2)_k\rangle$, etc. The statistical properties of the photon system have clearly been changed. Assume that the medium has an electric-dipole transition between atomic states $|\psi_2\rangle$ and $|\psi_1\rangle$ with frequency separation ω_{21}, which coincides with the photon frequency of the kth mode. The single-photon absorption can be described by the interaction Hamiltonian

$$\mathcal{H}_{\rm int}=\sum_i\{\xi c_{2i}^\dagger c_{1i}\mathbf{E}_k^{(-)}(\mathbf{r}_i)+\xi^* c_{2i}c_{1i}^\dagger\mathbf{E}_k^{(+)}(\mathbf{r}_i)\}. \quad (5)$$

Here, c_{1i}, c_{2i}, $c_{1i}^\dagger$, and $c_{2i}^\dagger$ are creation and annihilation operators for the ith atom in states 1 and 2, respectively. ξ is the electric-dipole matrix element for the transition. The positive-frequency part of the electric field at the ith atom is given by

$$\mathbf{E}_k^{(+)}(\mathbf{r}_i)=\mathbf{E}_k^{(-)}(\mathbf{r}_i)^\dagger=i(2\pi\hbar\omega_k)^{1/2}\mathbf{u}_k^*(r_i)a_k^\dagger. \quad (6)$$

In the interaction representation, the equation of

* Research was supported by the U. S. Office of Naval Research under Contract Nonr 3656(32). Preliminary results of this paper were reported in the Second Rochester Conference on Coherence and Quantum Optics, Rochester, New York, June, 1966.
† Alfred P. Sloan Research Fellow.
[1] R. Glauber, *Quantum Optics and Electronics*, edited by C. DeWitt *et al.* (Gordon and Breach Science Publishers, Inc., New York, 1965).
[2] See, for example, Abstracts on Second Rochester Conference on Coherence and Quantum Optics, Rochester (unpublished).
[3] See, for example, W. Heitler, *Quantum Theory of Radiation* (Clarendon Press, Oxford, England, 1954), p. 54.
[4] In general the coherent linear response of a medium to the fields can be described completely by a generalized linear dielectric tensor $\epsilon_k(\mathbf{r})$; see Y. R. Shen, Phys. Rev. 133, A511 (1964). In this paper, we shall assume that $\epsilon_k(\mathbf{r})$ is a scalar, and that all fields are linearly polarized.

motion for the density matrix ρ of the composite system is

$$i\hbar\partial\rho/\partial t=[\mathcal{H}_{\rm int}(t),\rho(t)]. \quad (7)$$

Iteration of ρ for small increment of t in the above equation gives[6]

$$\partial\rho(t_0+t)/\partial t=(1/i\hbar)[\mathcal{H}_{\rm int}(t_0+t),\rho(t_0)]+(-1/\hbar^2)\int_{t_0}^{t_0+t}[\mathcal{H}_{\rm int}(t_0+t),\times[\mathcal{H}_{\rm int}(t'),\rho(t_0)]]dt'+\cdots. \quad (8)$$

We now assume that the thermal equilibrium of the atomic system is not disturbed by photon fields. The density matrix can then be written as $\rho(t)=\rho_F(t)\times\prod_i\rho_{Ai}(0)$, where ρ_F and ρ_{Ai} are density matrix operators for the photon system and for the ith atom, respectively. This is known as the irreversible approximation.[6] We have, with the same approximation as used in the ordinary time-dependent perturbation calculation,[5,7] namely, $\hbar/|\mathcal{H}_{\rm int}|>t\gg 1/(\text{linewidth})$,

$$\partial\rho_F/\partial t=\mathrm{Tr}_A(\partial\rho/\partial t)=-\beta[(a_k^\dagger a_k\rho_i-2a_k\rho_F a_k^\dagger+\rho_F a_k^\dagger a_k)\rho_{1A}^0+(a_k a_k^\dagger\rho_F-2a_k^\dagger\rho_F a_k+\rho_F a_k a_k^\dagger)\rho_{2A}^0], \quad (9)$$

where

$$\beta=\sum_i\omega_k|\xi|^2|\mathbf{u}_k(\mathbf{r}_i)|^2g(\omega_k)/4\hbar\approx[\pi\omega_k|\xi|^2g(\omega_k)/\hbar]\int_V d^3r|\mathbf{u}_k(\mathbf{r})|^2N(\mathbf{r}).$$

Here $g(\omega_k)$ is the line shape function, $N(\mathbf{r})$ is the density of atoms at the position $\mathbf{r}$, and ρ_{1A}^0 and ρ_{2A}^0 are the thermal populations for the two atomic states. The integration extends over the volume of the medium. The constant β is related to the absorption coefficient. If $\rho_F(t)$ is known, statistical properties of the fields, such as temporal and spatial coherence, can readily be determined. From Eq. (9), one obtains

$$\partial\langle a_k\rangle/\partial t=-\beta(\rho_{1A}^0-\rho_{2A}^0)\langle a_k\rangle,$$
$$\partial\langle a_k^\dagger a_k\rangle/\partial t=-2\beta(\rho_{1A}^0-\rho_{2A}^0)\langle a_k^\dagger a_k\rangle+2\beta\rho_{2A}^0. \quad (10)$$

The last term in the above equation corresponds to spontaneous emission.

Equation (9) governs the change of statistical properties of the photon system in the single-photon absorption process. In particular, at zero temperature, if initially the photon system is in a coherent state,[1] $\rho_F(t_0)=|\alpha_k\rangle\langle\alpha_k|$, then it is easily shown that

$$\rho_F(t_0+\Delta t)=\{\sum_{n_k}[1-\beta\Delta t(n_k-|\alpha_k|^2)](\alpha_k^{2n_k}/n_k!)^{1/2}\times\exp(-\tfrac{1}{2}|\alpha_k|^2)|n_k\rangle\}\sum_{m_k}\langle m_k|\times[1-\beta\Delta t(m_k-|\alpha_k|^2)(\alpha_k^{2m_k}/m_k!)^{1/2}\times\exp(-\tfrac{1}{2}|\alpha_k|^2)\}\xrightarrow[\Delta t\to 0]{}|\alpha_k\exp(-\beta\Delta t)\rangle\times\langle\alpha_k\exp(-\beta\Delta t)|;$$
$$\rho_F(t_0+t)=|\alpha_k\exp(-\beta t)\rangle\langle\alpha_k\exp(-\beta t)|. \quad (11)$$

This shows that a coherent photon system remains coherent although the field amplitude decreases exponentially with time. More generally, if the initial photon field can be described by the P representation,[1]

$$\rho_F(t_0)=\int d^2\alpha_k P(\alpha_k)|\alpha_k\rangle\langle\alpha_k|,$$

one would get

$$\rho_F(t_0+t)=\int d^2\alpha_k P(\alpha_k)|\alpha_k\exp(-\beta t)\rangle\times\langle\alpha_k\exp(-\beta t)|. \quad (12)$$

The statistical properties of the fields are being changed in a rather trivial way, since it is simply a translation of the distribution $P(\alpha_k)$ in the α_k space.

No such simple solution exists if the equilibrium temperature of the atomic system is finite, since the spontaneous emission now comes into play. Consequently, the coherent properties of a beam will be disturbed in passing through the absorbing medium. The disturbance is, of course, small if the spontaneous emission process can be neglected in comparison with either the stimulated absorption or emission. This is certainly true for light beams in a medium at room temperature.

The same approach can be applied to the case of multiphoton transitions. Again, since the photon distribution can be disturbed by the transitions, statistical properties of the photon system are changed. The case of two-photon transitions, which includes Raman transitions, will be discussed in Sec. II. In general, even if the medium is not lossy, statistical properties of light are changed by nonlinear interaction of light with a medium, although the disturbance might be small for weak interaction. The nonlinear interaction couples different photon modes and leads to energy transfer between the modes. Photons in some modes may be annihilated, while those in other modes created, and hence the photon distribution is disturbed. Oftentimes the rate of energy transfer between the modes depends on the statistical properties of the light fields, usually higher for chaotic than for coherent sources.

For investigation of properties of a medium, incoherent scattering has long been a useful tool. Statistics

[6] C. P. Slichter, *Principles of Magnetic Resonance* (Harper and Row Publishers Inc., New York, 1963), p. 127.
[6] F. Bloch, Phys. Rev. 102, 104 (1956).
[7] See, for example, L. I. Shiff, *Quantum Mechanics* (McGraw-Hill Book Company, Inc., New York, 1955), p. 189.

is particularly important in this case for analyzing the results of experiments. In Sec. III, linear and nonlinear incoherent scattering are discussed. As is expected, the scattered radiation depends on the statistical nature of both the incident beam and the fluctuations in the medium. For nonlinear optics, one is perhaps more interested in coherent scattering. We shall discuss in Secs. IV and V two important cases, sum-frequency generation and parametric amplification, respectively. In all cases, there are one or more pump fields present. We shall not concern ourselves too much about how the statistical properties of the pump modes change. Instead, we are interested in finding the statistical properties of the generated modes, and the rate of generation as a function of the statistical nature of the pump modes. Conversely, from the statistical properties of the generated modes or the rate of generation, one could obtain some information about the statistical nature of the pump modes.

It must be noted that in our discussion of single-photon absorption, we have assumed a bounded system for the photon fields. This type of treatment is most conveniently applied to the case of a cavity; photons are neither coming into nor going out of the cavity. In principle, the same treatment can be applied to problems of light propagation in a medium. In practice, it is indeed successful in dealing with incoherent scattering (see Sec. III), but for coherent scattering, it becomes extremely difficult. Rigorously, the latter case should perhaps be treated by the method of many-body transport theory.[8] However, imagine an infinite medium and a box of finite volume in which the photon fields are quantized.[9] This box of photons interacts with the medium for a time t, as its center modes in the z direction from z_1 to z_1+ct, where c is the light velocity in the medium. The resultant change of statistical properties of fields in the box can now be calculated using the cavity treatment. A more general treatment of the propagation problems is given in the Appendix. For steady-state propagation, it is shown that the results are essentially the same as in the cavity case with t replaced by $-z/c$, as one would expect.

II. TWO-PHOTON ABSORPTION AND RAMAN TRANSITIONS

The calculation for two-photon absorption is essentially similar to that for single-photon absorption, except that the mathematics becomes more complicated. Here, an atom makes transition from the state $|\psi_1\rangle$ to the state $|\psi_2\rangle$ by absorbing one photon in the kth mode and another in the lth mode. The interaction Hamiltonian is

$$\mathcal{H}_{\rm int}=\sum_i \{\eta c_{2i}^{\dagger}c_{1i}\mathbf{E}_k^{(-)}(\mathbf{r}_i)\mathbf{E}_l^{(-)}(\mathbf{r}_i)+\text{adjoint}\}, \quad (13)$$

where η is the matrix element for the two-photon transitions.[10,11] Using the same procedure as in the case of single-photon absorption, one can find that the density matrix ρ_F for the photon system obeys the equation

$$\partial\rho_F/\partial t=-\beta^{(2)}[(a_k^{\dagger}a_l^{\dagger}a_ka_l\rho_F-2a_ka_l\rho_Fa_k^{\dagger}a_l^{\dagger}+\rho_Fa_k^{\dagger}a_l^{\dagger}a_ka_l)\rho_{1A}^0+(a_ka_la_k^{\dagger}a_l^{\dagger}\rho_F-2a_k^{\dagger}a_l^{\dagger}\rho_Fa_ka_l+\rho_Fa_ka_la_k^{\dagger}a_l^{\dagger})\rho_{2A}^0], \quad (14)$$

with

$$\beta^{(2)}\cong[2\pi^2\omega_k\omega_l|\eta|^2g(\omega_k+\omega_l)]\int_V d^3r\times N(r)|\mathbf{u}_k(\mathbf{r})|^2|\mathbf{u}_l(\mathbf{r})|^2.$$

The above equation governs the change of statistical properties of the photon system in the two-photon absorption process. The solution of Eq. (14) is difficult. However, it is clear that if the absorption is large, the statistical properties of the fields will be appreciably disturbed. A coherent beam will no longer be coherent after interacting with the medium.

From Eq. (14), we obtain

$$\partial\langle a_k\rangle/\partial t=-\beta^{(2)}(\rho_{1A}^0-\rho_{2A}^0)\langle a_ka_l^{\dagger}a_l\rangle+\beta^{(2)}\rho_{2A}^0\langle a_k\rangle, \quad (15a)$$

$$\partial\langle a_k^{\dagger}a_k\rangle/\partial t=\partial\langle a_l^{\dagger}a_l\rangle/\partial t,$$
$$=-2\beta^{(2)}(\rho_{1A}^0-\rho_{2A}^0)\langle a_k^{\dagger}a_ka_l^{\dagger}a_l\rangle+2\beta^{(2)}\rho_{2A}^0\langle(a_k^{\dagger}a_k+a_l^{\dagger}a_l+1)\rangle. \quad (15b)$$

In Eq. (15) the last term, which is proportional to the population ρ_{2A}^0 in the excited state, arises because $a^{\dagger}$ and a do not commute. It can be regarded as the spontaneous emission term in the two-photon absorption process. Assume that the two photon modes are independent initially. Then, as long as the photon distribution is not appreciably disturbed by the absorption, we can write

$$\langle a_k^{\dagger}a_ka_l^{\dagger}a_l\rangle\cong\langle a_k^{\dagger}a_k\rangle\langle a_l^{\dagger}a_l\rangle=\langle n_k\rangle\langle n_l\rangle.$$

The average rate of two-photon absorption depends on the average numbers of photons in the kth and the lth modes. However, if $k=l$, one would find

$$\partial\langle a_k\rangle/\partial t=-2\beta^{(2)}(\rho_{1A}^0-\rho_{2A}^0)\langle a_k^{\dagger}a_ka_k\rangle+4\beta^{(2)}\rho_{2A}^0\langle a_k\rangle,$$
$$\partial\langle a_k^{\dagger}a_k\rangle/\partial t=-4\beta^{(2)}(\rho_{1A}^0-\rho_{2A}^0)\langle a_k^{\dagger}a_k^{\dagger}a_ka_k\rangle+4\beta^{(2)}\rho_{2A}^0(2\langle a_k^{\dagger}a_k\rangle+1). \quad (16)$$

Here the absorption rate with $\rho_{2A}^0=0$ is twice as much as that of Eq. (15b) with $k=l$, since two photons in the same mode are being absorbed simultaneously. With the spontaneous-emission term being neglected, the average absorption rate is now proportional to the second-order correlation function $\langle a_k^{\dagger}a_k^{\dagger}a_ka_k\rangle$, and therefore depends

[8] See, for example, D. Ter Haar, Rept. Progr. Phys. 24, 304 (1961).

[9] The length of the box can be taken as the product of the light velocity and the response time of the photon detector.

[10] M. Göppert-Mayer, Ann. Physik 9, 273 (1931).

[11] P. Lambropoulos, C. Kikuchi, and R. K. Osborn, Phys. Rev. 144, 1081 (1966).

on the statistical nature of the fields.[11] It is two times higher for chaotic than for coherent sources, since[1]

$$\langle a^\dagger a^\dagger aa\rangle_{\text{chaotic}}=2(\langle a^\dagger a\rangle)^2,$$
$$\langle a^\dagger a^\dagger aa\rangle_{\text{coherent}}=(\langle a^\dagger a\rangle)^2. \quad (17)$$

Physically, a chaotic source has more irregularities in its intensity distribution than a coherent source. In a nonlinear response proportional to higher-order correlation functions of $a^\dagger$ and a, the peaks in the irregularities are weighted more strongly than the valleys. Consequently, the average nonlinear response from a source of more irregularities appears to be greater. It must be noted that if the absorption is appreciable, then $\langle a_k{}^\dagger a_k a_l{}^\dagger a_l\rangle(t)$ in Eq. (15) also depends on higher-order correlation functions of the initial field, as is seen by iteration on Eq. (15). A similar discussion can be given to the case where the fields contain many modes.

Assume that at each frequency there is a set of spatial modes, and for simplicity the fields consist of only two frequencies, ω_k and ω_l. The electric field at the position $\mathbf{r}$ is now given by

$$\mathbf{E}(\mathbf{r})=\mathbf{E}_k(\mathbf{r})+\mathbf{E}_l(\mathbf{r}),$$
$$\mathbf{E}_k{}^{(+)}(\mathbf{r})=\mathbf{E}_k{}^{(-)}(\mathbf{r})^\dagger=i(2\pi\hbar\omega_k)^{1/2}\sum_\lambda \mathbf{u}_{k_\lambda}{}^*(\mathbf{r})a_{k_\lambda}{}^\dagger. \quad (18)$$

By carrying out similar calculations as in the single-mode case, one would find at zero temperature

$$\partial\langle\sum_\lambda a_{k_\lambda}{}^\dagger a_{k_\lambda}\rangle/\partial t=2\gamma\int_V d^3r$$
$$\times N(r)\langle E_k{}^{(+)}E_k{}^{(+)}E_l{}^{(-)}E_l{}^{(-)}\rangle,$$
$$\gamma=[|\eta|^2g(\omega_k+\omega_l)/2\hbar^2], \quad (19)$$

assuming, for simplicity, that all fields are polarized in the same direction. If $\omega_k=\omega_l$, Eq. (19) becomes

$$\partial\langle\sum_\lambda a_{k_\lambda}{}^\dagger a_{k_\lambda}\rangle/\partial t=-4\gamma\int_V d^3r$$
$$\times N(r)\langle E_k{}^{(+)}E_k{}^{(+)}E_k{}^{(-)}E_k{}^{(-)}\rangle. \quad (20)$$

Using Glauber's P representation and the quasiprobability distribution for the field amplitude $\mathcal{E}_k$,[1] we can write for $t=0$

$$\langle E_k{}^{(+)}E_k{}^{(+)}E_k{}^{(-)}E_k{}^{(-)}\rangle$$
$$=\int d^2\mathcal{E}_k W(\mathcal{E}_k)|\mathcal{E}_k(\alpha,r)|^4. \quad (20a)$$

Then, if $N(\mathbf{r})=$constant, and $W(\mathcal{E}_k)\geq 0$, one would have a higher initial absorption rate in the multimode case than in the single-mode case since

$$\int_V d^3r|\mathcal{E}_k(\alpha,r)|^4/V>\left[\int_V d^3r|\mathcal{E}_k(\alpha,r)|^2/V\right]^2.$$

The discussion on two-photon absorptions can be applied with slight modification to Raman transitions between localized states. Here, instead of two photons being absorbed in a transition, one photon is now emitted, while the other is absorbed. Thus, for Raman transitions, the interaction Hamiltonian in Eq. (13) should be changed into the form

$$\mathcal{H}_{\text{int}}=\sum_i\{\eta_R c_{2i}{}^\dagger c_{1i}\mathbf{E}_k{}^{(-)}(\mathbf{r}_i)\mathbf{E}_s{}^{(+)}(\mathbf{r}_i)+\text{adjoint}\}. \quad (21)$$

In the single-mode case, the density matrix for the photon system becomes

$$\partial\rho_F/\partial t=-\beta_R[(a_k{}^\dagger a_s a_k a_s{}^\dagger\rho_F-2a_k a_s{}^\dagger\rho_F a_k{}^\dagger a_s$$
$$+\rho_F a_k{}^\dagger a_s a_k a_s{}^\dagger)\rho_{1A}{}^0+(a_k a_s{}^\dagger a_k{}^\dagger a_s\rho_F-2a_k{}^\dagger a_s\rho_F a_k a_s{}^\dagger$$
$$+\rho_F a_k a_s{}^\dagger a_k{}^\dagger a_s)\rho_{2A}{}^0], \quad (22)$$

where β_R has the same form as in Eq. (14). From the above equation, we find the average rate of Stokes photon generation or the pump photon absorption[12];

$$\partial\langle a_s{}^\dagger a_s\rangle/\partial t=-\partial\langle a_k{}^\dagger a_k\rangle/\partial t$$
$$=2\beta_R(\rho_{1A}{}^0-\rho_{2A}{}^0)\langle a_k{}^\dagger a_k a_s{}^\dagger a_s\rangle$$
$$+2\beta_R[\langle a_k{}^\dagger a_k\rangle\rho_{1A}{}^0-\langle a_s{}^\dagger a_s\rangle\rho_{2A}{}^0]. \quad (23)$$

The first term in Eq. (23) corresponds to stimulated Stokes emission, whereas the last term corresponds to spontaneous emission. The latter appears as a noise source and is responsible for the self-generation of the Stokes field. If the pump field is of high intensity and is not depleted appreciably in the Stokes generation, we can treat a_k and $a_k{}^\dagger$ as c numbers in the approximation and $\rho_F(t)=\rho_k(0)\rho_s(t)$, where ρ_k and ρ_s are the density matrices for the pump and the Stokes fields, respectively. From Eq. (22), we get

$$\partial\text{Tr}_s[\rho_s(t)a_s{}^\dagger a_s]/\partial t$$
$$=2\beta_R[(\rho_{1A}{}^0-\rho_{2A}{}^0)a_k{}^\dagger a_k-\rho_{2A}{}^0]$$
$$\times\text{Tr}_s[\rho_s(t)a_s{}^\dagger a_s]+2\beta_R a_k{}^\dagger a_k\rho_{1A}{}^0. \quad (24)$$

The solution of the above equation gives

$$\langle a_s{}^\dagger a_s\rangle(t)=\text{Tr}\rho_k(0)\{[\text{Tr}_s(\rho_s(0)a_s{}^\dagger a_s)+A/B]$$
$$\times\exp[B(a_k{}^\dagger,a_k)t]-A/B\},$$
$$B(a_k{}^\dagger,a_k)=[(\rho_{1A}{}^0-\rho_{2A}{}^0)a_k{}^\dagger a_k-\rho_{2A}{}^0]2\beta_R, \quad (25)$$
$$A(a_k{}^\dagger,a_k)=2\beta_R a_k{}^\dagger a_k\rho_{1A}{}^0.$$

By expanding $\exp(Bt)$ into power series, it is seen that $\langle a_s{}^\dagger a_s\rangle(t)$ is a function of the nth order correlation functions of $a_k{}^\dagger$ and a_k. Therefore, the Stokes generation must depend strongly on the statistical properties of the pump field. In particular, for a coherent pump field we have, assuming $\rho_{2A}{}^0\ll(\rho_{1A}{}^0-\rho_{2A}{}^0)a_k{}^\dagger a_k$,

$$\langle a_s{}^\dagger a_s\rangle(t)=[\langle a_s{}^\dagger(0)a_s(0)\rangle+(1-\rho_{2A}{}^0/\rho_{1A}{}^0)]$$
$$\times\exp[2\beta_R(\rho_{1A}{}^0-\rho_{2A}{}^0)\langle a_k{}^\dagger a_k\rangle t]-(1-\rho_{2A}{}^0/\rho_{1A}{}^0),$$

[12] R. W. Hellwarth, Phys. Rev. 130, 1852 (1963).

but for a chaotic pump field, since

$$\langle (a_k^\dagger)^n (a_k)^n \rangle = n! (\langle a_k^\dagger a_k \rangle)^n ,$$

we have

$$\langle a_s^\dagger a_s \rangle(t) = \{[\langle a_s^\dagger(0) a_s(0)\rangle + (1-\rho_{2A}^0/\rho_{1A}^0)]/ [1-2\beta_R(\rho_{1A}^0-\rho_{2A}^0)\langle a_k^\dagger a_k\rangle t]\} - (1-\rho_{2A}^0/\rho_{1A}^0).$$

Clearly, the average Stokes generation by chaotic pumps is much more effective than that by coherent pumps.

The multimode case in Raman transitions is somewhat complicated. For simplicity, we assume a uniform medium which fills up the entire volume of quantization. Assume also a set of spatial modes associated with each frequency, or a band of frequencies with a bandwidth much smaller than the Raman linewidth. Then, if the pump field is not highly depleted, we can show, for $\rho_{2A}^0 = 0$,

$$\partial \operatorname{Tr}_s[\rho_s(t) E_s^{(+)} E_s^{(-)}] / \partial t = 2\gamma_R \{ E_k^{(+)} E_k^{(-)} [\operatorname{Tr}_s(\rho_s(t) E_s^{(+)} E_s^{(-)}) + (\hbar\omega_s/2) \sum_\lambda |u_{s\lambda}|^2]\}, \quad (26)$$

$$\gamma_R = [\pi N \omega_s |\eta|^2 g(\omega_l - \omega_s)/\hbar],$$

assuming all fields to be polarized in the same direction. In deriving Eq. (26), we have used the approximation

$$\sum_\lambda u_{k\lambda}^*(\mathbf{r}) u_{k\lambda}(\mathbf{r}) \approx \delta(\mathbf{r}-\mathbf{r}'),$$

where the summation is over modes at the frequency ω_k. This approximation is equivalent to relaxation of the momentum matching condition in the Raman transitions.[13] The solution of Eq. (26) gives

$$\langle E_s^{(+)} E_s^{(-)} \rangle(r,t) = [\langle E_s^{(+)} E_s^{(-)} \rangle(r,0) + S(r)] \times (\exp(2\gamma_R E_k^{(+)} E_k^{(-)} t)\rangle - S(r), \quad (27)$$

$$S(r) = (\hbar\omega_s/2) \sum_\lambda |u_{s\lambda}(r)|^2.$$

If the quantity in the square brackets is independent of r, then $\langle E_s^{(+)} E_s^{(-)} \rangle(t)$ can be regarded as the average Stokes intensity in the volume. Since the magnitude of $\langle \exp(2\gamma_R E_k^{(+)} E_k^{(-)} t) \rangle$ is usually larger for multimodes than for a single mode, the average Stokes intensity should be higher for the multimode case. In the quasiprobability distribution, we have

$$\langle \exp(2\gamma_R E_k^{(+)} E_k^{(-)} t) \rangle = \int d^2\mathcal{E}_k W(\mathcal{E}_k) \exp(2\gamma_R |\mathcal{E}_k|^2 t).$$

For stationary fields with large numbers of modes,[1]

$$W(\mathcal{E}_k) = \exp[-|\mathcal{E}_k|^2/\langle E_k^{(+)} E_k^{(-)} \rangle]/\pi \times \langle E_k^{(+)} E_k^{(-)} \rangle. \quad (28)$$

Such a distribution gives

$$\int d^2\mathcal{E}_k W(\mathcal{E}_k) |\mathcal{E}_k|^{2n} = n! \langle E_k^{(+)} E_k^{(-)} \rangle^n .$$

Therefore, we would get

$$\langle E_s^{(+)} E_s^{(-)} \rangle(t) = [\langle E_s^{(+)} E_s^{(-)} \rangle(0) + S]/ \times [1 - 2\gamma_R \langle E_k^{(+)} E_k^{(-)} \rangle t] - S. \quad (29)$$

Equation (28) also leads to the conclusion that the probability of having at least $(1/N)$ part of the ensembles with a gain coefficient $2\gamma_R|\mathcal{E}_k|^2$ larger than the average gain $2\gamma_R\langle E_k^{(+)} E_k^{(-)}\rangle$ by a factor $\ln N$ is $1-e^{-1} = 0.63$, where N is the number of modes.[13] However, if the fields are nonstationary or there is phase correlation between modes, the factor $\ln N$ would be replaced by a much larger value, of the order of N for full phase correlation.

The statistical properties of the Stokes output in the Raman transitions are difficult to describe quantitatively. Qualitatively, they depend strongly on the initial statistical nature of both the pump and the Stokes field. If the pump is coherent and not appreciably disturbed, then the statistical properties of the Stokes output would be the same as those of a quantum oscillator.[14] In particular, if initially there is no Stokes input, the medium would appear as a Stokes noise generator.

III. INCOHERENT LINEAR AND NONLINEAR SCATTERING

Rayleigh and Brillouin scattering are often regarded as linear scattering processes. Nevertheless, they belong to the class of nonlinear optics in the sense that excitational waves in the medium actually play the equivalent role of light waves. Incoherent Rayleigh and Brillouin scattering are most frequently discussed in the classical language.[15] The transformation from classical to quantum terms is, however, straightforward.

Consider scattering due to density fluctuations in a dilute medium. The total Hamiltonian is

$$\mathcal{H} = \mathcal{H}_0 + \mathcal{H}_{\text{int}},$$

where $\mathcal{H}_0$, given by Eq. (4), includes the coherent interaction of light with the medium, and $\mathcal{H}_{\text{int}}$ describes solely the incoherent part of the interaction. In first order, with the trace taken over the atomic system, $\mathcal{H}_{\text{int}}$ can be written as

$$\mathcal{H}_{\text{int}} = -\sum_{i,k} [\mathbf{E}_k^{(+)}(\mathbf{r}_i) \cdot \mathbf{p} \cdot \mathbf{E}_{k_0}^{(-)}(\mathbf{r}_i) + \mathbf{E}_{k_0}^{(+)}(\mathbf{r}_i) \cdot \mathbf{p} \cdot \mathbf{E}_k^{(-)}(\mathbf{r}_i)], \quad (30)$$

[13] N. Bloembergen and Y. R. Shen, Phys. Rev. Letters 13, 720 (1964).

[14] J. P. Gordon, L. R. Walker, and W. H. Louisell, Phys. Rev. 130, 806 (1963).

[15] See, for example, L. D. Landau and E. M. Lifshitz, *Electrodynamics of Continuous Media* (Pergamon Press, Inc., New York, 1960), p. 377.

where $\mathbf{p}$ is the atomic polarizability in the electric-dipole approximation, k_0 is the pump mode, and k is the mode of the scattered radiation. By assuming running modes with

$$\mathbf{u}_k=\hat{e}_k(1/L^3\epsilon_k)^{1/2}\exp(i\mathbf{k}\cdot\mathbf{r}),$$

Eq. (30) takes the form

$$3\mathcal{C}_{\rm int}=\sum_k [a_{k1}(t)a_{k0}(t)f_k^*+a_{k0}^\dagger(t)a_k(t)f_k], \quad (31)$$

where in the Heisenberg representation

$$f_k=-\sum_i (2\pi\hbar\omega_k^{1/2}\omega_{k0}^{1/2}/\epsilon_k L^3)\hat{e}_k\cdot\mathbf{p}^*\cdot\hat{e}_{k0} \times\exp[i(\mathbf{k}-\mathbf{k}_0)\cdot\mathbf{r}_i],$$

the equation of motion is

$$da_k(t)/dt=i\omega_k a_k(t)-(i/\hbar)f_k^* a_{k0}(t). \quad (32)$$

If the pump field is of high intensity, and is not disturbed appreciably by the incoherent scattering, we can treat a_k and a_{k_0} as c numbers. This is actually equivalent to treating the pump field in the classical limit. Then, Eq. (32) can be solved readily. In fact, the problem reduces to the one of radiation by a prescribed current distribution discussed by Glauber.[1] The solution of Eq. (32) leads to the expression of an electric field at a point $\mathbf{r}$ for the scattered radiation,

$$\begin{aligned}\mathbf{E}_{sc}^{(-)}(\mathbf{r},t)&=-(1/c)\partial\mathbf{A}^{(-)}(\mathbf{r},t)/\partial t\\&=\left(\frac{-\partial}{c\partial t}\right)\left\{\hat{e}_k\left(\frac{iL^3}{8\pi^3}\right)\int d^3k\int_0^t dt'\left(\frac{2\pi c}{\hbar k\epsilon_k L^3}\right)^{1/2}\right.\\&\quad\times f_k^* a_{k0}(t')\exp[i\mathbf{k}-\mathbf{r}-i\omega(t-t')]\\&\quad\left.+\text{complex conjugate}\right\}.\end{aligned}$$

The integration in the above equation can be carried out explicitly.[16] At a point $\mathbf{r}$ sufficiently far from the scattering region, the electric field is approximately given by

$$\mathbf{E}_{sc}^{(-)}(\mathbf{r},t)=a_{k_0}\mathbf{F}(r,t)\exp(i\mathbf{k}_0\cdot\mathbf{r}) \times\int_V d^3r' N(\mathbf{r}',t)\exp[i(\mathbf{k}_0-\mathbf{k})\cdot\mathbf{r}'], \quad (33)$$

$$\mathbf{F}(\mathbf{r},t)=(\mathbf{k}\times i\mathbf{p}\cdot\hat{e}_{k_0})\times(\mathbf{k}/|\mathbf{r}-\mathbf{R}|)(2\pi\hbar\omega_0/\epsilon_k L^3)^{1/2} \times\exp(i\mathbf{k}\cdot\mathbf{r}-i\omega_0 t),$$

where V is the volume of interaction and $\mathbf{R}$ is the center of V. The calculation now follows essentially the same as the classical treatment.[15] Clearly, if the scattering medium is uniform and stationary, so that the density of atoms $N(\mathbf{r},t)$ is constant, the integral $\int_V d^3r$ in Eq. (33) would vanish if $\mathbf{k}_0\neq\mathbf{k}$, and, consequently, there is no scattering in the direction $\mathbf{k}\neq\mathbf{k}_0$. Thus, incoherent scattering appears as a result of density fluctuations. If we consider only one Fourier component of the total density fluctuations,

$$N(\mathbf{r},t)=\sum_q N_q\exp(i\mathbf{q}\cdot\mathbf{r}-i\omega_q t),$$

then we obtain from Eq. (33) the first-order correlation function

$$\begin{aligned}\langle\mathbf{E}_{sc}^{(+)}(r,t_1)\cdot\mathbf{E}_{sc}^{(-)}(r,t_2)\rangle&=|F(r)|^2 8\pi^3 V\langle a_{k_0}^\dagger a_{k_0}\rangle\\&\quad\times\langle N_q(t_1)N_q(t_2)^*\rangle\Delta(\mathbf{k}_0-\mathbf{k}\pm\mathbf{q})\\&\quad\times\exp[-i(\omega_0\pm\omega_q)(t_1-t_2)]\\\Delta(k_0-k\pm q)&\xrightarrow[V\to\infty]{}\delta(\mathbf{k}_0-\mathbf{k}\pm\mathbf{q}).\end{aligned} \quad (34)$$

For $N(r,t)=$constant, the scattered radiation in the direction $\mathbf{k}\neq\mathbf{k}_0+\mathbf{k}_0'$ vanishes. The Fourier transform of $\langle E_{sc}^{(+)}(r,t_1)E_{sc}^{(-)}(r,t_2)\rangle$ gives the power spectral density of the scattered radiation. Higher-order correlation functions can also be obtained from Eq. (33), and, hence the statistical properties of the scattered radiation can be described completely.

It is, however, interesting to note that for this case, an explicit expression of the density matrix for the scattered radiation can be written down immediately, following Glauber's treatment for the radiation by a prescribed current distribution.[1] If we assume P representation for both the pump field and the density fluctuations, such that

$$\begin{aligned}\langle(a_{k_0}^\dagger)^m(a_{k_0})^n\rangle&=\int d^2\alpha_{k_0}P(\alpha_{k_0})(\alpha_{k_0}^*)^m(\alpha_{k_0})^n,\\\langle(N_q)^m(N_q^*)^n\rangle&=\int d^2\sigma_q P(\sigma_q)(\sigma_q)^m(\sigma_q^*)^n,\end{aligned} \quad (35)$$

then we find for the scattered radiation

$$\rho_k(t)=\int d^2\alpha_{k_0}\int d^2\sigma_q P_{k_0}(\alpha_{k_0})P_q(\sigma_q)|\alpha_k(t)\rangle\langle\alpha_k(i)|,$$

with

$$\alpha_k(t)=(i/\hbar)\int_0^t dt\,\mathfrak{F}(\alpha_{k_0},\sigma_q), \quad (36)$$

where

$$\mathfrak{F}(\alpha_{k_0},\sigma_q)=-(2\pi\hbar\omega_{k_0}^{1/2}\omega_k^{1/2}/\epsilon_k L^3)\hat{e}_k\cdot\mathbf{p}\cdot\hat{e}_{k_0}\sigma_q.$$

This shows that statistical properties of the scattered radiation are determined by those of incident radiation and density fluctuations. Thus, measurements of statistical properties of the scattered radiation could yield information about the statistical properties of the density fluctuations, if those of the incident radiation are known. The analysis is particularly simple for coherent incident radiation.

[16] E. Fermi, Rev. Mod. Phys. 4, 87 (1932).

Recently, the question whether intensities of scattered radiation may be different for coherent and incoherent incident radiation has arisen.[17] It is clear from Eq. (34) that with our assumptions for linear incoherent scattering, the average scattering intensity is directly proportional to the average number of photons in the pump modes, and is independent of the coherent property of the pump field.

The above calculation can be extended to the case of incoherent nonlinear scattering, which has recently been investigated by Terhune *et al.*[18] We shall again consider only nonlinear scattering due to density fluctuations, in which two photons in the pump modes k_0 and k_0' are scattered into a single photon in the scattered mode k. The corresponding interaction Hamiltonian can be written as

$$\mathcal{H}_{\rm int}=-\sum_{i,k}[\mathbf{E}_k^{(+)}(\mathbf{r}_i)\cdot\mathbf{p}^{(2)}:\mathbf{E}_{k_0}^{(-)}(\mathbf{r}_i)\mathbf{E}_{k_0'}^{(-)}(\mathbf{r}_i)+\text{adjoint}], \quad (37)$$

where $\mathbf{p}^{(2)}$ is the second-order nonlinear polarizability.[19] Following the same procedure as in the linear case, one would find for the scattered radiation

$$\mathbf{E}_{sc}^{(-)}(\mathbf{r},t)=a_{k_0}a_{k_0'}\mathbf{F}(\mathbf{r},t)[\exp i(\mathbf{k}_0+\mathbf{k}_0')\cdot\mathbf{R}]\times\int_V d^3r'N(\mathbf{r}',t)\exp[i(\mathbf{k}_0+\mathbf{k}_0'-\mathbf{k})\cdot\mathbf{r}]$$

$$\mathbf{F}(\mathbf{r},t)=(\mathbf{k}\times\mathbf{p}^{(2)}:\hat{e}_{k_0}\hat{e}_{k_0'})\times\left(\frac{\mathbf{k}}{|\mathbf{r}-\mathbf{R}|}\right)\left(\frac{2\pi\hbar}{L^3}\right)\times\left(\frac{\omega_0\omega_0'}{\epsilon_{k_0}\epsilon_{k_0'}}\right)^{1/2}\exp[i\mathbf{k}\cdot\mathbf{r}-i(\omega_0+\omega_0')t]. \quad (38)$$

If only one Fourier component of the density fluctuations is taken into account, the first-order correlation function of the scattered radiation is

$$\langle\mathbf{E}_{sc}^{(+)}(\mathbf{r},t_1)\cdot\mathbf{E}_{sc}^{(-)}(\mathbf{r},t_2)\rangle=|F(r)|^2 8\pi^3 V\times\langle a_{k_0}^\dagger a_{k_0'}^\dagger a_{k_0}a_{k_0'}\rangle\langle N_q N_q^*\rangle\Delta(\mathbf{k}_0+\mathbf{k}_0'-\mathbf{k}\pm\mathbf{q})\times\exp[-i(\omega_0+\omega_0'\pm\omega_q)(t_1-t_2)], \quad (39)$$

where $F(r)$ is given in Eq. (38). Assuming Eq. (35) for both the pump modes and the density fluctuations, we find the density matrix for the scattered radiation

$$\rho_k(t)=\int d^2\alpha_{k_0}\int d^2\alpha_{k_0'}\int d^2\sigma_q P_{k_0}(\alpha_{k_0})P_{k_0'}(\alpha_{k_0'})\times P_q(\sigma_q)|\alpha_k(t)\rangle\langle\alpha_k(t)|,$$

$$\alpha_k(t)=\frac{i}{\hbar}\int_0^t dt\,\mathfrak{F}(\alpha_{k_0},\alpha_{k_0'},\sigma_q), \quad (40)$$

$$\mathfrak{F}(\alpha_{k_0},\alpha_{k_0'},\sigma_q)=-(8\pi^3\hbar^3\omega_k\omega_{k_0}\omega_{k_0'}/\epsilon_{k_0}\epsilon_{k_0'}\epsilon_k L^9)^{1/2}\times\hat{e}_k\cdot\mathbf{p}^{(2)}:\hat{e}_{k_0}\hat{e}_{k_0'}\alpha_{k_0}\alpha_{k_0'}\sigma_q.$$

From Eq. (39) it is seen that the scattering intensity, $\langle|E_{sc}^{(+)}(r,t)|^2\rangle$, for $k\neq l$ is proportional to $\langle a_{k_0}^\dagger a_{k_0}\rangle\langle a_{k_0'}^\dagger a_{k_0'}\rangle$, but for $k=l$, it is proportional to $\langle a_{k_0}^\dagger a_{k_0}^\dagger a_{k_0}a_{k_0}\rangle$, which from Eq. (17) is two times larger for chaotic than for coherent fields.

In the actual experiments, the incident radiation may contain many modes. However, as long as the divergence and the linewidth of the incident radiation are small compared with the acceptance angle of the photodetector and the linewidth of the scattered radiation, conservation of energy and momentum as expressed in Eq. (39) can be relaxed. We therefore have for the multimode case,

$$\langle|E_{sc}^{(+)}(\mathbf{r},t)|^2\rangle\cong|F(r)|^2(2\pi VL^6/\hbar^2\omega_0\omega_0')\times\langle E_{k_0}^{(+)}E_{k_0'}^{(+)}E_{k_0}^{(-)}E_{k_0'}^{(-)}\rangle(R,t)\times\langle N_q N_q^*\rangle\Delta(\mathbf{k}_0+\mathbf{k}_0'-\mathbf{k}\pm\mathbf{q}), \quad (41)$$

where

$$E_{k_0}^{(-)}(\mathbf{R})=\sum_\lambda(2\pi\hbar\omega_0/\epsilon_{k_0}L^3)^{1/2}a_{k_0\lambda}\exp(i\mathbf{k}_{0\lambda}\cdot\mathbf{R}-i\omega_{0\lambda}t).$$

and $\mathbf{R}$ is the center of the volume V. Then, if $k_0=k_0'$, from Eqs. (20a) and (28) we find for stationary fields, if the number of modes is large, $\langle E_{k_0}^{(+)}E_{k_0}^{(+)}E_{k_0}^{(-)}E_{k_0}^{(-)}\rangle=2\langle E_{k_0}^{(+)}E_{k_0}^{(-)}\rangle^2$. This shows that the scattering intensity in the multimode case is two times higher than in the single-mode case. The second-order incoherent nonlinear scattering is closely related to the second-order coherent scattering, which gives rise to sum-frequency and second harmonic generation, as we shall now discuss.

IV. SUM-FREQUENCY AND SECOND HARMONIC GENERATION

The coherent sum-frequency generation can be described by the same interaction Hamiltonian in Eq. (37) for incoherent nonlinear scattering. It was shown in Sec. III that if there are no fluctuations in the medium, scattered radiation can only appear in the direction where the wave vectors of incident and scattered radiation are matched. This corresponds to coherent scattering. Thus, coherent sum frequency generation described by the Hamiltonian of Eq. (37) appears in the direction $k_0+k_0'-2k=0$.

[17] T. V. George, L. Goldstein, L. Slama, and M. Yokoyama, Phys. Rev. 137, A369 (1965); R. D. Watson and M. K. Clark, Phys. Rev. Letters 14, 1057 (1965); R. C. C. Leite, R. S. Moore, S. P. S. Porto, and J. E. Ripper, *ibid.* 14, 7 (1965); D. H. Woodward, Appl. Opt. 2, 1205 (1963).

[18] R. W. Terhune, P. D. Maker, and C. M. Savage, Phys. Rev. Letters 14, 681 (1965); P. D. Maker, in *Proceedings of the Conference on Physics of Quantum Electronics, Puerto Rico, 1965*, edited by P. L. Kelley, B. Lax, and P. E. Tannenwald (McGraw-Hill Book Company, Inc., New York, 1966), p. 60.

[19] J. A. Armstrong, N. Bloembergen, J. Ducuing, and P. Pershan, Phys. Rev. 127, 1918 (1962).

The calculation follows essentially the same pattern as for the case of incoherent nonlinear scattering. Again, in the Heisenberg representation, the equation of motion is

$$da_k/dt=-i\omega_k a_k(t)-(i/\hbar)f_k a_{k_0}(t)a_{k_0'}(t),$$
$$f_k=-NV(8\pi^3\hbar^3\omega_0^{1/2}\omega_0'^{1/2}\omega_k^{1/2}/\epsilon_{k_0}\epsilon_{k_0'}\epsilon_k L^9)^{1/2}\times\hat{e}_k\cdot\mathbf{p}^{(2)}:\hat{e}_{k_0}\hat{e}_{k_0'}. \quad (42)$$

Here, we have assumed a uniform medium in a volume V. For intense pump fields, which have not yet been depleted appreciably by the sum-frequency generation, a_{k_0} and $a_{k_0'}$ can be treated as constant c numbers. Then, Eq. (42) yields

$$a_k(t)=[a_k(0)-(i/\hbar)f_k a_{k_0}a_{k_0'}t]\exp(-i2\omega_0 t). \quad (43)$$

From Eqs. (42) and (43), we find the average rate of sum-frequency generation;

$$d\langle a_k^\dagger a_k\rangle(t)/dt=(i/\hbar)[f_k^*\langle a_{k_0}^\dagger a_{k_0'}^\dagger a_k\rangle(0)-f_k\langle a_k^\dagger a_{k_0}a_{k_0'}\rangle(0)]+(\omega_k t/\hbar)[f_k^*\langle a_{k_0}^\dagger a_{k_0'}^\dagger a_k\rangle(0)+f_k\langle a_k^\dagger a_{k_0}a_{k_0'}\rangle(0)]+(2|f_k|^2t^2/\hbar^2)\langle a_{k_0}^\dagger a_{k_0'}^\dagger a_{k_0}a_{k_0}\rangle(0), \quad (44)$$

which can readily be integrated. Equation (44) shows that for $\mathbf{k}_0=\mathbf{k}_0'$, corresponding to second-harmonic generation, the average rate of generation depends on the initial statistical properties of the pump and the second-harmonic fields. In particular, if $\langle a_k(0)\rangle=0$, this rate is proportional to the second-order correlation function $\langle a_{k_0}^\dagger a_{k_0}^\dagger a_{k_0}a_{k_0}\rangle(0)$, and is therefore two times higher for a chaotic than for a coherent pump field.

Corresponding to the Hamiltonian of Eq. (37) with a_{k_0} and $a_{k_0'}$ treated as c numbers, the density matrix for the sum-frequency field is

$$\rho_k(t)=\int d^2\alpha_{k_0}d^2\alpha_{k_0'}P_{k_0}(\alpha_{k_0})P_{k_0'}(\alpha_{k_0'})\times D(\alpha_k)\rho_k(0)D^{-1}(\alpha_k),$$
$$D(\alpha_k)=\exp[\alpha_k a_k^\dagger-\alpha_k^* a_k], \quad (45)$$
$$\alpha_k=\frac{i}{\hbar}\int_0^t dt\, f_k\alpha_{k_0}\alpha_{k_0'},$$

where f_k is given in Eq. (42) and P representation is assumed for the pump fields,

$$\rho_{k_0}=\int d^2\alpha_{k_0}P_{k_0}(\alpha_{k_0})|\alpha_{k_0}\rangle\langle\alpha_{k_0}|,$$
$$\rho_{k_0'}=\int d^2\alpha_{k_0'}P_{k_0'}(\alpha_{k_0'})|\alpha_{k_0'}\rangle\langle\alpha_{k_0'}|.$$

If initially, $\rho_k(0)=\int d^2\beta_k P_k(\beta_k)|\beta_k\rangle\langle\beta_k|$, then Eq. (45) becomes

$$\rho_k(t)=\int d^2\alpha_{k_0}d^2\alpha_{k_0'}d^2\beta_k P_{k_0}(\alpha_{k_0})P_{k_0'}(\alpha_{k_0'})P_k(\beta_k)\times|\alpha_k+\beta_k\rangle\langle\alpha_k+\beta_k|, \quad (46a)$$

which, in the case of second-harmonic generation, reduces to

$$\rho_k(t)=\int d^2\alpha_{k_0}d^2\beta_k P_{k_0}(\alpha_{k_0})P_k(\beta_k)\times|\alpha_k+\beta_k\rangle\langle\alpha_k+\beta_k|, \quad (46b)$$

with $\alpha_k=(i/\hbar)\int_0^t dt\, f_k\alpha_{k_0}^2$. The above expressions lead to the following results. (1) For coherent pump fields, if $|\beta_k\rangle=|0\rangle$, the generated sum-frequency field is also coherent; but if $|\beta_k\rangle\neq|0\rangle$, the sum-frequency output has the same distribution function P_k as the input with $\rho_k(t)=\int d^2\beta_k P_k(\beta_k)|\alpha_k+\beta_k\rangle\langle\alpha_k+\beta_k|$. (2) If $|\beta_k\rangle=|0\rangle$, the sum-frequency output reflects the statistics of the pump fields. (3) In general, the sum-frequency output has the composite statistical properties of the pump fields and the sum-frequency input. Clearly, measurements of the statistics of the sum-frequency or second-harmonic output could yield information about the statistics of the pump fields. For example, if $|\beta_k\rangle=|0\rangle$, the nth-order correlation function of the second harmonics is proportional to the $2n$th-order correlation function of the fundamental.

The discussion can easily be extended to the multimode case. As discussed in the case of incoherent scattering, if the energy and momentum matching condition is relaxed, Eq. (44) gives

$$d\langle E_k^{(+)}E_k^{(-)}\rangle(\mathbf{r},t)/dt=(i/\hbar)[g_k^*\langle E_{k_0}^{(+)}E_{k_0'}^{(+)}E_{k_0}^{(-)}\rangle(\mathbf{r},0)-g_k\langle E_k^{(+)}E_{k_0}^{(-)}E_{k_0'}^{(-)}\rangle(\mathbf{r},0)]+(\omega_k t/\hbar)\times[g_k^*\langle E_{k_0}^{(+)}E_{k_0'}^{(+)}E_k^{(-)}\rangle(\mathbf{r},0)+g_k\langle E_k^{(+)}E_{k_0}^{(-)}E_{k_0'}^{(-)}\rangle(\mathbf{r},0)]+(2|g_k|^2t^2/\hbar^2)\times\langle E_{k_0}^{(+)}E_{k_0}^{(+)}E_{k_0'}^{(-)}E_{k_0'}^{(-)}\rangle(\mathbf{r},0), \quad (47)$$
$$g_k=-NV(2\pi\hbar\omega_k^{1/2}/\epsilon_k^{1/2}L^3)\hat{e}_k\cdot p^{(2)}:\hat{e}_{k_0}\hat{e}_{k_0'},$$

where $E_k^{(-)}(r,t)$ has the same expression as in Eq. (41). Again, for $k_0=k_0'$, if $\langle E_k(0)\rangle=0$, the average rate of second-harmonic generation is usually higher for multimode than for single-mode pump fields, since $\langle E_{k_0}^{(+)}E_{k_0}^{(+)}E_{k_0}^{(-)}E_{k_0}^{(-)}\rangle$ has a larger value in the former case. For stationary fields, there is a ratio of 2 in the rates of second-harmonic generation for the two cases.[20] The density matrix given in Eq. (46) can also easily be generalized to multimodes.

The above discussion is valid as long as there is no appreciable depletion of pump power by sum-frequency generation. For the more general case, the mathematics becomes much more complicated, since the reaction of the sum-frequency field on the pump fields must be

[20] J. Ducuing and N. Bloembergen, Phys. Rev. 133, A1493 (1964).

taken into account. The sum-frequency generation now depends on higher-order correlation functions of the initial pump fields. The output is no longer coherent even if the initial pump fields are coherent. Ducuing and Armstrong[21] have discussed the statistical aspects of second-harmonic generation with high conversion using the classical approach. A corresponding quantum-statistical discussion would be extremely difficult, if the noncommutability of the operators a and $a^\dagger$ is to be taken into account.

V. PARAMETRIC AMPLIFICATION

One of the most important subjects in nonlinear optics is parametric amplification. It is not only because the parametric amplification may lead to tunable oscillators at light frequencies,[22] but because in a broader sense, it also describes such important nonlinear processes as stimulated Raman and Brillouin scattering by elementary excitations.[23] In the latter cases, the idler photon mode is replaced by the mode of elementary excitations. The calculations remain the same if the elementary excitations are bosons.

The statistical properties of a parametric amplifier have been discussed in detail by Gordon *et al.*[24] However, they have assumed a constant field strength for the pump mode. From our discussion in the previous sections, we expect that the statistics of the pump field should influence the statistical output of the amplifier. Their results are valid only when the pump field is in a coherent state. In the following, we shall follow their calculations, but take into account the statistical properties of the pump field.

The interaction Hamiltonian for parametric amplification is also the same as in Eq. (37).

$$\mathcal{H}_{\rm int}=-\sum_{i,k}[\mathbf{E}_p^{(+)}(\mathbf{r}_i)\cdot\mathbf{p}^{(2)}:\mathbf{E}_s^{(-)}(\mathbf{r}_i)\times\mathbf{E}_I^{(-)}(\mathbf{r}_i)+\text{adjoint}]. \quad (48)$$

Here, however, the coherent scattering process is to destroy a photon in the pump mode p, and to create one photon in the signal mode s and another in the idler mode I, with $\omega_p=\omega_s+\omega_I$ and $\mathbf{k}_p=\mathbf{k}_s+\mathbf{k}_I$. The Heisenberg equations of motion are

$$\begin{aligned} da_s/dt&=-i\omega_s a_s(t)-i\kappa a_p(t)a_I^\dagger(t),\\ da_I^\dagger/dt&=i\omega_I a_I^\dagger(t)-i\kappa^* a_p^\dagger(t)a_s(t), \end{aligned} \quad (49)$$

where

$$\kappa=-NV(8\pi^3\hbar\omega_p\omega_s\omega_I/\epsilon_p\epsilon_s\epsilon_I L^6)^{1/2}\hat{e}_p\cdot\mathbf{p}^{(2)*}:\hat{e}_s\hat{e}_I.$$

If the pump field is of high intensity, and has not been depleted appreciably by the parametric process, then $a_p(t)\approx a_p(0)\exp(-i\omega_p t)$, where $a_p(0)$ and $a_p^\dagger(0)$ can be regarded as c numbers. Then the solution of Eq. (49) is

$$\begin{aligned} a_s(t)&=\{a_s(0)\cosh[|\kappa|(a_p^\dagger a_p)^{1/2}t]\\ &\quad+[i\kappa a_p/|\kappa|(a_p^\dagger a_p)^{1/2}]a_I(0)\\ &\quad\times\sinh[|\kappa|(a_p^\dagger a_p)^{1/2}t]\}\exp(-i\omega_s t),\\ a_I(t)&=\{a_I(0)\cosh[|\kappa|(a_p^\dagger a_p)^{1/2}t]\\ &\quad+[i\kappa a_p/|\kappa|(a_p^\dagger a_p)^{1/2}]a_s(0)\\ &\quad\times\sinh[|\kappa|(a_p^\dagger a_p)^{1/2}t]\}\exp(-i\omega_I t), \end{aligned} \quad (50)$$

$$\begin{aligned} \langle a_s^\dagger a_s\rangle(t)&=\mathrm{Tr}\rho_p(0)\{\langle a_s^\dagger a_s\rangle(0)\cosh^2[|\kappa|(a_p^\dagger a_p)^{1/2}t]\\ &\quad+(\langle a_I^\dagger a_I\rangle(0)+1)+\sinh^2[|\kappa|(a_p^\dagger a_p)^{1/2}t]\\ &\quad+i[\kappa a_p\langle a_s^\dagger a_I^\dagger\rangle(0)/|\kappa|(a_p^\dagger a_p)^{1/2}-\kappa^* a_p^\dagger\langle a_s a_I\rangle(0)/\\ &\quad|\kappa|(a_p^\dagger a_p)^{1/2}]\tfrac{1}{2}\sinh 2[|\kappa|(a_p^\dagger a_p)^{1/2}t]\}, \end{aligned} \quad (51)$$

with a similar expression for $\langle a_I^\dagger a_I\rangle(t)$. Equation (51) shows that the output signal in the parametric amplification depends on the initial statistical properties of the pump field. Assume $\langle a_s a_I\rangle(0)=0$. Then, for a coherent pump field, we have

$$\begin{aligned} \langle a_s^\dagger a_s\rangle(t)&=\tfrac{1}{2}[\langle a_s^\dagger a_s\rangle(0)-\langle a_I^\dagger a_I\rangle(0)-1]\\ &\quad+\tfrac{1}{2}[\langle a_s^\dagger a_s\rangle(0)+\langle a_I^\dagger a_I\rangle(0)+1]\\ &\quad\times\cosh[2|\kappa|\langle(a_p^\dagger a_p)^{1/2}\rangle t], \end{aligned} \quad (52)$$

but for a chaotic pump field, since

$$\langle(a_p^\dagger a_p)^n\rangle=n!\langle a_p^\dagger a_p\rangle^n,$$

we have

$$\begin{aligned} \langle a_s^\dagger a_s\rangle(t)&=\tfrac{1}{2}[\langle a_s^\dagger a_s\rangle(0)-\langle a_I^\dagger a_I\rangle(0)-1]\\ &\quad+\tfrac{1}{2}[\langle a_s^\dagger a_s\rangle(0)+\langle a_I^\dagger a_I\rangle(0)+1]\\ &\quad\times\sum_{n=0}^{\infty}[n!/(2n)!](2|\kappa|t)^{2n}\langle a_p^\dagger a_p\rangle_p. \end{aligned} \quad (53)$$

It is clear from the above expressions that the signal output is much larger for chaotic than for coherent pump fields.

For the multimode case, if the energy and momentum matching condition can be relaxed, as discussed in the previous sections, the calculations follow essentially the same as in the single-mode case with a replaced by $E^{(-)}(\mathbf{r},t)$, and κ in Eq. (49) by

$$\kappa'=-NV(2\pi/L^3)(\omega_s\omega_I/\epsilon_s\epsilon_I)^{1/2}\hat{e}_s\cdot\mathbf{p}^{(2)*}:\hat{e}_s\hat{e}_I. \quad (54)$$

The result is

$$\begin{aligned} \langle E_s^{(+)}E_s^{(-)}\rangle(\mathbf{r},t)&=\mathrm{Tr}\rho_p(0)\{\langle E_s^{(+)}E_s^{(-)}\rangle(\mathbf{r},0)\\ &\quad\times\cosh^2[|\kappa'|(E_p^{(+)}E_p^{(-)})^{1/2}t]+\langle E_I^{(-)}E_I^{(+)}\rangle(\mathbf{r},0)\\ &\quad\times\sinh^2[|\kappa'|(E_p^{(+)}E_p^{(-)})^{1/2}t]\}, \end{aligned} \quad (55)$$

assuming $\langle E_s^{(-)}E_I^{(-)}\rangle(\mathbf{r},0)=0$. Again, the output signal is usually larger for multimode than for single-mode

[21] J. Ducuing and J. A. Armstrong, in *Proceedings of the Third Quantum Electronics Conference, Paris, 1963*, edited by P. Grivet and N. Bloembergen, (Columbia University Press, New York, 1964), p. 1643.
[22] J. A. Giordmaine and R. C. Miller, Phys. Rev. Letters **14**, 973 (1965).
[23] Y. R. Shen and N. Bloembergen, Phys. Rev. **143**, 372 (1966).
[24] J. P. Gordon, W. H. Louisell, and L. R. Walker, Phys. Rev. **129**, 481 (1963). See also W. H. Louisell, *Radiation and Noise in Quantum Electronics* (McGraw-Hill Book Company, Inc., New York, 1964).

pump fields. For stationary fields with many modes, we have

$$\langle E_s^{(+)}E_s^{(-)}\rangle(r,t)=\tfrac{1}{2}[\langle E_s^{(+)}E_s^{(-)}\rangle(r,0)-\langle E_I^{(-)}E_I^{(+)}\rangle(r,0)]+\tfrac{1}{2}[\langle E_s^{(+)}E_s^{(-)}\rangle(r,0)+\langle E_I^{(-)}E_I^{(+)}\rangle(r,0)]\sum_{n=0}^{\infty}[n!/(2n)!](2\kappa' t)^{2n}\times\langle E_p^{(+)}E_p^{(-)}\rangle^n(r,0). \quad (56)$$

In principle, all higher-order correlation functions of the signal and the idler fields can be obtained from Eq. (50). However, to describe the statistical properties of fields, an explicit expression of the density matrix for the fields is usually of great interest. For the case of parametric amplification, the density matrices $\rho_s(t)=\mathrm{Tr}_I\rho_{s,I}(t)$ and $\rho_I(t)=\mathrm{Tr}_s\rho_{s,I}(t)$ for the signal and the idler fields can be obtained through the use of the characteristic functions,[24] which are defined as[25]

$$X_s(\gamma,t)=\mathrm{Tr}_{s,I}\{\rho_{s,I}(t)\exp[\gamma a_s^{\dagger}(0)]\exp[-\gamma^* a_s(0)]\}=\mathrm{Tr}_{s,I}\{\rho_s(0)\rho_I(0)\exp[\gamma a_s^{\dagger}(t)]\times\exp[-\gamma^* a_s(t)]\}, \quad (57)$$

$$X_I(\gamma,t)=\mathrm{Tr}_{s,I}\{\rho_s(0)\rho_I(0)\exp[\gamma a_I^{\dagger}(t)]\times\exp[-\gamma^* a_I(t)]\}.$$

Explicit expressions of X_s and X_I can be found by substituting into Eq. (57) the expressions of $a_s(t)$ and $a_I(t)$ in Eq. (50) and the known initial distribution $\rho_s(0)$ and $\rho_I(0)$.[24] Here, $a_p^{\dagger}$ and a_p are treated as c numbers. Then, the characteristic functions lead to the density matrices in the P representation,[25]

$$\rho_s(t)=\mathrm{Tr}_I\rho_{s,I}(t)=\int d^2\alpha_s P_s(\alpha_s,t)|\alpha_s\rangle\langle\alpha_s|,$$

$$P_s(\alpha_s,t)=\int d^2\alpha_p P_p(\alpha_p)\langle\alpha_p|\times\left[\int X(\gamma,t)\exp(\alpha_s\gamma^*-\alpha_s^*\gamma)d^2\gamma/\pi^2\right]|\alpha_p\rangle, \quad (58)$$

with a similar equation for $\rho_I(t)$. As an example, consider the case where initially both the signal and the idler modes are in the vacuum state.

$$\rho_s(0)=|0_s\rangle\langle 0_s|, \quad \rho_I(0)=|0_I\rangle\langle 0_I|.$$

From Eqs. (50) and (57), the characteristic function X_s is

$$X_s(\gamma,t)=\exp\{\tfrac{1}{2}|\gamma|^2(\cosh^2|\kappa|(a_p^{\dagger}a_p)^{1/2}t]+\sinh^2[|\kappa|(a_p^{\dagger}a_p)^{1/2}t]-1)\}. \quad (59)$$

Substitution of $X_s(\gamma,t)$ in Eq. (58) gives

$$P_s(\alpha_s,t)=\int d^2\alpha_p P_p(\alpha_p)(1/\pi\langle n_s\rangle)\times\exp[-|\alpha_s|^2/\langle n_s\rangle], \quad (60)$$

where

$$\langle n_s\rangle(t)=\sinh^2[|\kappa\alpha_p|t].$$

If the pump field is coherent, this corresponds to a Gaussian probability distribution for a chaotic field with an average number of photons $\langle n_s\rangle$.[24] Thus, with no input to the amplifier, the parametric amplifier acts as a noise oscillator. Characteristic functions for various input conditions have been obtained by Gordon *et al.*[24]

More generally, we should also consider the loss in the modes due to absorption. However, in the first approximation, we can simply take ω_s and ω_I in Eq. (49) as complex quantities. The mathematics is straightforward, and will not be reproduced here. The above discussion is valid as long as the pump field is not appreciably disturbed. The general calculations, taking into account the reaction of the parametric process on the pump field, becomes extremely complicated.

VI. CONCLUSION

Nonlinear optical effects often depend on the statistical properties of the fields present. The rate of nonlinear absorption, emission, and amplification is higher for chaotic than for coherent, and higher for multimode than for single-mode pump fields. The statistics of the fields generated in the nonlinear effects is a partial function of the statistics of the pump fields. Measurements of the statistics of the output fields may yield information about the statistics of the input fields, and the statistical properties of the medium.

APPENDIX

Classically, a cavity problem of coherent scattering can usually be converted to a corresponding steady-state propagation problem by simply replacing t by $-z/c$ in the field amplitudes, where $\hat{z}$ is the direction of propagation. It is expected that the same is true in the quantum treatment. This can be realized by using a localized momentum operator instead of the Hamiltonian operator.

For steady-state propagation, the field amplitudes at fixed spatial points remain unchanged. The vector potential for a plane wave propagating in the z direction can be written as

$$A(z,t)=c\sum_k(\hbar/2\omega_k\epsilon_k L^3)^{1/2}\times\{\psi_k(z)\exp(-i\omega_k t)+\psi_k^{\dagger}(z)\exp(i\omega_k t)\},$$
$$\psi_k(z)=b(z)\exp(ikz), \quad (A1)$$
$$[b_k(z),b_{k'}^{\dagger}(z)]=\delta_{kk'}.$$

[24] R. Glauber, in *Proceedings of Conference on Physics of Quantum Electronics, 1965*, edited by P. L. Kelley, B. Lax, and P. E. Tannenwald (McGraw-Hill Book Company, Inc., New York, 1966), p. 788.

For free fields, $\psi_k(z)=a_k\exp(ikz)$. Here, we have defined localized annihilation and creation operators $b(z)$ and $b^\dagger(z)$ under the assumption that $\langle(b_k^\dagger)^m(b_k)^n\rangle$ does not vary much in a distance d large compared with the wavelength. We also assume that $k=2\pi n/d$, where n is an integer. Thus, the corresponding localized photon number operator is[26]

$$\hat{n}(z)=(\mathfrak{A}d/L^3)\sum_k b_k^\dagger(z)b_k(z), \tag{A2}$$

where $\mathfrak{A}$ is the cross-sectional area of the beam, and L^3 is the volume of quantization. We can also define a localized momentum operator,

$$\begin{aligned}\mathcal{P}(z_0,t)&=\hat{z}\mathfrak{A}\mathcal{H}(z_0,t)/c\\&=\hat{z}\frac{L^2}{cd}\int_{z_0-d/2}^{z_0+d/2}H(z,t)dz,\end{aligned} \tag{A3}$$

where $H(z,t)$ is the Hamiltonian density, and $\mathcal{H}(z_0,t)$ is the Hamiltonian corresponding to a system which has the same Hamiltonian density

$$(1/d)\int_{z_0-d/2}^{z_0+d/2}H(z,t)dz$$

everywhere in the volume L^2. Therefore, $\mathcal{H}(z_0,t)$ here has the same form as given for the various cases discussed in this paper, but with $b_k(z_0)$ and $b_k^\dagger(z_0)$ replacing a_k and $a_k^\dagger$, assuming that the medium has a uniform density $N(z_0)$, which fills the entire quantization volume for free fields,

$$\mathcal{P}(z,t)=\hat{z}\sum_k \hbar k[b_k^\dagger(z)b_k(z)+\tfrac{1}{2}].$$

The momentum operator acts as a translation operator:

$$\begin{aligned}d\psi(z)/dz&=(-1/i\hbar)[\psi(z),\mathcal{P}(z)],\\dE^{(-)}(z)/dz&=(-1/i\hbar)[E^{(-)}(z),\mathcal{P}(z)].\end{aligned} \tag{A4}$$

Thus, for example, in the case of sum-frequency generation, Eq. (A4) yields

$$\begin{aligned}dE_k^{(-)}(z)/dz-ikE_k^{(-)}(z)&=i[2\pi\omega_k/c\epsilon(z)]\\&\times N(z)\hat{e}_k\cdot\mathbf{p}^{(2)}:\hat{e}_{k_0}\hat{e}_{k_0'}E_{k_0}(z)E_{k_0'}(z),\end{aligned} \tag{A5}$$

which agrees with the corresponding classical equation. According to Eq. (A4), the unitary translation operator is

$$U(z,z_0)=\left\{\exp\left[(i/\hbar)\int_{z_0}^{z}\mathcal{P}(z)dz\right]\right\}_+. \tag{A6}$$

Here, the space-ordered product $\{\ \}_+$ has the similar definition as the time-ordered product. Field operators at different spatial points are connected by this unitary operator:

$$E(z,t)=U^{-1}(z,z_0)E(z_0,t)U(z,z_0). \tag{A7}$$

We can now define a localized density matrix operator,

$$\rho(z)=U(z,0)\rho(0)U^{-1}(z,0), \tag{A8}$$

assuming free space for $z<0$. Then the correlation function of fields at different times is given by

$$\begin{aligned}&\langle E^{(+)}(z,t_1)\cdots E^{(+)}(z,t_n)E^{(-)}(z,t_n)\cdots E^{(-)}(z,t_1)\rangle\\&\quad=\mathrm{Tr}[\rho(0)E^{(+)}(z,t_1)\cdots E^{(+)}(z,t_n)E^{(-)}(z,t_n)\\&\qquad\times\cdots E^{(-)}(z,t_1)]\\&\quad=\mathrm{Tr}[\rho(z)E^{(+)}(0,t_1)\cdots E^{(+)}(0,t_n)E^{(-)}(0,t_n)\\&\qquad\times\cdots E^{(-)}(0,t_1)].\end{aligned} \tag{A9}$$

The equation of motion for the density matrix $\rho(z)$ is

$$\partial\rho/\partial z=(-1/i\hbar)[\mathcal{P}(z),\rho(z)]. \tag{A10}$$

With the help of these localized operators, the calculations for steady-state propagation in a medium become exactly the same as the corresponding calculations for a cavity with t replaced by $-z/c$.

Physically, the density matrix $\rho(z)$ describes an ensemble of photon systems which has all the statistical properties of fields at z. If a photon system is taken as the section of the light beam emerged from the plane at z in a time T, where T can be the counting time of photodetectors,[9] then $\rho(z)$ actually describes an ensemble of such photon systems. This is the ensemble we measure in experiments.

The problem of beam splitting has been deliberately avoided in this paper. It requires some modification of our formalism. Qualitatively, the split beams would have different statistical properties than the unpslit beam, and they are correlated with each other. The equivalent problem in the cavity case corresponds to the splitting of the photon ensemble with time.

[26] L. Mandel, Phys. Rev. 144, 1071 (1966).

APPENDIX XII

Reprinted from THE PHYSICAL REVIEW, Vol. 167, No. 3, 818–821, 15 March 1968
Printed in U. S. A.

Permutation Symmetry of Nonlinear Susceptibilities and Energy Relation*

Y. R. SHEN†
Physics Department, University of California, Berkeley, California
(Received 2 October 1967)

Permutation symmetry for generalized nonlinear susceptibilities is derived from the microscopic theory. It is shown that this permutation symmetry is essential for the existence of a time-averaged stored energy density or free energy for wave propagation in a nonlinear, nondissipative medium.

FOR propagation of electromagnetic waves in a linear, nondissipative but dispersive medium, it is well known that a simple energy relation exists. The rate of time-averaged energy propagated out of a closed volume is equal to the rate of decrease of time-averaged energy stored in the volume.[1] The question arises on whether the same energy relation holds for wave propagation in a nonlinear, nondissipative medium. We shall show in this note that the permutation symmetry of nonlinear susceptibilities would in fact lead to the existence of such an energy relation in the nonlinear case. Pershan[2] derives the permutation symmetry of nonlinear susceptibilities from energy consideration by assuming the existence of time-averaged free energy. However, his expressions for time-averaged free energy are correct only for nondispersive media.

From the Maxwell equations

$$\begin{aligned}\nabla\times\mathbf{E}&=-(1/c)\partial\mathbf{B}/\partial t\,,\\ \nabla\times\mathbf{B}&=(1/c)\partial\mathbf{E}/\partial t+(4\pi/c)\mathbf{J}\,,\end{aligned}\tag{1}$$

one obtains the energy conservation equation

$$(c/4\pi)\nabla\cdot(\mathbf{E}\times\mathbf{B})=-(1/8\pi)(\partial/\partial t)[E^2+B^2]-\mathbf{E}\cdot\mathbf{J}\,,\tag{2}$$

where $\mathbf{J}$ is the total current density which can often be written in terms of multipole moments:

$$\mathbf{J}=\mathbf{J}_{\text{conduction}}+(\partial/\partial t)\mathbf{P}+c\nabla\times\mathbf{M}-(\partial/\partial t)\nabla\cdot\mathbf{Q}+\cdots.\tag{3}$$

However, the expansion of Eq. (3) is physically meaningless, if the wavelength of the propagating waves is small compared with the dimension of the medium.[1] It is then more appropriate to keep $\mathbf{J}$ as a single physical quantity. We can define a generalized polarization $\mathfrak{P}$ as[3]

$$\mathbf{J}-\mathbf{J}_{dc}=\partial\mathfrak{P}/\partial t.\tag{4}$$

Moreover, the Fourier component of $\mathfrak{P}$ can often be expanded into a series

$$\mathfrak{P}(\mathbf{k},\omega)=\sum_{n=1}^{\infty}\mathfrak{P}^{(n)}(\mathbf{k},\omega)\,,\tag{5}$$

where

$$\mathfrak{P}^{(1)}(\mathbf{k},\omega)=\chi^{(1)}(\mathbf{k},\omega)\cdot\mathbf{E}(k,\omega)\,,$$

$$\mathfrak{P}^{(2)}(\mathbf{k}=\mathbf{k}_1+\mathbf{k}_2,\,\omega=\omega_1+\omega_2)=\chi^{(2)}(\mathbf{k}=\mathbf{k}_1+\mathbf{k}_2,\,\omega=\omega_1+\omega_2):\mathbf{E}(\mathbf{k}_1,\omega_1)\mathbf{E}(\mathbf{k}_2,\omega_2)\,.$$

The tensors $\chi^{(1)}$, $\chi^{(2)}$, etc., denote the (generalized) linear susceptibility, the second-order nonlinear susceptibility, etc., respectively.

Consider first the linear case, where $\mathfrak{P}^{(n)}$ with $n\geq 2$ can be neglected. Let us assume a quasimonochromatic wave which can be represented by

$$\mathbf{E}(t)=\mathcal{E}(t)\exp(-i\omega t)+\mathcal{E}^*(t)\exp(i\omega t)\,,\tag{6}$$

where $|\partial\mathcal{E}(t)/\partial t|\ll|\omega\mathcal{E}(t)|$. Then, it can be shown that for a nondissipative medium, since $\chi_{ij}^{(1)}=\chi_{ji}^{(1)}$ from the microscopic theory, Eq. (2) averaged over a period of time $2\pi/\omega$ can be written as[1]

$$(c/4\pi)\nabla\cdot\langle\mathbf{E}\times\mathbf{B}\rangle_{\text{av}}=-\partial\bar{U}^{(1)}/\partial t\,,\tag{7}$$

where the time-averaged stored energy density is

$$\bar{U}^{(1)}=(1/4\pi)[|\mathcal{E}|^2+|\mathcal{B}|^2+4\pi\mathcal{E}^*\cdot(\partial\omega\chi^{(1)}/\partial\omega)\cdot\mathcal{E}].\tag{8}$$

From energy consideration, we would expect that there may also exist in general a time-averaged stored energy density $\bar{U}$ for wave propagation in a nonlinear medium. To show this, we must first derive the permutation symmetry for the generalized nonlinear susceptibilities. The microscopic expressions for nonlinear susceptibilities can be obtained from density matrix calculation[3,4] which is summarized as follows.

In the semiclassical treatment, the Hamiltonian of the nondissipative system is

$$\mathcal{H}=\mathcal{H}_0+\mathcal{H}_{\text{int}}\,,\tag{9}$$

where

$$\mathcal{H}_0|n\rangle=\hbar\omega_n|n\rangle\,,$$

$$\mathcal{H}_{\text{int}}=\mathcal{H}_{\text{int}}^{(1)}+\mathcal{H}_{\text{int}}^{(2)}\,,$$

$$\mathcal{H}_{\text{int}}^{(1)}=(e/2mc)(\mathbf{p}\cdot\mathbf{A}+\mathbf{A}\cdot\mathbf{p})+(eh/mc)\mathbf{s}\cdot\nabla\times\mathbf{A}\,,$$

$$\mathcal{H}_{\text{int}}^{(2)}=(e^2/2mc^2)\mathbf{A}\cdot\mathbf{A}\,.$$

* This research was supported by the joint sponsorship of the Advanced Research Projects Agency and the Office of Naval Research under Contract No. Nonr-3656(32).
† A. P. Sloan Research Fellow.
[1] See, for example, L. D. Landau and E. M. Lifshitz, *Electrodynamics in Continuous Media* (Addison-Wesley Publishing Co., Inc., Reading, Mass., 1959), p. 252.
[2] P. S. Pershan, Phys. Rev. 130, 919 (1963). See also N. Bloembergen, *Nonlinear Optics* (W. A. Benjamin, Inc., New York, 1965), p. 55.
[3] Y. R. Shen, Phys. Rev. 133, A511 (1964).
[4] N. Bloembergen and Y. R. Shen, Phys. Rev. 133, A37 (1964).

The vector potential $\mathbf{A}$ can be written as

$$\mathbf{A}(\mathbf{r},t)=\sum_m [\mathbf{A}_m(\mathbf{r})\exp(-i\omega_m t)+\mathbf{A}_m^*(\mathbf{r})\exp(i\omega_m t)], \quad (10)$$

$$\mathbf{A}_m(\mathbf{r})=(c/i\omega_m)\mathcal{E}(\mathbf{k}_m,\omega_m)\exp(i\mathbf{k}_m\cdot\mathbf{r}),$$

with $\nabla\cdot\mathbf{A}=0$. The equation of motion for the density matrix ρ is

$$i\hbar\partial\rho/\partial t=[\mathcal{H}_0+\mathcal{H}_{\rm int},\rho]. \quad (11)$$

If $\mathcal{H}_{\rm int}^{(1)}$ and $\mathcal{H}_{\rm int}^{(2)}$ are treated as first-order and second-order perturbations, respectively, then ρ can be expanded into series in ascending orders of the perturbation.

$$\rho=\sum_{n=0}^{\infty}\rho^{(n)}.$$

The various orders of ρ can then be found from the following hierarchy of equations

$$\begin{aligned}
&i\hbar\partial\rho^{(1)}/\partial t=[\mathcal{H}_0,\rho^{(1)}]+[\mathcal{H}_{\rm int}^{(1)},\rho^{(0)}],\\
&i\hbar\partial\rho^{(2)}/\partial t=[\mathcal{H}_0,\rho^{(2)}]+[\mathcal{H}_{\rm int}^{(1)},\rho^{(1)}]+[\mathcal{H}_{\rm int}^{(2)},\rho^{(0)}],\\
&i\hbar\partial\rho^{(n)}/\partial t=[\mathcal{H}_0,\rho^{(n)}]+[\mathcal{H}_{\rm int}^{(1)},\rho^{(n-1)}]\\
&\qquad\qquad+[\mathcal{H}_{\rm int}^{(2)},\rho^{(n-2)}]. \quad (12)
\end{aligned}$$

These equations can be solved successively through Fourier decomposition of $\rho^{(n)}$

$$\rho^{(n)}(t)=\sum_m \rho^{(n)}(\omega_m)\exp(-i\omega_m t). \quad (13)$$

From the density matrix, we can calculate the expectation value of a Fourier component of the current density.

$$\mathbf{J}(\mathbf{k},\omega)\exp(i\mathbf{k}\cdot\mathbf{r}-i\omega t)=\mathrm{Tr}\{\mathbf{J}^{0p}(\mathbf{k},\omega)\rho(\omega)\}\times\exp(i\mathbf{k}\cdot\mathbf{r}-i\omega t), \quad (14)$$

where $\mathbf{J}^{0p}(\mathbf{k},\omega)=\mathbf{J}_0^{0p}(\mathbf{k},\omega)+\mathbf{J}_1^{0p}(\mathbf{k},\omega)$ have matrix elements

$$\begin{aligned}
\langle n|\mathbf{J}_0^{0p}(\mathbf{k},\omega)|n'\rangle&=-(e/mc)\langle n|\{\exp(-i\mathbf{k}\cdot\mathbf{r})\mathbf{p}\\
&\quad+(p-2i\hbar\mathbf{s}\times\mathbf{k})\times\exp(-i\mathbf{k}\cdot\mathbf{r})\}|n'\rangle, \quad (15)\\
\langle n|\mathbf{J}_1^{0p}(\mathbf{k},\omega)|n'\rangle&=(e^2/mc)\langle n|\mathbf{A}\exp(-i\mathbf{k}\cdot\mathbf{r})|n'\rangle.
\end{aligned}$$

The nth-order term of the current density is now given by

$$J^{(n)}(k,\omega)=\sum_{n,n'}\{\langle n|\mathbf{J}_0^{0p}(\mathbf{k})|n'\rangle\langle n'|\rho^{(n)}(\omega)|n\rangle+\langle n|J_1^{0p}(\mathbf{k},\omega)|n'\rangle\langle n'|\rho^{(n-1)}(\omega)|n\rangle\}. \quad (16)$$

Subsequently, the nth-order generalized susceptibility tensor can be obtained from the relation

$$\mathbf{J}^{(n)}(\mathbf{k},\omega)=(-i\omega)\chi^{(n)}(\mathbf{k}=\sum_{i=1}^{n}\mathbf{k}_i,\ \omega=\sum_{i=1}^{n}\omega_i):\mathcal{E}(\mathbf{k}_1,\omega_1)\cdots\mathcal{E}(\mathbf{k}_n,\omega_n). \quad (17)$$

The above procedures lead, for example, to the second-order generalized susceptibility tensor

$$\begin{aligned}
\chi^{(2)}(\mathbf{k}_3=\mathbf{k}_1+\mathbf{k}_2,\ \omega_3=\omega_1+\omega_2)&=\sum_{n,n'}\frac{-iNe^3}{m^2\omega_1\omega_2\omega_3}(\rho_{n'}^{(0)}-\rho_n^{(0)})\Big\{\frac{\mathbf{R}_{n'n}^{\dagger}(\mathbf{k}_3)[\exp(i\mathbf{k}_3\cdot\mathbf{r})]_{nn'}}{\hbar(\omega_3-\omega_{nn'})}\\
&+\frac{[\exp(-i\mathbf{k}_2\cdot\mathbf{r})]_{n'n}\mathbf{R}_{nn'}(\mathbf{k}_2)}{\hbar(\omega_2-\omega_{nn'})}+\frac{[\exp(-i\mathbf{k}_2\cdot\mathbf{r})]_{n'n}\mathbf{R}_{nn'}(\mathbf{k}_1)}{\hbar(\omega_1-\omega_{nn'})}\Big\}+\sum_{n,n',n''}\frac{-iNe^3}{m^2\omega_1\omega_2\omega_3}\\
&\times\{\mathbf{R}_{n'n}^{\dagger}(\mathbf{k}_3)\mathbf{R}_{nn'}(\mathbf{k}_1)\mathbf{R}_{n''n'}(\mathbf{k}_2)\}\Big[\frac{\rho_{n'}^{(0)}}{\hbar^2(\omega_3-\omega_{nn'})(\omega_2-\omega_{n''n'})}+\frac{\rho_n^{(0)}}{\hbar^2(\omega_3-\omega_{nn'})(\omega_1-\omega_{nn''})}\\
&-\frac{\rho_{n''}^{(0)}}{\hbar^2(\omega_1-\omega_{nn''})(\omega_2-\omega_{n''n'})}\Big]+\mathbf{R}_{n'n}^{\dagger}(\mathbf{k}_3)\mathbf{R}_{nn''}(\mathbf{k}_2)\mathbf{R}_{n''n'}(\mathbf{k}_1)\Big[\frac{\rho_n^{(0)}}{\hbar^2(\omega_3-\omega_{nn'})(\omega_2-\omega_{nn''})}\\
&+\frac{\rho_{n'}^{(0)}}{\hbar^2(\omega_3-\omega_{nn'})(\omega_1-\omega_{n''n'})}-\frac{\rho_{n''}^{(0)}}{\hbar^2(\omega_1-\omega_{n''n'})(\omega_3-\omega_{nn''})}\Big], \quad (18)
\end{aligned}$$

where

$$\begin{aligned}
\mathbf{R}_{nn'}(\mathbf{k})&=[(\mathbf{p}+i\hbar\mathbf{s}\times\mathbf{k})\exp(i\mathbf{k}\cdot\mathbf{r})]_{nn'}\\
&=[\mathbf{R}_{n'n}^{\dagger}(\mathbf{k})]^*=[\mathbf{R}_{n'n}(-\mathbf{k})]^*,\\
\hbar\omega_{nn'}&=\hbar\omega_n-\hbar\omega_{n'}.
\end{aligned}$$

N is the number of atoms per unit volume. The term $\exp(\pm i\mathbf{k}\cdot\mathbf{r})$ in the above equations can be expanded into power series of $(\mathbf{k}\cdot\mathbf{r})$. One would find[5]

$$\mathbf{R}_{nn'}(\mathbf{k})=im\omega_{nn'}\mathbf{r}_{nn'}-\tfrac{1}{2}m\omega_{nn'}[\mathbf{r}(\mathbf{k}\cdot\mathbf{r})]_{nn'}+\tfrac{1}{2}i\hbar[\mathbf{l}+2\mathbf{s}]_{nn'}\times\mathbf{k}+\cdots, \quad (19)$$

where $\mathbf{l}$ is the orbital angular momentum of electrons.

[5] J. S. Griffith, *The Theory of Transition Metal Ions* (Cambridge University Press, London, 1961), p. 54.

Equation (19) is clearly the multipole expansion of $\mathbf{R}_{nn'}$. In the electric-dipole approximation, only the first term in the expansion of $\exp(\pm i\mathbf{k}\cdot\mathbf{r})$ is retained. The expression for $\chi^{(2)}$ in Eq. (18) should then reduce to the one obtained by Armstrong *et al.*[6] From Eq. (18), one finds readily the permutation symmetry for the generalized susceptibility tensor.[7]

$$\begin{aligned}\chi_{lmn}^{(2)*}(\mathbf{k}_3=\mathbf{k}_1+\mathbf{k}_2,\ \omega_3=\omega_1+\omega_2)&=\chi_{mnl}^{(2)}(\mathbf{k}_1=-\mathbf{k}_2+\mathbf{k}_3,\ \omega_1=-\omega_2+\omega_3)\\&=\chi_{nlm}^{(2)}(k_2=k_3-k_1,\ \omega_2=\omega_3-\omega_1).\end{aligned}\tag{20}$$

In a dense medium, there should also be a Lorentz-Lorenz correction factor in the expression for $\chi^{(2)}$, but the permutation symmetry relation of $\chi^{(0)}$ is unchanged.[8]

Consider now the presence of three waves in the nonlinear medium.

$$\begin{aligned}\mathbf{E}_m(\mathbf{r},t)&=\mathcal{E}_m(t)\exp(i\mathbf{k}_m\cdot\mathbf{r}-i\omega_m t)\\&\quad+\text{complex conjugate (c.c.)},\quad m=1,2,3,\\&\mathbf{k}_3=\mathbf{k}_1+\mathbf{k}_2,\quad \omega_3=\omega_1+\omega_2,\end{aligned}\tag{21}$$

where $|\partial\mathcal{E}_m(t)/\partial t|\ll|\omega_m\mathcal{E}_m|$. These three waves are coupled through the nonlinear susceptibility $\chi^{(2)}$, and consequently there is energy transfer among them. We expect that a time-averaged energy for the coupling of the three waves should exist. The term involving coupling of the three waves in Eq. (2) is

$$\mathbf{E}\cdot\mathbf{J}^{(2)}=\sum_{m=1,2,3}\mathbf{E}_m\cdot\partial\mathfrak{P}_m^{(2)}/\partial t,\tag{22}$$

where we can write

$$\mathbf{E}_m(t)=\int d\eta_m\mathcal{E}_m(\omega_m+\eta_m)\exp[i\mathbf{k}_m\cdot\mathbf{r}-i\omega_m t-i\eta_m t]+\text{c.c.},$$

$$\begin{aligned}\frac{\partial}{\partial t}\mathfrak{P}_1^{(2)}(t)&=\int d\eta_2 d\eta_3(-i)(\omega_3-\omega_2+\eta_3-\eta_2)\chi^{(2)}(\omega_1+\eta_1=-\omega_2-\eta_2+\omega_3+\eta_3):\mathcal{E}_2^*(\omega_2+\eta_2)\mathcal{E}_3(\omega_3+\eta_3)\\&\quad\times\exp[i\mathbf{k}_1\cdot\mathbf{r}-i(\omega_1+\eta_3-\eta_2)t]\\&\approx\left\{\chi^{(2)}(\omega_1=-\omega_2+\omega_3):\left[(-i\omega_1)\mathcal{E}_2^*(t)\mathcal{E}_3(t)+\frac{\partial\mathcal{E}_2^*(t)}{\partial t}\mathcal{E}_3(t)+\mathcal{E}_2^*(t)\frac{\partial\mathcal{E}_3(t)}{\partial t}\right]\right.\\&\quad+\omega_1\left[-\frac{\partial\chi^{(2)}(\omega_1)}{\partial\omega_2}+\frac{\partial\chi^{(2)}(\omega_1)}{\partial\omega_1}\right]:\frac{\partial\mathcal{E}_2^*(t)}{\partial t}\mathcal{E}_3(t)+\omega_1\left[\frac{\partial\chi^{(2)}(\omega_1)}{\partial\omega_3}+\frac{\partial\chi^{(2)}(\omega_1)}{\partial\omega_1}\right]:\mathcal{E}_2^*(t)\left.\frac{\partial\mathcal{E}_3(t)}{\partial t}\right\}\\&\quad\times\exp(i\mathbf{k}_1\cdot\mathbf{r}-i\omega_1 t)+\text{c.c.},\end{aligned}\tag{23}$$

$$\begin{aligned}\frac{\partial}{\partial t}\mathfrak{P}_2^{(2)}(t)&\approx\left\{\chi^{(2)}(\omega_2=\omega_3-\omega_1):\left[(-i\omega_2)\mathcal{E}_3(t)\mathcal{E}_1^*(t)+\frac{\partial\mathcal{E}_3(t)}{\partial t}\mathcal{E}_1^*(t)+\mathcal{E}_3(t)\frac{\partial\mathcal{E}_1^*(t)}{\partial t}\right]\right.\\&\quad+\omega_2\left[\frac{\partial\chi^{(2)}(\omega_2)}{\partial\omega_3}+\frac{\partial\chi^{(2)}(\omega_2)}{\partial\omega_2}\right]:\frac{\partial\mathcal{E}_3(t)}{\partial t}\mathcal{E}_1^*(t)+\omega_2\left[\frac{\partial\chi^{(2)}(\omega_2)}{\partial\omega_2}-\frac{\partial\chi^{(2)}(\omega_2)}{\partial\omega_1}\right]:\mathcal{E}_3(t)\left.\frac{\partial\mathcal{E}_1^*(t)}{\partial t}\right\}\\&\quad\times\exp(i\mathbf{k}_2\cdot\mathbf{r}-i\omega_2 t)+\text{c.c.},\\\frac{\partial}{\partial t}\mathfrak{P}_3^{(2)}(t)&\approx\left\{\chi^{(2)}(\omega_3=\omega_1+\omega_2):\left[(-i\omega_3)\mathcal{E}_1(t)\mathcal{E}_2(t)+\frac{\partial\mathcal{E}_1(t)}{\partial t}\mathcal{E}_2(t)+\mathcal{E}_1(t)\frac{\partial\mathcal{E}_2(t)}{\partial t}\right]\right.\\&\quad+\omega_3\left[\frac{\partial\chi^{(2)}(\omega_3)}{\partial\omega_1}+\frac{\partial\chi^{(2)}(\omega_3)}{\partial\omega_2}\right]:\frac{\partial\mathcal{E}_1(t)}{\partial t}\mathcal{E}_2(t)+\omega_3\left[\frac{\partial\chi^{(2)}(\omega_3)}{\partial\omega_2}+\frac{\partial\chi^{(2)}(\omega_3)}{\partial\omega_3}\right]:\mathcal{E}_1(t)\left.\frac{\partial\mathcal{E}_2(t)}{\partial t}\right\}\\&\quad\times\exp(i\mathbf{k}_3\cdot\mathbf{r}-i\omega_3 t)+\text{c.c.}\end{aligned}$$

From the above expressions, and with the help of permutation symmetry of $\chi^{(2)}$ in Eq. (20), it can readily be shown that the time average of Eq. (22) is given by

$$\sum_{m=1,2,3}\langle\mathbf{E}_m\cdot\partial\mathfrak{P}_m^{(2)}/\partial t\rangle_{\text{av}}=\partial\bar{U}^{(2)}/\partial t,\tag{24}$$

[6] J. Armstrong, N. Bloembergen, J. Ducuing, and P. S. Pershan, Phys. Rev. 127, 1918 (1962).

[7] Permutation symmetry for $\chi^{(3)}$ in the electric-dipole approximation was derived in Ref. 6.

[8] The proof of this statement is given in Ref. 6 for the electric-dipole approximation. However, it can also be applied to the present case with slight modification. Equation (A1) in Ref. 6 is now defined for each wave with wave vector $\mathbf{k}$ and frequency ω separately. The Lorentz tensor L_{ij} is a function of both $\mathbf{k}$'s and ω's. Both the linear polarizability $\alpha^{(1)}$ and the Lorentz tensor L_{ij} are self-adjoint and the derivation in Ref. 6 should be modified accordingly.

where the time-averaged coupling density stored in the medium is

$$\bar{U}^{(2)}=2\mathcal{E}_1^*(t)\cdot\chi^{(2)}(\omega_1):\mathcal{E}_2^*(t)\mathcal{E}_3(t)+\mathcal{E}_1^*\cdot\left[\omega_1\frac{\partial\chi^{(2)}(\omega_1)}{\partial\omega_1}+\omega_2\frac{\partial\chi^{(2)}(\omega_1)}{\partial\omega_2}+\omega_3\frac{\partial\chi^{(2)}(\omega_1)}{\partial\omega_3}\right]:\mathcal{E}_2^*(t)\mathcal{E}_3(t)+\text{c.c.} \quad (25)$$

More generally, one can show, from the microscopic expression for $\chi^{(n)}$ for a nondissipative medium, the general permutation symmetry

$$\begin{aligned}&\chi_{l_{n+1},l_1\cdots l_n}^{(n)*}(\mathbf{k}_{n+1}=\sum_{i=1}^{n}\mathbf{k}_i,\ \omega_{n+1}=\sum_{i=1}^{n}\omega_i)\\&=\chi_{l_1\cdots l_n,l_{n+1}}^{(n)}(\mathbf{k}_1=-\sum_{i\neq1}\mathbf{k}_i+\mathbf{k}_{n+1},\ \omega_1=-\sum_{i\neq1}\omega_i+\omega_{n+1})\\&=\cdots=\chi_{l_n,l_{n+1},l_1\cdots l_{n-1}}^{(n)}(\mathbf{k}_n=\mathbf{k}_{n+1}-\sum_{i\neq n}\mathbf{k}_i,\ \omega_n=\omega_{n+1}-\sum_{i\neq n}\omega_i).\end{aligned} \quad (26)$$

With Eq. (26), one finds

$$\sum_{m=1}^{n+1}\langle\mathcal{E}_m\cdot\partial\mathfrak{P}_m^{(n)}/\partial t\rangle_{\text{av}}=\partial\bar{U}^{(n)}/\partial t, \quad (27)$$

where the time-averaged energy density stored in the nonlinear medium for the coupling of the $(n+1)$ waves is

$$\bar{U}^{(n)}=n\mathcal{E}_1^*(t)\cdots\mathcal{E}_n^*(t)\chi^{(n)*}(\mathbf{k}_{n+1},\omega_{n+1})\mathcal{E}_{n+1}(t)+\mathcal{E}_1^*(t)\cdots\mathcal{E}_n^*(t)\left[\sum_{i=1}^{n+1}\omega_i\frac{\partial\chi^{(n)*}(\mathbf{k}_{n+1},\omega_{n+1})}{\partial\omega_i}\right]\times\mathcal{E}_{n+1}(t)+\text{c.c.} \quad (28)$$

Conversely, the existence of $\bar{U}^{(n)}$ in the form of Eq. (28) implies the permutation symmetry for $\chi^{(n)}$. The energy conservation relation of Eq. (2) after time average can now be written as

$$(c/4\pi)\nabla\cdot(\mathbf{E}\times\mathbf{B})=-\partial\bar{U}/\partial t,$$

where

$$\bar{U}=\sum_{n=1}^{\infty}\bar{U}^{(n)},$$

with $\bar{U}^{(1)}$ and $\bar{U}^{(n)}$ $(n\geq2)$ given by Eqs. (8) and (28), respectively.

In conclusion, we have shown in this paper that the permutation symmetry of the generalized nonlinear susceptibilities leads to the existence of a time-averaged stored energy density for electromagnetic wave propagation in a nonlinear, nondissipative, but dispersive medium.[9] The discussion can of course be generalized to include other types of excitational waves in the medium.

[9] The derivation here is strictly correct only for waves with $\mathbf{k}_3=\mathbf{k}_1+\mathbf{k}_2$ and $\omega_3=\omega_1+\omega_2$. However, it is also a good approximation when these matching conditions are approximately satisfied. This is in the same spirit as one can define a linear dielectric constant $\epsilon(\omega)$ for a pulse of waves of frequency ω as long as ω is much larger than the inverse of the pulse width.